HIGH-THROUGHPUT INTRACELLULAR DELIVERY OF PROTEINS AND PLASMID

A Thesis
Presented to
The Academic Faculty

by

Seonhee Park

In Partial Fulfillment
of the Requirements for the Degree
Doctor of Philosophy in the
School of Chemical and Biomolecular Engineering

Georgia Institute of Technology
May 2015

HIGH-THROUGHPUT INTRACELLULAR DELIVERY OF PROTEINS AND PLASMID

Approved by:

Dr. Mark R. Prausnitz, Advisor
School of Chemical and Biomolecular Engineering
Georgia Institute of Technology

Dr. Wilbur A. Lam
School of Biomedical Engineering
Georgia Institute of Technology

Dr. Gang Bao
School of Biomedical Engineering
Georgia Institute of Technology

Dr. Hang Lu
School of Chemical and Biomolecular Engineering
Georgia Institute of Technology

Dr. Michelle R. Dawson
School of Chemical and Biomolecular Engineering
Georgia Institute of Technology

Date Approved: February 3, 2015

To my family

ACKNOWLEDGEMENTS

First of all, I would like to thank my advisor, Dr. Mark R. Prausnitz, for giving me the opportunity to be part of the lab and work on the project. Over the years, I have learned many valuable lessons in research and I could not have been more grateful for his patience and guidance. I would also like to thank Dr. Gang Bao, Dr. Michelle R. Dawson, Dr. Wilbur A. Lam, and Dr. Hang Lu, for serving as member of my thesis committee and providing valuable advices in the past years.

I would like to thank the members of NDC project center for the collaboration and guidance for the past four years I have been a part of the center. I was very fortunate to have collaborators who were a continuous motivation for me to learn and provided scientific guidance in their area of expertise for my project during the meetings and video conferences. I would like to specially acknowledge few of the collaborating labs/members: I would like to thank members of Bao lab, especially Annie Zheng, Harsha Deshmukh, and Renee Cottle, for their help with microinjection and cell culture. I would like to thank members of Lam lab, Dr. David Myers, Reggie Tran, Dr. Byungwook Ahn, for their technical support on microfluidic devices and fabrication for the nanoneedle mediated intracellular delivery, even though the devices did not work as well as we hoped for. I would like to thank members of Dr. Porteus lab (Gabe Washington and Stacey Wirt) and Dr. Dynan lab (Dr. Lahcen Jaafar) for their generous giving of the reagents and materials for us to try.

I would like to acknowledge collaborators in my thesis work, without whom I could not have completed my study. First, I would like to thank the members of Dr. Mark

Allen's lab, Dr. Seungkeun Choi and Dr. Seung-joon Paik, for their wonderful fabrication work and the advice on the nanoneedle mediated intracellular delivery study. I would like to also thank SQZ Biotech and Dr. Armon Sharei for providing the microfluidic devices for our study and sharing number of tips for the experiment. I would like to thank Emily Jackson and Agustin Lopez Marquez for their help in setting up the microfluidic device and technical support.

I would like to thank the core facility staff in the IBB for their technical expertise in the confocal microscopy and flow cytometry: Andrew Shaw for the assistance with the confocal microscopy every time I ran into the problem and Nadia Boguslavsky for the help with flow cytometry.

I am truly grateful for the past and present members of the drug delivery lab, where I spent majority of time here at Georgia Tech and made many unforgettable memories. I would like to especially thank Dr. Seong-O Choi for the fabrication work on nanoneedles and being a great mentor in research. I would like to thank Dr. Vladimir Zarnitsyn and Dr. Xin Dong Guo, who helped me in the early years on the nanoneedle work. I would like to also thank Dr. Hong-wei Yang for making several types of nanoparticles and helping me with the experiment. I would like to thank Dr. Ying Liu and Dr. Aritra Sengupta for teaching me mammalian cell culture and helping me get started. I would like to thank number of others who had helped me with experiment and provided valuable feedbacks: Dr. Devin McAllister, Dr. Priya Kalluri, Dr. Yoo Chun Kim, Dr. Jeong Woo Lee, Dr. Wilmarie Medina-Ramos, Matt Mistilis, Stefany Holguin, Pradnya Samant, Jaya Arya, Bryce Chiang, Jessica Joyce, and Andrew Tadros. I would like to also thank Paul Choi, an undergraduate student, and Aidan O'Reilly, high school intern

student, for helping me with experiments, especially with the image analysis. Last but not least, I would like to thank Donna Bondy for all the support and work on paper work and scheduling.

I would like to thank my friends. Without their encouragement and support throughout the years, I could not have completed thesis work and survived these years in the graduate school. I would like to thank friends here in Georgia Tech for being a great support and sharing good and bad times together. I would like to thank friends in Surgarloaf Korean Baptist Church, who provided encouragement and shared wonderful times together as a family in Jesus Christ.

Last but not least, I would like to thank my family for their continuous love and support in the past and now. Their encouragement, trust and care has always been a source of strength for me in the past years whenever I faced homesickness, weaknesses and challenges in undergraduate and graduate schools.

TABLE OF CONTENTS

LIST OF TABLES

LIST OF FIGURES

SUMMARY

Intracellular delivery of macromolecules is crucial for the success of many research and clinical applications. Especially, increasing interest in delivery of pharmaceutical agents requires effective methods to transport drugs across the cell membrane. Intracellular delivery methods, such as lipofectamine, electroporation, and microinjection, have been developed and used for many years due to the simplicity of the method and the efficiency of intracellular uptake. However, these conventional methods are still inadequate for several applications because of the issues associated with toxicity, low-throughput, and/or difficulty to target certain cell types. In this study, we developed and evaluated new high-throughput intracellular delivery methods for the efficient delivery of macromolecules while maintaining high cell viability.

First, we studied the feasibility of using an array of nanoneedles to physically make transient holes in cell membranes for intracellular delivery. The array of nanoneedles was fabricated to have sharp tip diameters in the range of tens of nanometers and contain 250,000 needles per array. Two delivery methods, puncture loading and centrifuge loading, were developed and assessed for the intracellular uptake of fluorescent molecules in human prostate cancer cells. For each method, we studied the effect of various experimental parameters on cell viability and delivery efficiency of fluorescent molecules. We observed effective intracellular delivery of up compounds as large as 500 kDa FITC-dextran molecules using the puncture loading method and determined the dependence of delivery efficiency and viability on puncture force and time. We also examined the effect of nanoneedle type, centrifugal force, and time on the viability and intracellular uptake in centrifuge loading. In both methods, high-throughput intracellular delivery was feasible by creating transient holes in cell membranes with the sharp tips of the nanoneedles.

The second physical intracellular delivery method we studied was a novel microfluidic device that created transient holes in the cell membrane by mechanical deformation and shear stress to the cell. We observed efficient delivery of fluorescent molecules to prostate cancer cells and leukemia cells and studied the effect of device

design and flow pressure on the delivery efficiency compared to data in the literature. Furthermore, we observed the delivery of proteins, which are similar to the size of other pharmaceutical proteins. We accounted for cell loss and clogging in the constriction channels of the microdevices and determined the true loss of cell viability associated with this delivery method by accounting for all cells introduced into the device.

Lastly, we investigated the possibility of intracellular delivery using nanoparticles on a target cell line. We screened for suitable nanoparticle materials among a number of candidate materials based on maintaining cell viability of leukemia cells and on plasmid transfection efficiency. Mesoporous silica/poly-L-lysine nanoparticles were selected for further intracellular delivery study based on cell viability and intracellular delivery capability. We demonstrated the co-delivery of protein and plasmid by encapsulating into and coating onto the surface of the nanoparticles, respectively, which would be advantageous for certain therapeutic strategies.

In summary, this work introduced two new intracellular delivery methods involving nanoneedles and novel nanoparticles, and provided an early, independent assessment of microfluidic delivery, showing the strengths and weaknesses of each method. With continued research, these methods can be further optimized for a number of laboratory and clinical applications.

CHAPTER I

INTRODUCTION

Delivery of drugs and molecules into cells in an effective and efficient manner is of widespread interest and studied extensively due to its many applications in biology and medicine. Effective intracellular delivery of pharmaceutical agents, such as proteins, antibodies, enzymes, plasmids, and drug-loaded nanocarriers, can be utilized for the treatment of cancer, genetic disorders, and other acquired diseases by targeting the site of genetic mutation, stimulating the immune response, or modifying cellular information [1, 2]. For these pharmaceutical agents to be therapeutically active, they often need to be delivered intracellulary inside cytoplasm or onto the nucleus [3].

The major barrier for the delivery of these pharmaceutical agents is the cell membrane, which has a bilayer structure from phospholipids and is lipophilic in nature. While molecules can enter the cytoplasm by the endocytic pathways, they may end up within endosomes and be degraded by lysosomal enzymes. Only portion of molecules are likely to end up in cytoplasm and there may be other barriers such as cytoplasm trafficking and nuclear membrane, for the delivery to be successful [4]. Instead, number of methods are developed to make transient holes on the cell membrane by exerting external forces but will compromise the viability of the cells. Thus, an ideal intracellular delivery method should have following features; protection of pharmaceutical agents, specific targeting, prevention of non-specific interaction with other components, reaching required intracellular dose, low toxicity, and cost-effectiveness [5].

There are a number of biological, chemical, and physical methods that have been developed and are commercially available for intracellular delivery in laboratory settings. Although these systems are widely used and highly efficient, there are a number of drawbacks with these systems, such as low throughput and toxicity. To address limitations of previously developed methods, we studied three alternative intracellular delivery techniques, using nanoneedles, a microfluidic device, and nanoparticles, for the delivery of macromolecules, protein, and plasmid. In each chapter, the intracellular delivery techniques used are characterized and optimized for high viability and uptake of

fluorescent molecules by varying experimental parameters. Once the uptake of fluorescent molecules of various sizes has been demonstrated, the feasibility of delivery of functional protein and plasmid has been further investigated, which usually requires the delivery not only inside cytoplasm but also onto the nucleus.

The first part of the study is on a nanoneedle-mediated intracellular delivery method. Among many other delivery methods, microinjection is known as a universal intracellular delivery mechanism for its capability to by-pass both physical and chemical barriers. However, there is a major drawback to the method as the injection is done manually at the single cell level [6]. In order to address the limitation of microinjection, we propose an alternative method using multi-needle arrays of nanoneedles which can achieve high-throughput delivery of molecules and will resemble the delivery mechanism similar to that of microinjection. Broad experience with microneedles in our lab demonstrated the possibility of drug delivery in skin and eyes as well as preliminary intracellular delivery using solid microneedles [7]. Nanoneedles, fabricated out of silicon with high needle density and very sharp tip diameter, in the nanometer range, are utilized in two different loading techniques; centrifuge and puncture loading. Uptake of fluorescent molecules and cell viability in human prostate cancer cells are quantitatively measured at varying parameters, such as force and time applied.

Two other intracellular delivery methods, microfluidic device and nanoparticles, are explored as nanoneedle-mediated intracellular delivery works well with adherent cells but showed poor result with suspension cells. The microfluidic device consists of tens of constrictions channels to squeeze the cells and create transient holes in the cell membrane for the diffusion of molecules into the cell [8]. The method is tested in different cell lines, prostate cancer cells and leukemia cell lines, which are suspension cells in nature. We studied the effect of varying parameters, such as constriction width and pressure, on the cell loss and viability after the treatment.

Nanoparticles can be made of many different materials, including polymers, inorganic metals, quantum dots, etc., and delivered intracellularly by endocytic pathways and/or ligand-receptor interaction [9]. We tested nanoparticles made of different materials for DNA delivery to a leukemia cell line for high cell viability and high GFP

expression. We also studied the feasibility of co-delivery of protein and plasmid using mesoporous nanoparticle.

CHAPTER II

BACKGROUND

2.1 Intracellular delivery

Intracellular delivery has been an area of interest to many, especially in the medical and pharmaceutical field. Intracellular delivery is the process of delivering the molecules or therapeutic agents to cellular or organ compartments across the cell membrane. Despite years of research and the existence of some already established methods, there is still much on-going research on new intracellular delivery methods for more efficient and effective delivery method.

2.1.1 Barriers

The cell membrane, which has a bilayer structure from phospholipids and is lipophilic in nature, is the major barrier for intracellular delivery. Direct intracellular delivery of compounds from the surroundings is restricted by cell membrane, such that macromolecules, such as proteins and plasmids, cannot be delivered without the active transport mechanism [3]. Under certain conditions, molecules can enter the cytoplasm by the endocytic pathways by receptor-mediated endocytosis [4]. However, molecules taken in by endocytosis may end up within endosomes and can be degraded by lysosomal enzymes [10]. Thus, only a small portion of molecules entering cytoplasm may be unaffected. The small portion of unaffected molecules in the cytoplasm may face other barriers, such as cytoplasm trafficking in the dense meshwork of the cytoskeleton and the membrane of target organelles. Therapeutic agents and molecules often need to be delivered to the specific organelles, such as nuclei, mitochondria, and endoplasmic reticulum, in order to be effective.

2.1.2 Applications

Intracellular delivery has been studied extensively for many years due to the number of possible applications. Some of the prevalent applications and delivery agents will be discussed in more detail below.

2.1.2.1 Imaging and tracking

Imaging and tracking in cells is important in understanding the complex system of cells; how cells behave, carry out functions, and respond to changes in the surroundings. While there are number of fluorescent sensors and proteins available for use, quantum dots have several characteristics that are more desirable for imaging and tracking; composition- and size-dependent absorption and emission, long fluorescence lifetime, and surface functionalization [11]. Using little amount of quantum dots and different surface functionalization, quantum dots can label live cells, the specific organelles, and surface proteins for imaging and tracking. For targeting and labeling, the quantum dots need to be delivered into the cytoplasm and/or nucleus without being trapped in the endocytic pathway [11]. Due to the size of quantum dots, they cannot cross the cell membrane barrier and need to be intracellularly delivered by methods, such as electroporation, microinjection, and lipofection [12, 13]. A study showed that a number of delivery methods, with the exception of microinjection, are not able to easily deliver quantum dots without forming aggregation or getting trapped in the endosomes [14]. Another limitation is the difficulty of washing away excess quantum dots.

2.1.2.2 Cellular engineering

Cellular engineering is an emerging area of studying the role of engineering in basic cell biology and making products out of living cells [15]. One well-known example of cellular engineering is the generation of induced pluripotent stem cells (iPSCs) from adult human fibroblasts by four transcription factors [16]. With number of possible applications using stem cells, the cell engineering of stem cell is being studied extensively [17]. Two cell engineering possibilities are the direct differentiation from pluripotent stem cells and direct conversion from other somatic cells [18, 19]. Finding the right transcription factors and protocol for desired state is crucial, but delivery of these

transcription factors in efficient and safe way is also important for the further use of generated stem cells. In addition, choosing a right delivery method that will not alter the stem cell behavior or identity is of importance.

2.1.2.3 Gene therapy

Gene therapy is the delivery of genetic materials as a drug to stem cells or immune cells for the treatment of cancer, genetic disorder, and other acquired diseases. With increasing amount of research on genome editing tools, such as zinc finger nucleases (ZFNs), transcription activator-like effector nucleases (TALENs), and clustered regularly interspaced short palindromic repeats (CRISPRs), the area of gene therapy is growing [20-22]. These restriction enzyme pairs can be designed to target and induce double strand break at specific DNA sequence. The cell can respond with two repair mechanisms, non-homologous end joining and homology directed repair, to introduce the donor template, which encodes the correct DNA sequence, at the site of double strand break. By delivering restriction enzymes, either as a protein or a plasmid encoding these proteins, with a donor template, gene correction at the targeted site can be accomplished [23].

Gene therapy can be completed by efficient intracellular delivery of therapeutic agents to immune cells or stem cells, which can be treated ex vivo and transplanted back to the patient to treat cancer, genetic disorder, and other acquired diseases [1, 2, 24]. Manipulation of immune cells, like natural killer (NK)-cells and T cells, have been considered as the possible cancer immunotherapy after years of studying immune responses against tumors [25-27]. In recent years, some successes of treating leukemia with genetically modified T cells, to recognize a variety of tumor-associated antigens, have been demonstrated [28-30]. Stem cells can also be used as a possible treatment for genetic disease due to stem cells' ability to differentiate into several tissues. Mesenchymal stem cells (MSCs) can differentiate into mesenchymal tissues and have been investigated to treat patients with heart diseases and autoimmune diseases [31, 32]. Hematopoietic stem cell (HSC) transplantation is known as one of the effective treatments available for the sickle cell disease and was first used 25 years ago [33]. Although HSCs are rare in the body, the potential of a single HSC to rebuild the entire

blood system after the transplantation has been demonstrated [34, 35]. Other types of stem cells, endothelial progenitor cells and neural stem cells, also have potential to differentiate into endothelial and neural cells lineage and have been investigated for the gene therapy [36].

2.2 Current intracellular delivery techniques

For any applications to succeed, the construction of working therapeutic agents will be necessary along with the good gene delivery methods. Thus, an ideal intracellular delivery method should have the following features; protection of pharmaceutical agents, specific targeting, prevention of non-specific interaction with other components, reaching required intracellular dose, low toxicity, and cost-effectiveness [5]. A number of intracellular delivery methods are available and used in many laboratories for different applications. Three main categories of the intracellular delivery methods are biological, chemical, and physical methods and will be discussed in more details below.

2.2.1 Biological methods

Biological method involves the use the viral vectors as a carrier and is most commonly used in laboratories for the delivery of plasmid. Viral vectors, such as lentivirus, retrovirus, adeno-associate and adeno-derived vectors, have been used to introduce the therapeutic gene into the cells by a process called transduction [37]. Viral vectors have been used widely due to the stable gene expression and the high efficiency as virus has natural tendency to infect the host cell and replicate [38]. In addition, the ease of design and use of viral vectors is one of the advantages of the method. However, number of problems has limited the further use of viral vectors in clinical applications. The packaging capacity of plasmid DNA is limited and the preparation in a large-scale is difficult and expensive. Number of potential problems in clinical application also includes the risk of mutagenesis, induction of immune responses, and pathogenic risk [5, 24, 39, 40]. Due to these problems that may raise safety concerns with biological methods, a substantial effort is focused on the development of non-viral systems.

2.2.2 Chemical methods

In an effort to move away from viral vectors, development of synthetic vectors has been of interest. The non-viral vectors are relatively simple for quantitative production and are safer alternative due to low host immunogenicity [41]. The therapeutic agents can be encapsulated into the cationic lipids or synthetic polymers, such as polyethylenimine (PEI), and polylactic acid (PLA), to be delivered across the cell membrane.

Lipofection, a transfection mediated by liposomes, is one of the most widely used chemical methods. Liposomes are formed by a self-assembly of cationic lipids, which have polar heads and non-polar tails. The positive charge present in these structures allows the interaction with negatively charged plasmids. Plasmids can bind to the surface or can be placed inside the aqueous phase of liposomes to form lipoplexes for delivery [42]. Similarly, polyplexes can be formed by plasma binding on polymers [43]. Lipoplex and polyplex can be taken inside the cell by endocytosis and destabilized inside the cytoplasm to release DNA [5, 44]. Since the method is simple to use and safe, many products are commercially available to be used for cell transfection. Despite the use of lipofection in many laboratories, there are major limitations of low delivery efficiency and toxicity associated the lipoplexes. The lipofection suffers from poor transfection efficiency since the uptake across the cell membrane via endocytosis is low, which could be order of magnitude lower than the efficiency of viral vectors. In addition, lipoplex are recognized as foreign and trigger the production of cytokines once taken inside the cell [45]. The toxicity of liposome may be questionable for the use of lipofection in gene therapy and have been studied to develop safer cationic lipids.

2.2.3 Physical methods

Physical methods use different types of external forces to temporarily disrupt the cell membrane and have been investigated in the recent years due to the advantage of delivering the therapeutics agents without encapsulation in lipids or polymers, which reduces the immune response, the toxicity associated with polymers, and the modification of therapeutic agents [45-47]. Although a lack of protection might result in DNA degradation and low efficiency, minimal immune response makes the physical methods a

desirable alternative for gene therapy. Some widely used physical methods are discussed in details below.

2.2.3.1 Electroporation

Electroporation is one of the widely used physical methods for cell transfection and has been known as the standard for plasmid delivery. When the short electrical pulse is applied to the cells, cell membrane is transiently disrupted and molecules can enter the cytoplasm by diffusion and electrophoresis before the membranes reseal [48]. The method has been used in various applications, such as cancer treatment, DNA transfection and gene therapy, and proven to be effective in both in vivo and in vitro treatment [49, 50]. Extensive study on the method has led to high percentage of cell permeabilization with low cell death using the optimum conditions. However, due to the differences between different types of cells, optimization of different parameters, such as pulse electric field intensity, electrical pulse type, electropulsation buffer conductivity, and electroporation temperature, is required for different cell types [5]. Cell lines with large heterogeneity in cell size or non-spherical orientation are difficult to optimize due to inverse correlation between cell size and the external field for permeabilization [1]. Electroporation of cells in suspension also requires a voltage up to 1 kV and such high voltage can affect the stability of plasmids. Due to vulnerability of cells after the treatment, post-pulse manipulations of cells are also important to maintain the high cell viability and to maintain the proper biological functions, especially for the application of gene therapy.

2.2.3.2 Ultrasound

Ultrasound has been exploited in number of biological application, as a sensor, an acoustic microscopy, and a method for intracellular delivery of fluorescent molecules, genetic materials, and chemotherapeutic compounds by transient mechanical disruption of cell membranes [51]. It is assumed that the acoustic cavitations or acoustically-induced bubble activity causes cell membranes to transiently enhance the permeability and increase the efficiency of intracellular delivery [52-55]. Effective in vitro delivery of chemotherapeutic agents, such as BH3 peptides and doxorubicin, encapsulated in

microbubbles or micelles using ultrasound has been demonstrated [56, 57]. Despite the promising results of ultrasound, there are number of disadvantages to the method. The application of this method is limited to a specific tissue type of anatomical region and requires complex equipment [58]. Effect on cell viability depends on the acoustic intensity and has been of concern due to the damage on the cell membrane during the ultrasound. The effect of ultrasound is also non-homogeneous and not consistent since same condition can result in various results in terms of membrane poration and cell viability due to difference in the cell structure [59].

2.2.3.3 Fluid mechanical delivery

Fluid mechanical delivery employs the physical force generated by fluid motion for permeabilization of the cell membrane and delivery of macromolecules. Increase in membrane tension due to shear forces is believed to induce the cell membrane poration [60, 61]. Intracellular delivery of macromolecules has been demonstrated by directly applying shear forces to cells by rapid flow through small-gauge hypodermic needles, called syringe loading [62]. Using microchannel devices, shear-induced loading of cells with fluorescent molecules of different sizes has been studied [63]. The effect of varying flow conditions, such as shear forces and time, and device design on intracellular delivery and cell viability have been studied. Recent work on the new device with constriction channels to deform and shear cells has demonstrated the delivery of various fluorescent molecules, proteins, and nanotubes on number of different cell types [8]. While the delivery technique is high throughput method, easy to use and relatively inexpensive, the delivery is mainly limited to cytoplasm and further studies need to be conducted to understand the delivery mechanism.

2.2.3.4 Magnetofection

Magnetofection is a delivery technique utilizing magnetic fields to concentrate nanoparticles containing nucleic acids into the cells [64]. Particles are chosen based on the following properties; functionality for association with nucleic acid, magnetic properties to react under certain magnetic force, physical and chemical stability, and biocompatibility [65]. These particles can be associated with nucleic acids, such as DNA,

and RNA, and concentrated on the target cell by magnetic field. The uptake of these particles is accomplished by endocytosis and the nucleic acids can be released in the cytoplasm [66]. The method has shown promising results in vitro and in vivo studies but further studies on the effect of magnetic field on the cellular level and plasmid are to be done.

2.2.3.5 Gene gun

Gene gun is a technique first developed in 1987 for the delivery of nucleic acids into the plant cells using high-velocity microprojectiles [67]. Also known as a biolistic or particle bombardment, the technique accelerates the particles, heavy metal particles coated with plasmid DNA, by pressurized gas or electric discharge to penetrate into cells and release DNA for transfection. The technique was utilized for mammalian cells starting in the early 1990s [68]. Delivery of plasmid has been demonstrated in DRG neurons and in C. elegans [69, 70]. The technique can be used in vivo for delivery of DNA vaccine to skin or exposed tissue [70, 71]. Some limitations of this technique is that the cells need to be firmly attached to the substrate to withstand the force of gold projectiles and that use of heavy metals can be toxic to the cells or expensive to use [72].

2.2.3.6 Microinjection

Microinjection is well-known method that has been used to inject molecules into the cells and is known as a universal intracellular delivery mechanism due to its capability to by-pass both physical and chemical barriers. The microinjection system is composed of a glass needle of outside diameter about 0.5 to 1 μm, a microinjector for suspension cells, and a positioning device to control the micropipette movement. The needle, containing a fluid of genetic material, is precisely controlled by a micromanipulator using inverted microscope for visual control. Once needle is placed on top of the target cell, hydrostatic pressure is applied to inject the material [6, 48]. Since materials by-pass the cell membrane and are directly entered to the cells, there is little or no degradation of materials or diffusion limitations and the method is very effective and reproducible. However, there are number of disadvantages to the method. Since the injection is controlled by the injection time and pressure, the volume of the materials

entered is difficult to precisely control and the clogging of the micropipette can occur over time. Throughput of the method is also of concern since only one cell at a time can be injected; i.e. a trained person can only inject up to few hundred cells per day. Due to low throughput, microinjection is impractical for gene delivery applications and has limited potential. In order to solve this issue of low throughput, many approaches of combining the microinjection with microfluidics are being developed [73, 74].

2.3 Developing intracellular delivery techniques: Nanobiotechnology

Nanotechnology refers to a system that has the dimensions of 1 – 100 nm and has become an important technology as microelectronic devices become smaller [75]. Nanotechnology has offered new tools for studying biology, especially at cellular and molecular levels, because of the similarity in dimensions [76, 77]. The advance in nanotechnology provided new ways to visualize, manipulate, and characterize cells and sub-cellular components inside the cells. In particular, nanoneedle, nanowires, and nanoparticles are methods that are similar or used in this thesis and will be further discussed below.

2.3.1 Microfabrication

Microfabrication is the collection of processes used to make physical objects with dimensions in the micrometer to millimeter range. The microfabrication process has been used and developed for the semiconductor manufacturing in early years, but has been extensively explored in other applications, such as microelectromechanical systems (MEMS), microfluidics/lab-on-a-chip, and the extension into nanoscale. In a representative process, first, thin film growth or deposition onto the substrate, such as silicon, glass, and plastics, is conducted by chemical-reaction-driven or physical processes to form one or more thin films for different applications [78, 79]. Afterward, the process called photolithography is used to transfer a pattern by coating positive or negative photoresist, a photosensitive organic polymer, and exposing under UV light [80]. Another method, microcontact printing using a soft polymeric stamp, has been introduced and used mainly for non-cleanroom-compatible materials or chemicals [81]. Thin film or substrate can be removed according to the transferred pattern by etching

process. Using liquid chemicals or plasma, films and substrate can be etched to form different structures using either isotropic etching or anistropic etching, or the combination of both [82-84]. The fabricated devices are ready to use after washing residual photoresist or films and bonding different parts together. Microfabrication process offers many advantages in designing new devices by precise control of geometry and dimensions in millimeter range. The process is explored in bio-MEMS applications for sensors, lab-on-chip device, and medical devices [85]. With advancement in the process and the increasing interest in nanobiotechnology, there are more possibilities for the device designs in biological applications.

2.3.2 Nanoneedles

Nanoneedle is one-dimensional nanostructure with nanoscale geometry and high-aspect ratio, with a diameter of 1 – 100 nm and a length of 1 – 20 μm [86]. One-dimensional nanostructure, such as carbon nanotubes and boron nitride nanotubes, can be fabricated by chemical synthesis to have physical properties appropriate for nanoneedle with diameter of 1 – 100 nm [87, 88]. Because of the difficulties to precisely align and reliably assemble nanostructure into needle-like probe configuration, other approaches are taken to develop nanotube-tipped AFM probes [89, 90]. Alternative method to fabricate nanoneedle is nanofabrication techniques, such as focused-ion-beam machining, electrochemical fountain pen nanofabrication, and direct-write nanofabrication techniques, which usually makes nanoneedle with diameters larger than 100 nm [91-93].

Some applications of nanoneedle include the use in biosensors, delivery systems, and bio-imaging as these nanostructures can penetrate the cell membrane with minimal invasiveness and access the interiors of living cells. Carbon nanotubes have been used as a biosensor to detect proteins, antibody-antigen interactions, glucose, and DNA hybridization, due to the electrical properties and sensitivity to changes in the surrounding environment [94, 95]. Nanotubes can be covalently or non-covalently functionalized with proteins and polymers to be more suitable for biological applications. Semiconducting boron nitride nanotube has been also used as an electrochemical probe to measure signaling processes and electrochemical reactions by coating with layers of metal and insulating polymer [96].

2.3.2.1 Applications in intracellular delivery

Nanoneedle has been explored as alternative options for intracellular delivery to overcome the barrier of cell membrane with minimal invasiveness and deliver macromolecules. Nanoneedle delivery system is composed of three components; an individual nanoneedle, a manipulator, and an optical microscope [86]. Fabricated needle can be attached to the atomic force microscopy (AFM) probes or incorporated into the system similar to the microinjection for manipulation and injection. Delivery can be achieved either by loading molecules inside hollow nanotubes or nanopipettes, which is similar to microinjection, or by loading molecules on the surface of solid nanoneedles by surface functionalization [91, 97-99]. Efficient intracellular delivery by both techniques has been demonstrated, but the system still has the same issue as in microinjection of low throughput due to the single cell process. Another drawback could be the limited volume of loading on nanoneedle, which reduces the number of cells that can be treated per each nanoneedle.

2.3.3 Nanowire

Nanowire is a nanostructure with aspect ratios of 1000 or more and with the diameter in the nanometer range. Various materials, polymers, metal oxides, and silicon, have been used for producing nanowires [100-102]. Nanowires can be synthesized in two different approaches: top-down and bottom-up. The former approach reduces a bulk material to nanowires by lithography or electrophoresis, but is mostly limited to the single needle instead of arrays [101, 103]. The latter approach uses surface chemistry to grow nanowires on semiconductor materials, using vapor-liquid-solid synthesis, and is used more commonly for the synthesis of nanowire arrays [104-106]. The size of the nanowires can be controlled precisely by the liquid alloy droplets on the surface.

Due to nanowires' physical properties and the materials used for synthesis, nanowires have been studied for many different applications in recent years, including solar cells, and biological applications. Silicon nanowire arrays have been explored for photovoltaic applications for its optical absorption properties, owing to the sub-visible wavelength of the wires [107, 108]. Studies in recent years showed the feasibility of using nanowires for solar cells, but further studies are being done to increase the solar-

energy-conversion with different materials and physical properties. In biological applications, silicon nanowires have been attractive option for a sensor due to nanowires' high selectivity and sensitivity. Nanowire-based sensors have been explored for the detection of real-time biological macromolecules, DNA, cancer markers, and chemical detection [109-111].

2.3.3.1 Applications in intracellular delivery

Nanowires have been utilized in the recent years for the intracellular delivery to deliver molecules in high throughput manner. Carbon nanofibers are grown on a flat substrate with the tip diameter less than 100 nm and used for intracellular delivery to Chinese Hamster Ovary cells [112]. Vertical silicon nanowires have also been developed for the intracellular delivery of proteins and plasmids to neural and neural precursor cells [113]. Other materials, such as gallium arsenide and copper oxide, have been used for making nanowires [114, 115]. Intracellular delivery using nanowires has demonstrated the intracellular delivery with high cell viability. The method also has shown the ability to treat many cells at one time. However, most works on nanowires are relatively new and still requires further improvement to be reliably used for intracellular delivery.

2.3.4 Nanoparticles

Nanoparticles are synthesized particles with the diameters of 1 – 100 nm [116]. Using different methods and materials, various types of nanoparticle can be prepared; inorganic nanoparticle, polymeric nanoparticles, nanocrystals, nanoboxes, and solid-lipid nanoparticle [117-121]. Surface coating of nanoparticles is important for tuning the properties, such as stability, solubility, and targeting, based on the application.

Nanoparticles are explored in optical and electronic field applications as nanoparticles' small size gives rise to unexpected properties [122]. Quantum dots are example of nanoparticles with size-dependent optical and electrical properties [123]. Because of high quantum yield, high resistance to photobleaching, and broad excitation spectra of quantum dots, quantum dots offer many advantages for imaging, labeling and sensing over the other fluorescent proteins or labeling techniques [124]. Another field of interest for nanoparticles is electronic field. Magnetic nanocrystals, which are iron oxide-

based particles, have been evaluated for biological applications, including imaging, diagnosis and therapy [125]. Improvement in magnetic resonance-imaging by internalization of superparamagnetic nanoparticle in mesenchymal stem cells has been a promising result [126].

2.3.4.1 Applications in intracellular delivery

Nanoparticles have been used for the intracellular delivery of therapeutic agents by either encapsulating inside or coating on the surface of the nanoparticle. By modulating polymer characteristics, release of therapeutic agents from nanoparticle can be targeted and controlled to desired level for required duration while therapeutic agents can be protected from enzymatic degradation [127, 128]. In addition, compared to the microparticles, which have diameters of 1 and 10 μm, nanoparticles demonstrated the increase in uptake efficiency due to its smaller size [129, 130]. Because of several advantages of nanoparticles, there are number of in vivo and in vitro studies on-going for drug delivery, such as anticancer drugs, siRNA, and glaucoma drugs [131, 132]. Although nanoparticles seem to be an effective intracellular delivery method, the answers regarding the pathway and the interaction with biological systems are still unknown.

CHAPTER III

DEVELOPMENT AND ASSESSMENT OF A HIGH-THROUGHPUT INTRACELLULAR DELIVERY SYSTEM USING NANONEEDLES

3.1 Introduction

Among the many different intracellular delivery methods, microinjection is known as a universal delivery mechanism that works in almost all cell types. Since the glass pipette is used to directly enter into the cells, the system is advantageous to overcome both the physical barrier of the plasma membrane and possibly the nuclear membrane and the chemical barrier of diffusion limitations or plasmid degradation [133]. These advantages make the microinjection system very effective in drug delivery across the cell membrane and desirable to use in other applications. However, the microinjection system requires a number of expensive pieces of equipment to visualize the cells and needles, to hold the cells in place (for the suspension cells), and to control the injection process [134]. In addition, since the injection is done at a single cell level, the number of cell injected is very limited and the throughput is extremely low compared to most other intracellular delivery methods. We hypothesized that an array of nanoneedles can be used for intracellular delivery by adapting the mechanism of microinjection to make transient holes in the cell membrane but with increased throughput of delivery.

Microneedles have been studied for years to achieve drug delivery to the eye and skin [135, 136]. Using microneedles, preliminary results on intracellular delivery were demonstrated in human prostate cancer cells. Very small microneedles (i.e., nanoneedles) used in the experiment were 25 μm-tall solid silicon needles assembled in an array of 160,000 needles and imaged by scanning electron microscopy (Figure 3.1, left). On a confluent monolayer of cells, the nanoneedles were inserted briefly and intracellular uptake was observed by the uptake of calcein, a cell-impermeant fluorescent marker. The green fluorescence image showed the bright fluorescence on the left side, which indicated

the uptake of calcein by cells treated with microneedles (Figure 3.1, right). On the right side, there was little fluorescence as the cells were untreated.

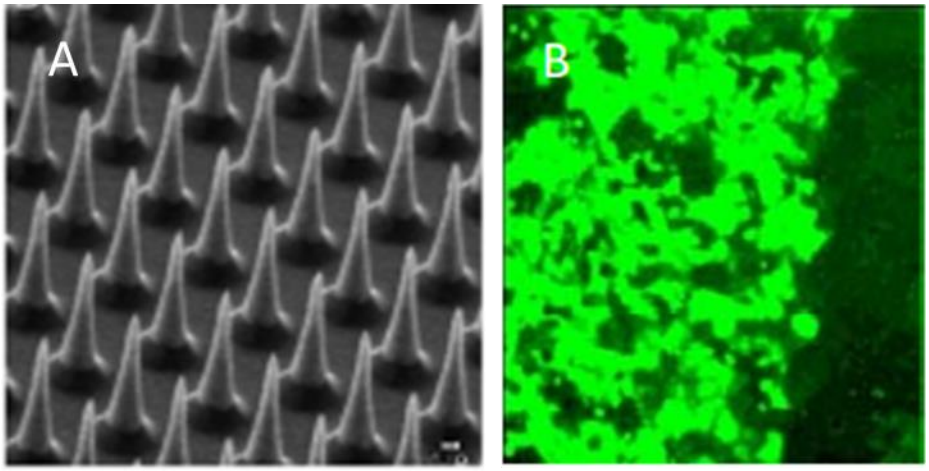

Figure 3.1. SEM image of 25 µm tall solid silicon nanoneedles in an array of 160,000 (A). The fluorescence image of prostate cancer cells after treatment with the nanoneedles (B). The bright fluorescence on the left indicates the uptake of calcein after treatment with nanoneedles while the untreated right side shows little or no fluorescence. Reproducd from reference [7]. (No scale bars available)

Based on this preliminary result, we investigated the intracellular delivery method using a new design of nanoneedles. By reducing the dimensions of the nanoneedles further, the nanoneedles can more efficiently target the drug delivery across the cell membrane. First, we assessed the feasibility of impalement by nanoneedles across the cell membrane and developed the methods of intracellular delivery using the nanoneedles. Next, we examined each method by varying experimental parameters to determine the range of parameters required for the intracellular uptake and to optimize the delivery efficiency of fluorescent molecules and cell viability

3.2 Methods

3.2.1 Cell culture

Human prostate cancer cells (DU145, American Type Culture Collection, Manassas, VA) were cultured as a monolayer in a humidified atmosphere of 95% air and 5% CO_2 at 37°C [137]. RPMI-16490 medium (Cellgro, Herndon, VA) was supplemented with 10% (v/v) heat-inactivated fetal bovine serum (FBS, Corning, Palo Alto, CA) and 1% penicillin/streptomycin (Cellgro). DU145 cells were used as a model cell line because they are well characterized and have been used extensively in previous intracellular delivery studies [50, 138, 139].

3.2.2 Nanoneedle fabrication

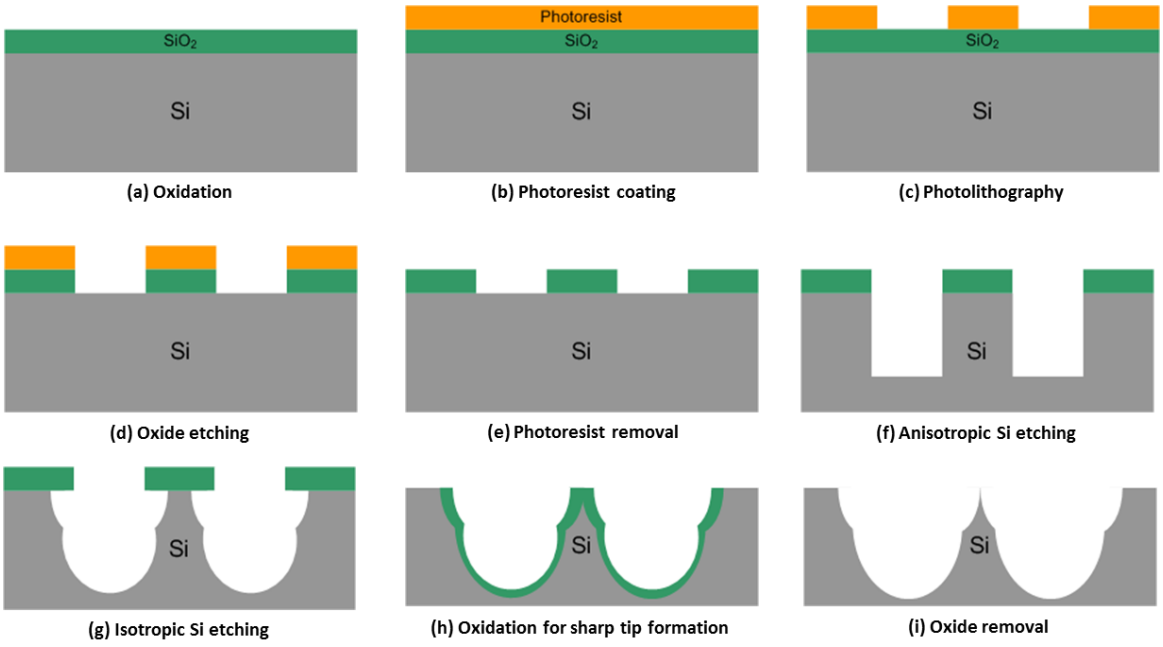

Figure 3.2. Nanoneedle fabrication method. Gray, green, and yellow coloring represents the silicon wafer, silicon dioxide layer, and photoresist layer, respectively. The surface of a silicon wafer was first patterned by creating a silicon dioxide layer by oxidation (a), applying photoresist (b) and patterning it by photolithography (c), transferring the pattern to the silicon dioxide layer by oxide etching (d) and leaving behind a hard mask of silicone dioxide after removing the photoresist (e). The nanoneedles were then created by anisotropic (f) and then isotropic (g) etching. The tips were sharpened by oxidation (h) and then the oxide layer was removed (i).

Nanoneedles were fabricated using silicon as a structural material since it has good mechanical strength and processing capability in the range of microns down to the nanoscale [140, 141]. As shown in the schematic in Figure 3.2, a silicon wafer (Siltronic, Portland, OR) was covered with a 0.7 µm film of thermal oxide, SiO_2, with a TYTAN Mini Furnace (Tystar, Torrance, CA) and was patterned using a positive photoresist mask (Microposit S1813, Shipley, Marlborough, MA). The etch mask pattern was designed with square patterns of 7 µm with an edge-to-edge gap between squares of 3 µm. The center-to-center spacing of the spots was 10 µm, which is somewhat smaller than the average diameter of DU145 cells in a confluent monolayer (i.e., 15 – 20 µm). Oxide etching was performed using an inductively coupled plasma etcher (ICP, Plasma-Therm, St. Petersburg, FL) to yield an array of SiO_2 spots.

After oxide etching, anisotropic dry etching of silicon was performed using SF_6-based gas mixture in the ICP to form 12 µm-tall square pillars under each masked spot. Isotropic dry etching of the silicon with an SF_6 plasma in the ICP followed, which produced tapered tips at the top of each pillar by utilizing under-etching of silicon under the etch mask. After removing residual masks by hydrofluoric acid and cleaning with DI water, tips were further sharpened to nano-scale sharpness using an oxidation sharpening process [142]. The resulting array of nanoneedles was die cut into individual 5 mm x 5 mm chips using a dicing saw (Advanced Dicing Technologies, Horsham, PA) and cleaned with acetone, isopropyl alcohol, and piranha solution, which is a mixture of sulfuric acid and hydrogen peroxide. These fabrication methods have been presented in greater detail previously [143].

3.2.3 Puncture loading

3.2.3.1 Sample preparation

DU145 cells were harvested by trypsin/EDTA (Cellgro) and plated on a 35 mm cell culture dish (Corning, Tewksbury, MA) or µ-Slide 8-well chambered coverslip (ibidi, Martinsried, Germany) 1 - 2 days prior to the experiment. The confluent monolayer of cells was washed once with PBS before adding a solution of fluorescent molecules: calcein or 70 kDa FITC-dextran prepared in RPMI at a concentration of 100

μM, or 500 kDa FITC-dextran (Sigma-Aldrich) prepared at a concentration of 12.5 μM to avoid excessive dye sticking to the cell membrane at higher concentration.

Doubled-sided tape (3M, Saint Paul, MN) was attached to an SEM sample holder (Ted Pella, Redding, CA) or a captive female threaded round standoff (McMaster-Carr). A 1/16”-thick, deformable adhesive foam tape (Medco Coated Products, Bedford Heights, OH) was attached to allow self-correcting of possible non-parallel contact between the nanoneedles array and the cell monolayer. A nanoneedle array was mounted onto the adhesive foam tape.

3.2.3.2 Delivery method

Puncture loading was conducted using an ESM301 motorized test stand (Mark-10, Copiague, NY), which was used to control the speed of nanoneedle array application to cells, the puncture time contacting the cells, and the speed of nanoneedle array removal from the cells. Unless otherwise noted, the application and removal speeds were 150 mm/min and 10 mm/min, respectively, and the puncture time was varied from 1 to 120 s. The sample holder to which the nanoneedle array was attached was screwed onto a digital force gauge (Series 5 M5-05, Mark-10) in order to control the force of nanoneedle puncture, which was varied from 0.1 to 0.5 N. A cell culture dish containing a cell monolayers was placed underneath the nanoneedle array for puncture after the cell culture medium was replaced with a solution containing fluorescent dye.

After puncture, the cells were left for 15 min to recover. The cells were then washed with PBS four times to remove the extracellular fluorescent molecules, after which RPMI with 2.5 μg/ml PI was added to stain non-viable cells 10 min before imaging.

3.2.3.3 Analysis and quantification

Cells were imaged using an inverted fluorescence microscope (Olympus IX70, Olympus, Center Valley, PA). Using cellSense Standard software (Olympus), images were taken at 4x magnification and captured using three filters: brightfield, green fluorescence, and red fluorescence images for the analysis of cell detachment, uptake of

fluorescent molecules, and cell viability, respectively. Sufficient numbers of images were taken to create a composite image of the entire area treated by the nanoneedle array.

The images captured were patched together to form one composite image for each of the three filters to show the entire area treated by nanoneedles. The images were then analyzed by Adobe Photoshop CS3 (Adobe Systems, Mountain View, CA) to quantify uptake and cell viability based on the cells with green and red fluorescence, respectively. The fluorescence threshold for identifying a cell as containing a dye was set based on the background fluorescence of untreated areas in the images, which served as the sham control. The percentage of cells with calcein or FITC-dextran uptake was determined by dividing the area with green fluorescence above threshold by the total area contacted by the nanoneedle array. The percentage of non-viable cells was similarly determined by dividing the area with red fluorescence above threshold by the total area contacted by the nanoneedle array and multiplying by the ratio of the nucleus area to the cell area, because PI only stains the nucleus of the cell.

Confocal microscopy imaging was also conducted to visualize the interaction between nanoneedles and cells at higher magnification and to further study the process of intracellular uptake. The cells were plated on a glass cover slip after trypsinization and cultured for 1 - 2 days before imaging. Prior to nanoneedle puncture, the cell nucleus was stained with Hoechst 33342 (trihydrochloride, Invitrogen) at a final concentration of 2 μg/ml for 20 min and the cell membrane was subsequently stained with 1x working solution of CellMask orange or green (Invitrogen) for 10 min at 37°C. Either propidium iodide or calcein AM (Invitrogen) was used as an uptake marker, as these dyes are fluorescent only intracellularly. Cells were either imaged live or fixed by 4% formaldehyde (Sigma-Aldrich). The cell-coated overslip was placed on a microscope slide or a sheet of PDMS, punctured with nanoneedles and sealed with nail polish.

The prepared samples were images using an LSM 700 confocal laser scanning microscope (Carl Zeiss Microscopy,Thornwood, NY) at 60x magnification to visualize the physical puncture by nanoneedles and associated molecular uptake. Images were captured and analyzed using the software ZEN lite black edition (Carl Zeiss Microscopy).

3.2.4 Centrifuge loading

3.2.4.1 Sample preparation

Tubes for centrifuge loading were made out of 1.5 ml microcentrifuge tubes (Eppendorf, Hauppauge, NY), modified to hold nanoneedle arrays at the bottom of the tube parallel to the bottom surface. A poly(methylmethacrylate) (PMMA; McMaster-Carr, Atlanta, GA) sheet with a thickness of approximately 5 mm was cut by CO_2 laser (Universal Laser systems, Scottsdale, AZ) into a T shape. Poly(dimethylsiloxane) (PDMS, Sylgard 184, Dow Corning, Midland, MI) was prepared by mixing the elastomer and curing agent at a ratio of 10 to 1. After degasing, the PDMS was poured into the microcentrifuge tube and the T-shaped piece of PMMA was placed inside the tube while the PDMS was curing at 37°C. After 12 h, the PMMA was removed from the tube, forming a square well at the bottom of which the nanoneedle array was placed.

DU145 cells were harvested by trypsin/EDTA (Cellgro) and re-suspended in RPMI. Cell concentration was measured by a Multisizer 3 Coulter Counter (Beckham Coulter, Fullerton, CA) and prepared for the experiment at 10^6 cells/ml. Cells were mixed with calcein (Molecular Probes, Eugene, OR), 20 kDa FITC-labeled dextran (Sigma-Aldrich, St. Louis, MO), and FITC-labeled BSA (Sigma-Aldrich) to a final concentration of 10 μM to serve as markers of intracellular uptake.

3.2.4.2 Delivery method

In each custom-made microcentrifuge tube, a nanoneedle array was placed on the bottom surface of the well with the nanoneedles facing up and 300 μl of a solution containing cells and a fluorescent dye was added to the microcentrifuge tube. The tubes were spun at varying centrifugal force and time using one of two swing-bucket centrifuges, Centrifuge 5702RH (Eppendorf) and Sorvall Legend RT+ centrifuge (Thermo Scientific, Waltham, MA).

Fifteen minutes after the spin, cells were transferred to unmodified 1.5 ml microcentrifuge tubes by pipetting with RPMI to detach cells off the nanoneedles. To remove extracellular fluorescent molecules in the medium and on the surface of the cell membrane, cells were washed three times with PBS (Cellgro) at 300 x g for 5 min. After

the third wash, the cells were resuspended in PBS and transferred to flow cytometry tubes for analysis. Propidium iodide (PI, Invitrogen, Grand Island, NY) was added at a final concentration of 5 µg/ml 10 min before flow cytometry analysis to stain non-viable cells and thereby measure cell viability.

3.2.4.3 Analysis and quantification

The uptake of fluorescent dyes and cell viability were measured using a bench-top flow cytometer (BD LSRII, BD Biosciences, San Jose, CA) based on methods described previously [50, 139]. The data were collected and analyzed in FACSDiva software (BD Biosciences). Approximately 10,000 events were collected per sample. For cell viability, PI was analyzed using a PerCP-Cy5, 670 nm longpass filter for emission. The uptake of calcein, FITC-BSA or FITC-dextran was measured by a FITC, 530/30 nm bandpass filter for emission.

The cell gate was constructed based on forward- and side-scatter light of the untreated control cells. Any events within this gate were considered to be intact cells while any events outside the gate were considered to be cell debris or other noise. To determine which cells had taken up fluorescent marker compounds (i.e., calcein, BSA and dextran for uptake; PI for viability), histogram gates were set by the sham control which had fluorescent dyes in the solution but was not treated with nanoneedles to account for extracellular staining and other noise. To set gates and account for possible spectral overlap between the dyes, compensation controls were prepared and tested. The positive control was prepared by staining cells with calcein AM (Invitrogen), which stained all viable cells. The negative control was prepared by incubating cells in 70% methanol for 30 min and staining with PI.

3.2.5 Statistical analysis

A minimum of three replicates was performed for all conditions. Means and standard deviations were calculated from the replicates. An unpaired Student's t-test or analysis of variance (ANOVA) was performed using Minitab 17 (Minitab, State College, PA). A value of $p < 0.05$ was interpreted as significant.

3.3 Results

3.3.1 Nanoneedle fabrication

Nanoneedles were designed and microfabricated out of silicon to puncture monolayers of mammalian cells for intracellular delivery (Figure 3.3). The nanoneedles were spaced 10 µm apart (i.e., tip to tip), which is similar to the diameter of many mammalian cells in general (e.g., 4 to 25 µm [144]) and of the DU145 cells used in this study specifically (i.e., 15 – 20 µm), so as to direct at least one nanoneedle per cell in a confluent monolayer (Figure 3.3.a). The height of each nanoneedle was 12 µm, which is again similar to the cell diameter so that the nanoneedles can puncture deeply into the cell and overcome possible cell membrane deformation during puncture. More specifically, the nanoneedles were designed to have a base pedestal of 6 µm height and approximately 3 µm width topped with a 6 µm tall pyramidal portion tapering to a 23 nm sharp tip (Figure 3.3.b). A tip diameter below 100 nm was desirable in order to achieve the high cell viability shown in previous studies of single-needle intracellular delivery [87, 88, 145]. The nanoneedles were etched on silicon wafers, which were diced to 5 mm x 5 mm chips, which contained approximately 250,000 nanoneedles per chip.

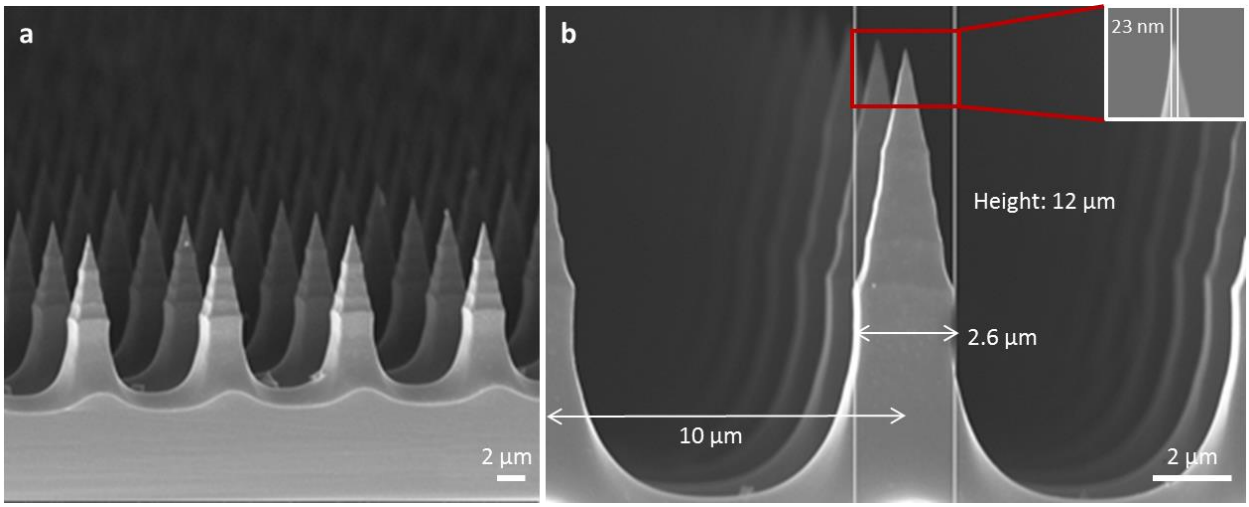

Figure 3.3. Scanning electron microscopy images of nanoneedles. (a) Section of an array of nanoneedles. (b) Further magnified view of a nanoneedle showing its dimensions.

We also made two variations on the nanoneedle design: nanoneedle tips and nanoblades (Figure 3.4). The nanoneedles tips were fabricated as the tapered pyramidal tips of the nanoneedles without the base pedestals (Figure 3.4. a). The nanoneedle tips had a height of approximately 3 µm and tip diameter of 20 – 30 nm. The nanoblades were fabricated with the same geometry as the nanoneedles, except with a wider tip in one dimension (Figure 3.4.b). The height of the nanoblades was the same as the nanoneedles, but the tip width and thickness were 1 µm and 25 nm, respectively. Although the nanoblade tips were bigger than the sharp-tipped nanoneedles, they were still smaller than the glass pipettes commonly used for microinjection, which often have an outer diameter of approximately 0.5 - 1 µm [134]. Chips containing the nanoneedle tips or the nanoblades still had a tip-to-tip pitch of 10 µm and contained the same number of needles.

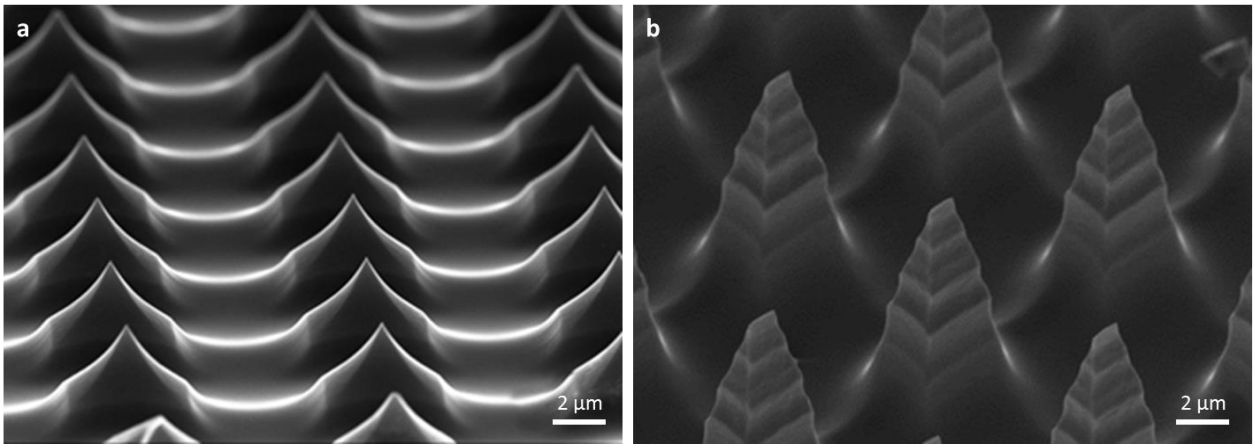

Figure 3.4. Scanning electron microscopy images of (a) nanoneedle tips and (b) nanoblades.

3.3.2 Puncture loading of adherent cells

Nanoneedles were used to puncture monolayers of adherent cells and thereby enable intracellular delivery of molecules. DU-145 human prostate cancer cells were cultured on a petri dish as a confluent monolayer and nanoneedles were brought down onto the cells to puncture them. Nanoneedle movement was controlled along the z-axis (i.e., vertical movement) by a force gauge mounted on a motorized test stand. The position on x or y-axis was fixed.

As a first assessment of intracellular delivery using nanoneedles, nanoneedle arrays were applied to cells incubated in a solution of calcein (used as a marker of intracellular uptake) using a puncture force of 0.1 N and left in contact with the cells for 2 min. The nanoneedles were brought down upon the cells at an application speed of 150 mm/min and back up from the cells at a retraction speed of 10 mm/min. The retraction speed was slow in order to reduce the chances of cells being pulled off the petri dish during retraction. These speeds are in the range of speeds used for insertion of micropipettes during conventional microinjection [146, 147].

After nanoneedle puncture, we imaged the cell monolayers using fluorescence microscopy to assess cell detachment from the petri dish, intracellular uptake of calcein and cell viability measured by staining with propidium iodide (Figure 3.5). The brightfield images were used primarily to assess possible detachment of cells from the petri dish after nanoneedle treatment (Figure 3.5.a). At the conditions used, there was only minor detachment observed (i.e., < 10% of cells). In contrast, more significant detachment was observed when greater contact was made with the cells using blunt nanoneedle base pedastals (without the tapered pyramidal tips) and using bare silicon without nanoneedle structures (data not shown). Altogether, these findings suggest that adhesion between cells and nanoneedles can lead to cell detachment, but that sharp-tipped nanoneedles and slow retraction minimize this effect.

The green fluorescence images indicate the extent of intracellular uptake of calcein, which occurred extensively in the area treated by the nanoneedle array, which is clearly evident as a square of green fluorescence (Figure 3.5.b). The surrounding non-fluorescent cells serve as an internal negative control of cells that were exposed to calcein and subjected to the same procedures as the other cells, except they were not contacted with nanoneedles.

Cells that were non-viable after the nanoneedle treatment were marked by the red fluorescence of propidium iodide (Figure 3.5.c). This analysis shows that some of the cells were rendered non-viable by the process, but that most of the cells remained viable. To supplement this propidium iodide assay, cells were cultured for 24 h after nanoneedle puncture and viability was assessed relative to untreated controls (Figure 3.6). In the untreated controls, the percentage of intact cells and viable cells were statistically same at

both time points (Student's t-test, $p = 0.258$ and 0.163 for 0 and 24 h, respectively). When the cells were treated with the nanoneedles, the detachment of cells from the surface was observed initially but was not significant compared to the untreated control (Student's t-test, $p = 0.062$). Due to the membrane puncture by nanoneedles, the viability decreased slightly (Student's t-test, $p = 0.018$) but most of the cells remained viable at an applied force of 0.1 N. After 24 h incubation, the percentage of intact cells were comparable to the percentage of viable cells at 0 h (Student's t-test, $p = 0.995$) and the majority of the cells were also viable (Student's t-test, $p = 0.568$). The ratio of intact cells in treated sample to untreated control was 0.782 and 0.604 at $t = 0$ and 24 h, respectively, and the difference was not significant (Student's t-test, $p = 0.3012$). The ratio of viable cells in treated sample to untreated control was 0.679 and 0.564 at $t = 0$ and 24 h, respectively, and the difference was also not significant (Student's t-test, $p = 0.6296$). Thus, there was a good correlation between viability measured by the propidium iodide assay shortly after nanoneedle puncture and viability determined after 24 h.

This qualitative analysis demonstrates that application of nanoneedles to cells can deliver molecules into the cells while maintaining cell viability. Quantitative measures of uptake and viability are presented further below.

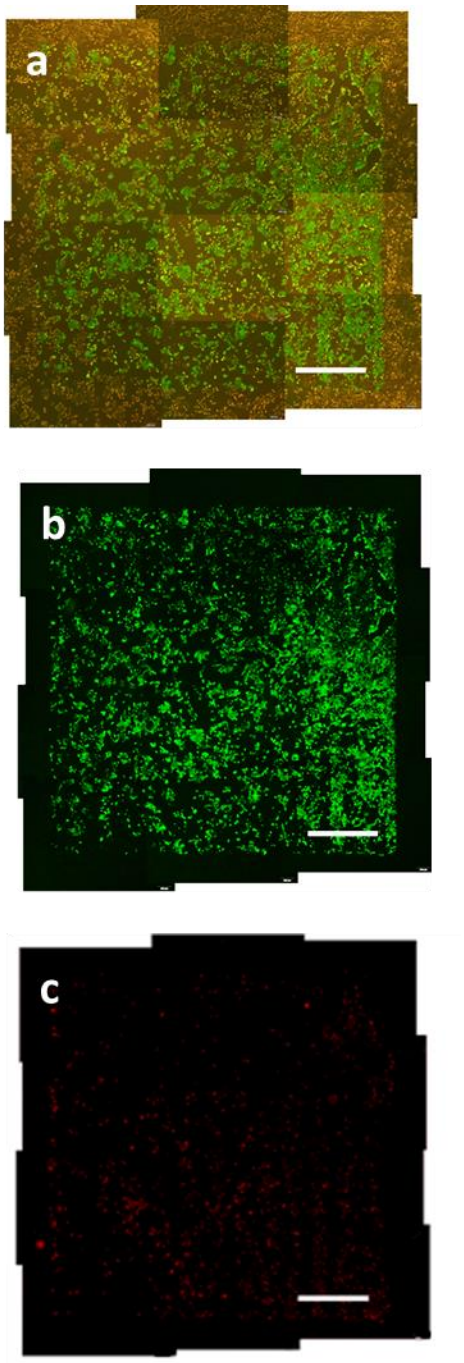

Figure 3.5. Representative fluorescence microscopy imaging of cell monolayers after puncture with nanoneedles. Brightfield (a), green fluorescence (b), and red fluorescence (c) images of DU145 cells are shown after puncture loading using nanoneedles applied with a force of 0.1 N for 2 min. Green fluorescence indicates the intracellular uptake of calcein. Red fluorescence indicates propidium iodide staining, which is a marker for non-viable cells. Scale bars are 1 mm.

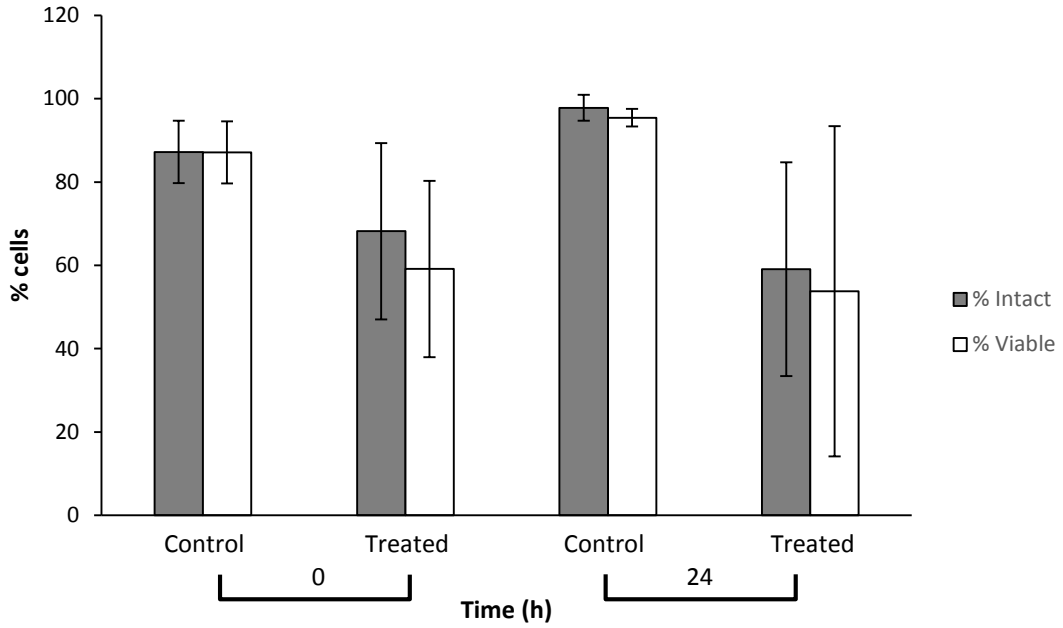

Figure 3.6. The percentage of intact (gray) and viable (white) cells at 0 and 24 h with and without the puncture loading. Control cells were untreated. Treated cells were punctured with nanoneedles at the applied force of 0.1 N for 2 min. Data show average ± SD, n ≥ 4.

3.3.2.1 Imaging of cells during puncture loading

This research is based on the hypothesis that nanoneedles puncture cells and thereby permit entry of molecules into the cells. To further test this hypothesis, we imaged cells by confocal microscopy during puncture by nanoneedles (Figure 3.7). The cells were stained with Hoechst dye to stain the nucleus blue and CellMask Orange to stain the cell membrane red. In untreated cells, the blue nuclei can be seen surrounded by red cell membranes (Figure 3.7.a). Cells punctured by nanoneedles (i.e., with the nanoneedles still in place) similarly show blue nuclei and red cell membranes, but also display a regular array of black dots (Figure 3.7. b and c). Because the spacing of these black dots is approximately 10 μm and the size of each black dot is approximately 0.5 μm, we interpret these black dots as representing the presence of nanoneedles (which do not fluoresce green or red). There were typically a few nanoneedles associated with each cell, since the cell diameter was 15 – 20 μm when spread on the culture dish. Images of x-z and y-z planes (Figure 3.7.d and e) show cell deformation associated with the nanoneedles during their apparent puncture into the cells by shape of the needle tips on z-stack images along the cell membrane and brighter red fluorescence at the sites of the puncture.

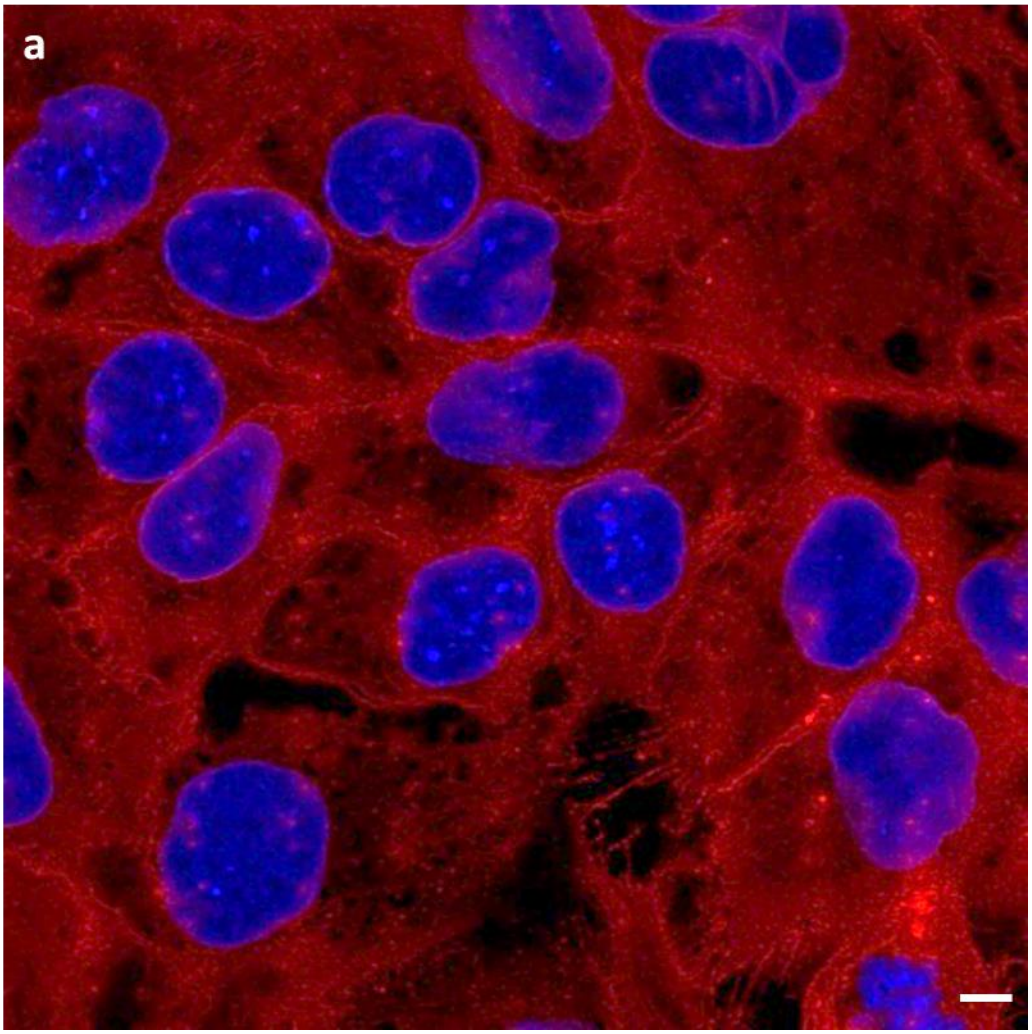
a

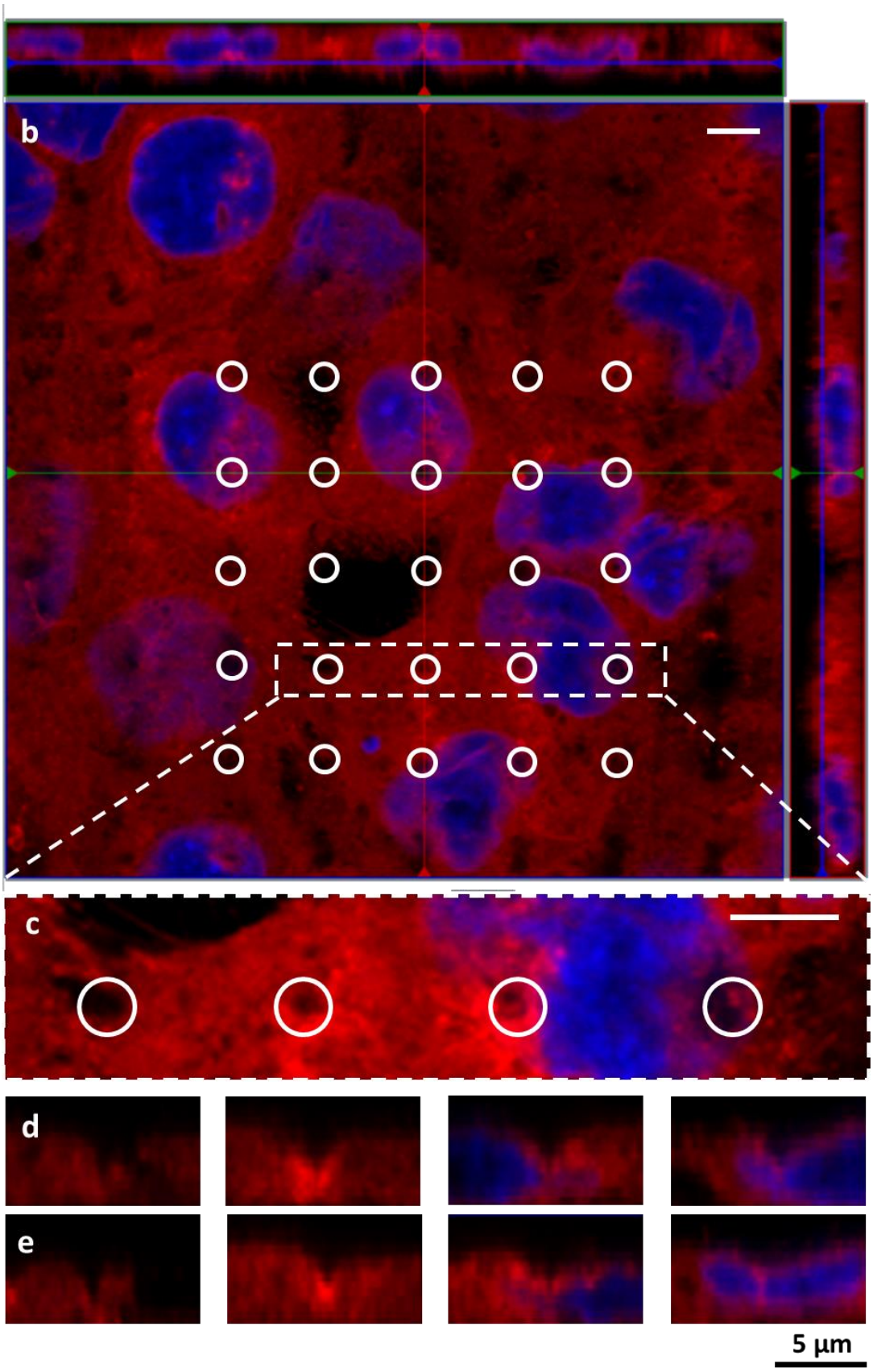
b
c
d
e
5 µm

Figure 3.7. Imaging of a monolayer of cells punctured by an array of nanoneedles by confocal microscopy (z-stack). (a) Untreated cells. (b) Cells punctured by nanoneedles, with nanoneedles still in place. Cells were stained with Hoechst (blue) and CellMask orange (red) to label the nucleus and cell membrane, respectively. Red, green, and blue lines in (b) indicate the positions on x, y, and z-axes, respectively. The white dotted line box in (b) is magnified in (c) at higher resolution. The white circles in (b) and (c) show the array of nanoneedle punctures. (d) and (e) show the x-z and y-z plane images, respectively, for the corresponding puncture site shown by white circles in (c). Scale bars (white in (a), (b), and (c) and black in (d) and (e)) are 5 μm.

We performed additional imaging with using cells loaded with an intracellular marker, calcein AM, to observe molecular transport associated with the puncture loading method. The cells were loaded with calcein AM prior to the puncture and stained with Hoechst and CellMask Orange, as above. Successful nanoneedle puncture of the cells would therefore be indicated by loss of green intracellular fluorescence due to transport of calcein out of the cell. In this study, the cells were imaged a few minutes after puncture loading was initiated with the nanoneedles still in place (Figure 3.8).

In untreated control cells, the imaging shows cells with blue nuclei and red cell membranes filled with green calcein surrounded by a dark extracellular space (Figure 3.8.a). In cells punctured with nanoneedles, the blue nuclei and red cell membranes are again evident (Figure 3.8.b). However, the calcein molecule leaked out of the cell as the cell membrane was permeabilized by the nanoneedles. The intracellular and extracellular calcein concentration equilibrated and resulted in similar level of green fluorescence inside and outside of the cell. The presence of nanoneedles is also seen as a regular array of black dots with a spacing of 10 μm. The nanoneedles are clearly seen due to good contrast with the green color.

We conducted additional experiments with calcein in the extracellular environment instead of preloading cells with calcein AM. These uptake experiments showed similar results, with dark cells in the absence of nanoneedle puncture and green cells with nanoneedle puncture (data not shown), consistent with the fluorescence microscopy images above. To better understand the kinetics of transport, cells were punctured with nanoneedles in the presence of calcein and then the calcein solution was

replaced with fresh cell media 1 min after nanoneedle puncture, but before the nanoneedles were removed. In this case, there was similarly good uptake (data not shown), indicating that most transport happens with a min after nanoneedle puncture.

To further investigate transport kinetics, we punctured the cells with nanoneedles in the absence of calcein for 2 min, and then added calcein within 1 s or 1 min after the nanoneedles were removed and found that intracellular uptake was minimal (data not shown). These findings suggest that intracellular uptake occurs at the time of nanoneedle puncture and/or shortly thereafter and does not significantly occur after nanoneedle removal. Previous studies employing other methods of intracellular delivery associated with physical breaches of the cell membrane have reported cell membrane resealing times on the order of 1 to 100 s after electroporation [148], 10 – 30 s after puncture with a microinjection [149] and 1 min or more after exposure to acoustic cavitation [55]. The relatively rapid cell membrane resealing time observed here, apparently within seconds after nanoneedle removal, could be explained by the extremely sharp nanoneedle tips (i.e., 20 – 30 nm diameter) that minimize cell membrane disruption.

a

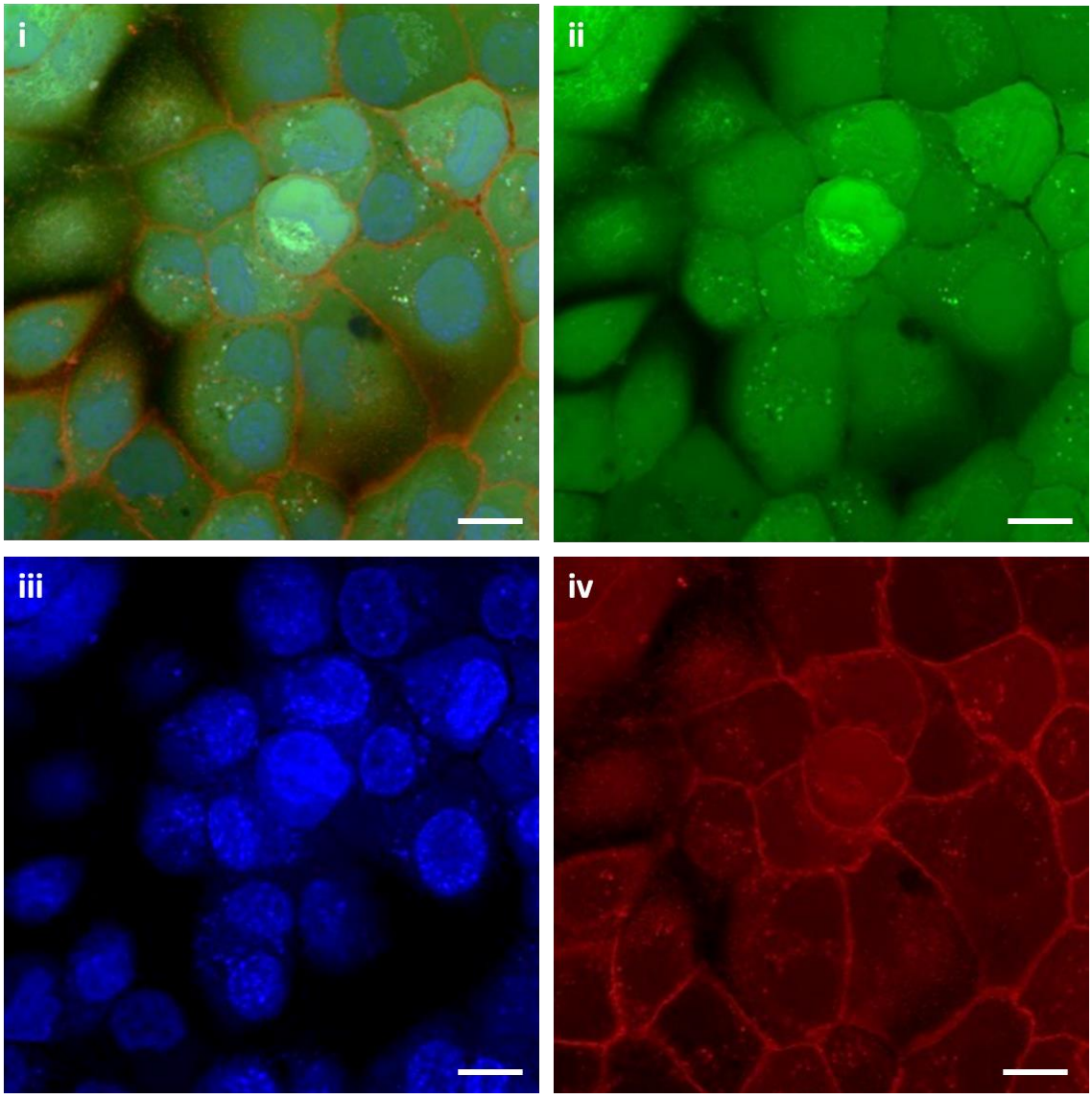

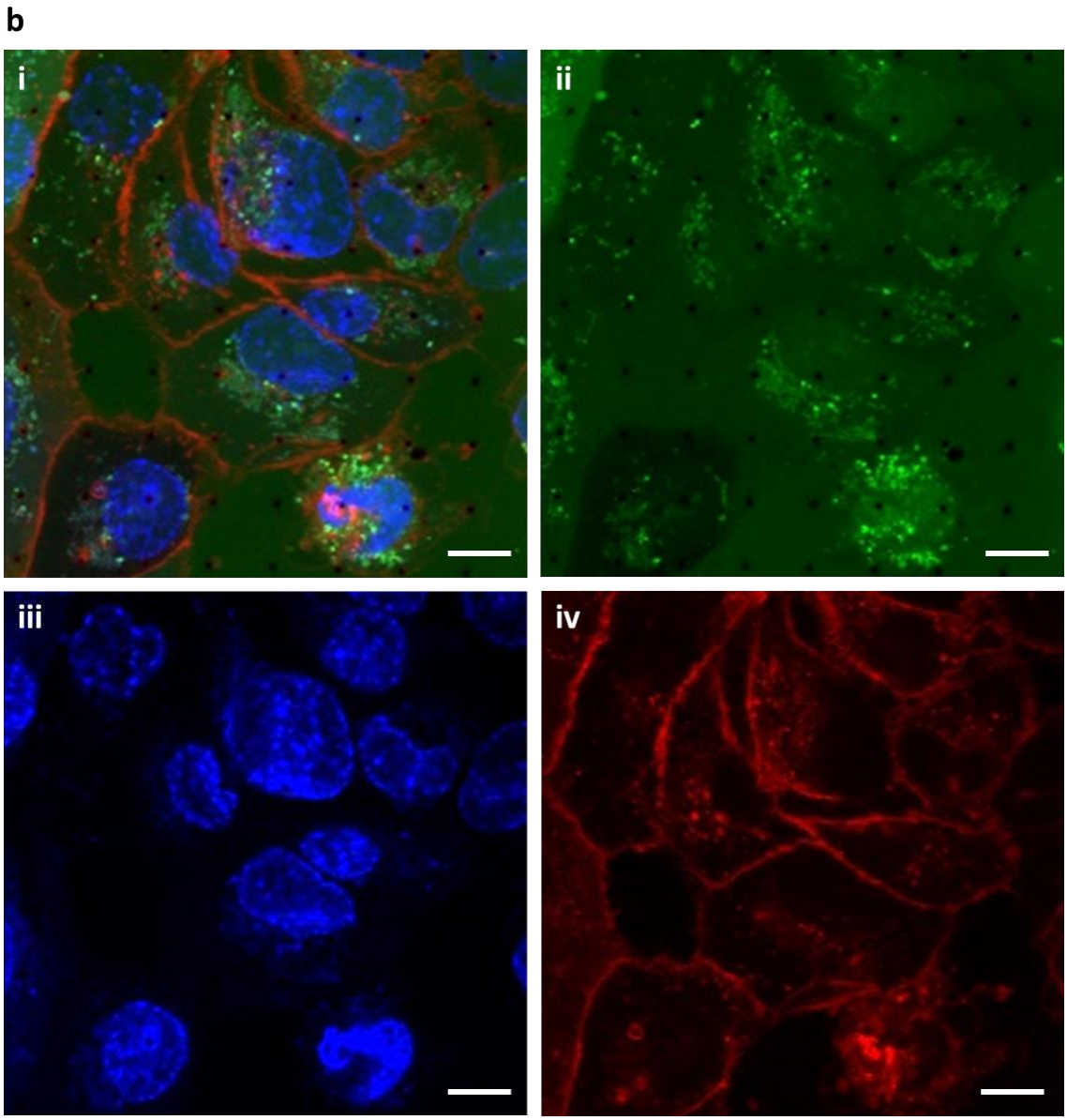

Figure 3.8. Imaging of a monolayer of DU145 cells pre-loaded with calcein AM and punctured by an array of nanoneedles by confocal microscopy. (a) Untreated cells. (b) Cells punctured by nanoneedles, with nanoneedles still in place. Each image is shown with (i) three channels merged, (ii) only the FITC channel for calcein AM, (c) only the Hoechst channel for the nucleus stain and (d) only the TRITC channel for the cell membrane stain (CellMask Orange). An array of black dots, with approximately 10 µm in spacing, is visible especially in FITC channel showing the tips of the nanoneedles. Green fluorescence in the extracellular space and lack of green fluorescence intracellularly in image (b) indicate that the calcein molecules have leaked from the cells due to nanoneedle puncture. Scale bars are 10 µm.

3.3.2.2 Effect of molecular weight of uptake marker on uptake and viability

Building off the initial evidence for intracellular delivery of calcein and nanoneedle puncture into cells, we next studied the effect of molecular weight on delivery efficiency by measuring uptake of three different fluorescent molecules (Figure 3.9). Fluorescence microscopy shows that all of the fluorescent molecules were delivered into cells in the treated area, marked by the dotted line (Figure 3.9.a). Quantitative analysis of these images shows that intracellular uptake decreased with increasing molecular weight (ANOVA, $p = 0.027$), ranging from ~50% delivery efficiency for calcein (i.e., 50% of cells contained calcein) to ~20% delivery efficiency for the dextrans (Figure 3.9.b). The delivery efficiency of calcein (623 Da) was significantly higher than either of the dextrans (Student's t-test, $p = 0.035$ and 0.025 for 70 kDa and 500 kDa dextran, respectively), but there was no significant difference in delivery efficiency between the two dextrans despite a difference in molecular weight of almost an order of magnitude (Student's t-test, $p = 0.97$). Since the puncture condition was same in each case, the viability was ~90% for all three molecules (ANOVA, $p = 0.56$).

We also conducted a preliminary study on intracellular delivery of other macromolecule using the same puncture conditions. Plasmid DNA encoding for green fluorescent protein (GFP) was also delivered to cells, but only low levels of transfection (i.e., < 5%) were observed 24 h post-treatment (Figure 3.10). We conclude that molecules over a range of different sizes can be delivered into cells using nanoneedles, but delivery of low molecular weight compounds appears to be more efficient that macromolecules.

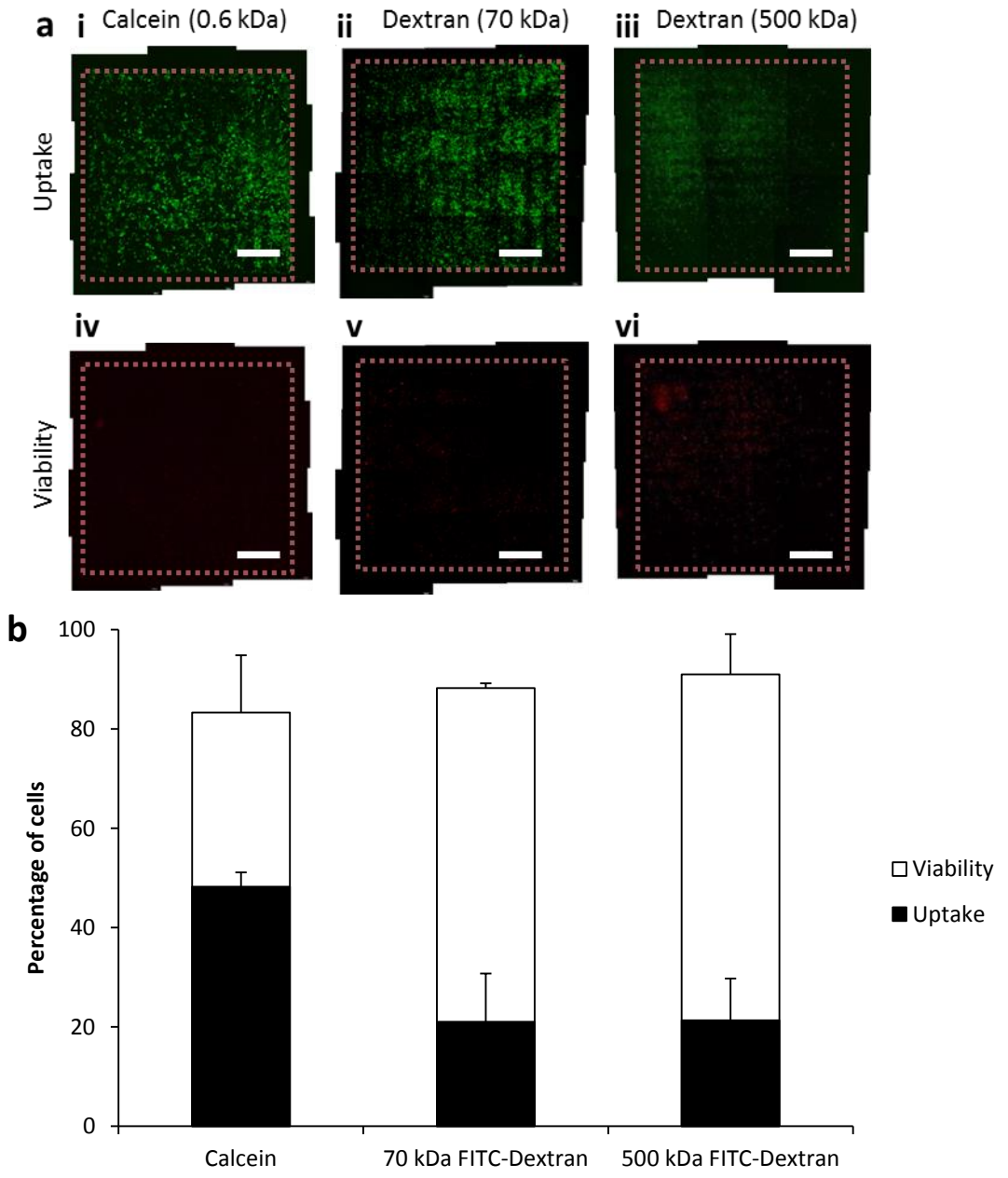

Figure 3.9. Effect of molecular weight on intracellular uptake and viability of DU145 cells after nanoneedle puncture. Puncture for was 0.1 N, puncture time was 2 min and the down and up speeds were 150 and 10 mm/min, respectively. (a) Representative green fluorescence images show cells with intracellular uptake of (i) calcein, (ii) 70 kDa FITC-dextran and (iii) 500 kDa FITC-dextran. Representative red fluorescence images show the corresponding non-viable cells (iv, v, vi). Dotted lines indicate the area treated with nanoneedles. Scale bars are 1 mm. (b) Quantitative data on delivery efficiency and viability were generated from image analysis of the micrographs in (a). Data show average ± SD, n ≥ 3.

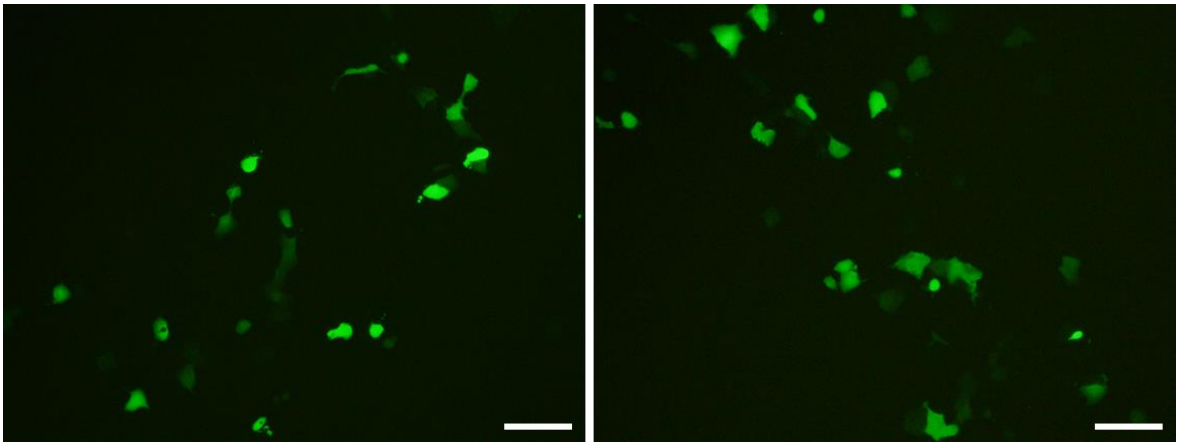

Figure 3.10. Green fluorescence images showing the transfection of plasmid DNA encoding for green fluorescent protein in DU145 cells 24 h-post puncture with a applied force of 0.1 N for 2 min. Scale bars (white) are 50 µm.

3.3.2.3 Effects of puncture force and time on intracellular uptake and viability

We next examined the effect of puncture force on cell viability and delivery efficiency of 70 kDa FITC-dextran while maintaining a fixed puncture time of 120 s (Figure 3.11). Fluorescence microscopy shows that all of the conditions tested were effective in delivering the fluorescent dextran molecule to many cells, while also killing some of the cells in the treated area marked by the dotted line (Figure 3.6.a). Quantitative analysis of the images shows that intracellular uptake of the dextran molecule increased (ANOVA, $p = 0.022$) and cell viability decreased (ANOVA, $p = 0.027$) with increasing puncture force. At 0.1 N puncture force, viability was ~90% but delivery efficiency was only about 20%. At 0.5 N, most of the viable cells (~50%) showed uptake of dextran. We conclude that greater puncture force can increase intracellular uptake, but there is a trade-off between the delivery efficiency and cell viability.

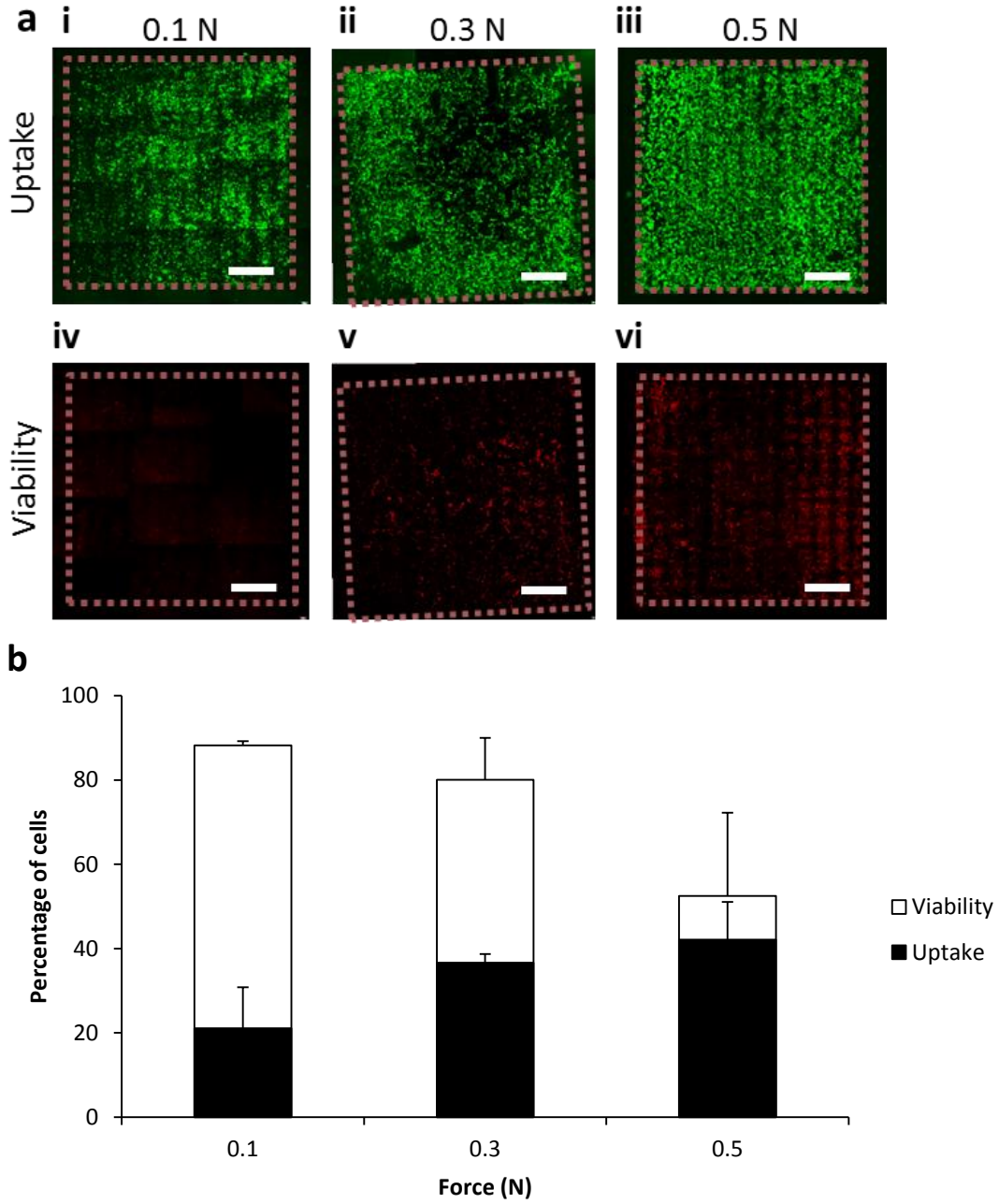

Figure 3.11. Effect of nanoneedle puncture force on intracellular uptake and viability of DU145 cells. Puncture time was 2 min and the down and up speeds were 150 and 10 mm/min, respectively. (a) Representative green fluorescence images show cells with intracellular uptake of 70 kDa FITC-dextran after puncture at 0.1 N (i), 0.3 N (ii) and 0.5 N (iii). Representative red fluorescence images show the corresponding non-viable cells (iv, v, vi). Dotted lines indicate the area treated with nanoneedles. Scale bars are 1 mm. (b) Quantitative data on delivery efficiency and viability were generated from image analysis of the micrographs in (a). Data show average ± SD, n = 3.

We next quantified intracellular uptake and viability at varied puncture times while maintaining a constant puncture force of 0.5 N (Figure 3.12). There was a small increase in delivery efficiency with longer puncture time, but it was not statistically significant (ANOVA, $p = 0.66$). The viability decreased significantly with longer puncture time (ANOVA, $p = 0.016$), from ~90% after 1 s puncture time to just ~50% after 120 s puncture time. These data suggest that longer puncture times compromise viability with little benefit to delivery efficiency. It appears that the initial force of puncture may be the more important factor in the uptake process.

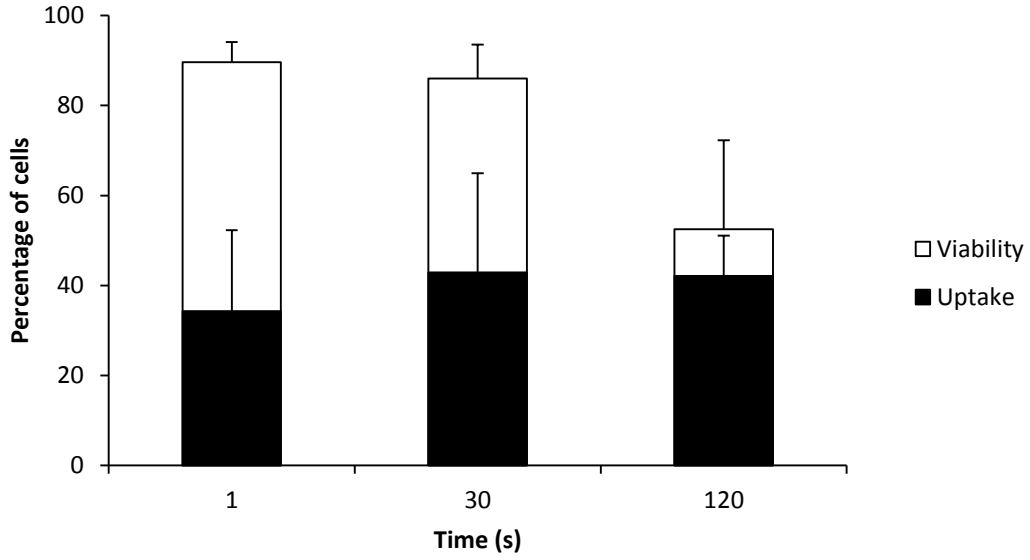

Figure 3.12. Effect of nanoneedle puncture time on intracellular uptake and viability of DU145 cells. Puncture for was 0.5 N and the down and up speeds were 150 and 10 mm/min, respectively. Data were generated from image analysis of fluorescence micrographs of cells after nanoneedle treatment. Data show average ± SD, n = 3.

3.3.2.4 Cell morphological changes associate with puncture loading

Lastly, we examined for any noticeable morphological changes that might be associated with the puncture loading method. Morphological changes are expected to be associated with the non-viable cells, i.e. apoptotic and necrotic cells. Apoptosis is a programmed cell death and is associated with the cell shrinkage and condensation as a result of protein denaturation [150, 151]. Subsequently, apoptotic bodies packed with cellular constituents form and degrade. Necrosis signaled by irreversible changes in the nucleus and in the cytoplasm and characterized by the cells swelling [152].

The fluorescence images were analyzed to compare the area of viable and non-viable cells after the treatment by nanoneedles array (Figure 3.13). The green and black cells were viable cells with and without intracellular uptake of calcein or FITC-dextran, respectively. And the red cells were non-viable cells that were stained with propidium iodide for necrotic and late apoptotic death. Non-viable cells were slightly smaller than the viable cells, both uptake and non-uptake, but were statistically the same (ANOVA, $p = 0.304$). In the short-term, from a few minutes to an hour post-treatment, we did not observe any significant difference in morphology of the cells after the treatment by the puncture loading method. Since the difference was minimal, it is difficult to determine what changes the non-viable cells are going through with the nanoneedles. Further study in more detail, i.e. to distinguish between apoptotic and necrotic cells, and over the long-term may be necessary to better understand the effect of nanoneedle-mediated intracellular delivery.

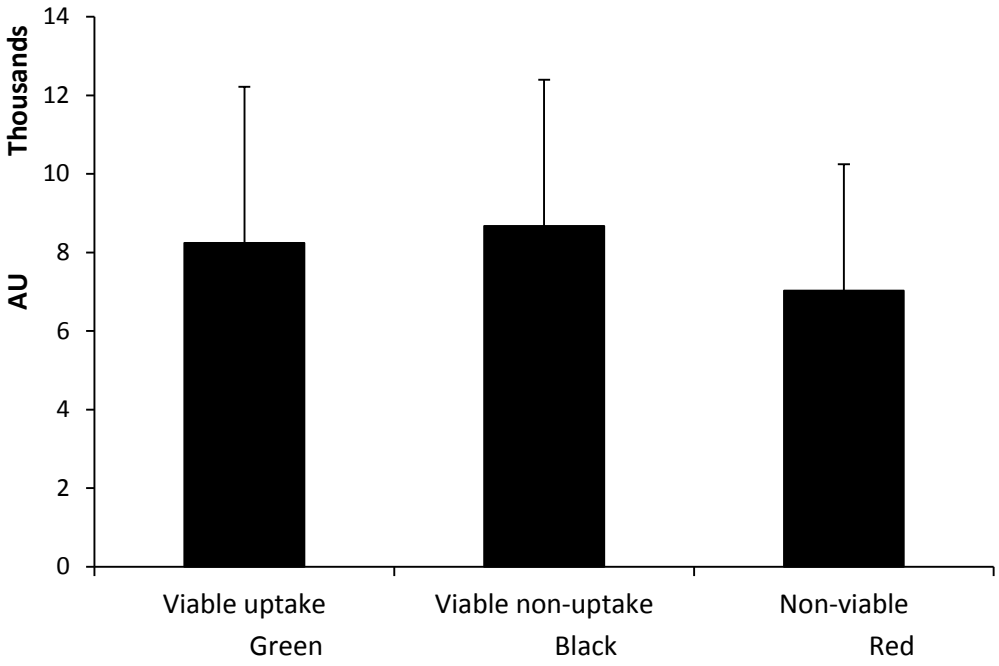

Figure 3.13. Comparison of cell size by area (arbitrary units) for any morphological changes associated with the puncture loading method by image analysis. From each image, several green (viable uptake), black (viable non-uptake), and red (non-viable) cells were measured. Data show average ± SD, n ≥ 30.

3.3.3 Puncture loading of suspension cells

The puncture loading method was further implemented with suspension cells, since we have observed the successful intracellular delivery with the adherent cells. In order to use the method on suspension cells, it was necessary to investigate the measures to attach the cells firmly onto the surface with good cell viability. There are a number of methods available to chemically and biologically attach cells onto the surface for various other purposes. Among those methods, we selected a few potential candidates to try: poly-L-lysine, Cell-Tak, fibronectin, and retronectin. Poly-L-lysine is a cationic polymer [153, 154] that will enable the cells to bind to the surface due to the negative charge of the cell membrane [155, 156]. Cell-Tak is the commercially available protein solution derived from mussels and is used as a cell and tissue adhesive on a variety of substrates [157, 158]. Fibronectin is a glycoprotein which binds to integrins, the receptor protein on the cell membrane [159]. Fibronectin has been applied commonly onto microfabricated surfaces for the attachment of cells [160, 161]. Similar to fibronectin, retronectin is a

recombinant fibronectin containing three functional domains to improve gene therapy viral transduction [162]. Successful DNA delivery via microinjection was demonstrated in CD34+ cells, adhered to the surface by retronectin, with high cell viability [163]. We tested these methods as they were widely used in many applications for attaching cells onto varying substrates.

For each adhesion method, the degree of adhesion and the cell viability (i.e. morphology and propidium iodide staining) were observed by fluorescence microscopy after the treatment. Cell morphology retained the spherical shape and viability did not show any noticeable difference from the untreated sample (data not shown), as demonstrated in the previous studies for the other applications. Adhesion to the surface was determined by observing cell movement under the brightfield view while slightly tapping on the side of the petri dish. Minor movement of the cell was observed but a majority of the cells were immobilized to the surface (data not shown).

We also attempted adding a centrifugation step in order to increase the possible area of adherence to the surface by cell spreading. Once the surface was treated with Cell-Tak, the cells were centrifuge onto the surface with various centrifugal forces. Cells were resuspended in media afterwards to determine the cell viability (Figure 3.14). At lower centrifugal forces, such as 500 and 1000 g-force, cell viability was similar to the control sample (Student's t-test, $p > 0.05$). At higher centrifugal force of 3000 g-force, cell viability decreased from the control (Student's t-test, $p = 0.007$), but was still about 90%. From these studies, we concluded that these commercially available methods were effective in attaching the cells onto the surface with good cell viability as demonstrated in the previous applications.

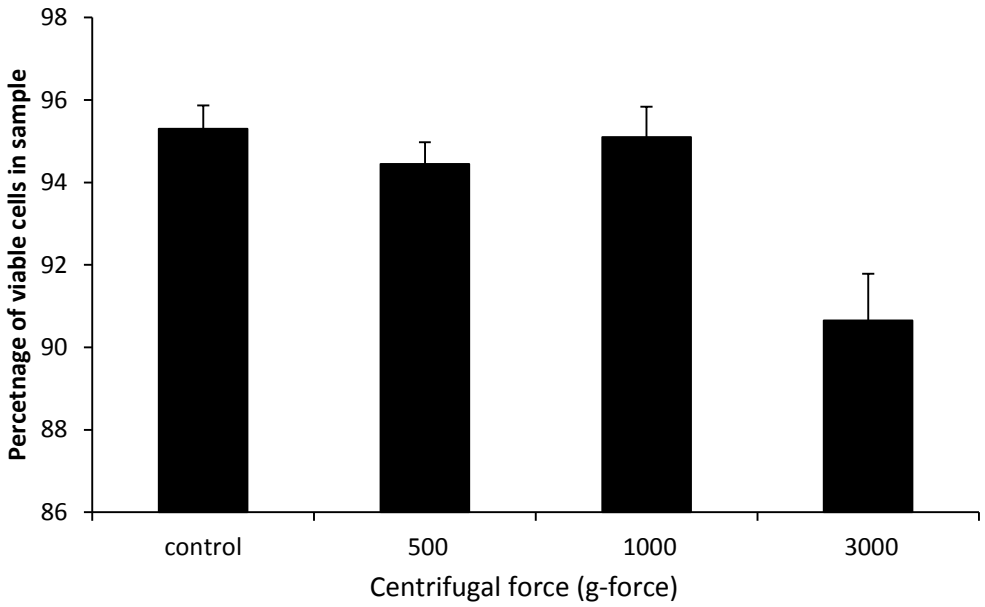

Figure 3.14. Percentage of viable cells after re-suspending K562 cells that were attached to the petri dish with Cell-Tak at varying centrifugal force (500, 1000, and 3000 g-force). Data show average ± SD, n = 4.

As we observed the attachment of the suspension cells onto the surface with the methods discussed, we moved on to apply puncture loading for intracellular delivery. Once the suspension cells were attached to the surface treated with retronectin, cells were treated with nanoneedles using the puncture condition of 0.20 N for 30 s for the intracellular delivery of 70 kDa FITC-dextran. Down and up speed of the force gauge were fixed at 150 and 10 mm/min, respectively. Cells were observed under the fluorescence microscope for detachment and intracellular uptake (Figure 3.15).

In the brightfield images, the untreated area outside the nanoneedles array still showed good attachment of the cells. However, the excessive detachment was observed, especially along the edges of the nanoneedles array, while the cells were piling up in the center of the treated area as seen in each close-up image. The cell detachment and migration to the center of the area was possibly due to the surface tension and/or convective motion of the liquid when the nanoneedles were lifted after the puncture. The delivery efficiency of dextran molecule was very low compared to the puncture loading on the adherent cells. The cells were not as firmly attached to the surface as adherent cells were and the movement of nanoneedles could induce the cells to shake and stick in-

between nanoneedles instead of puncture at the tip. We concluded that intracellular delivery into suspension cells would be difficult unless there is a better method of cell immobilization due to cell detachment and migration with the nanoneedles movement.

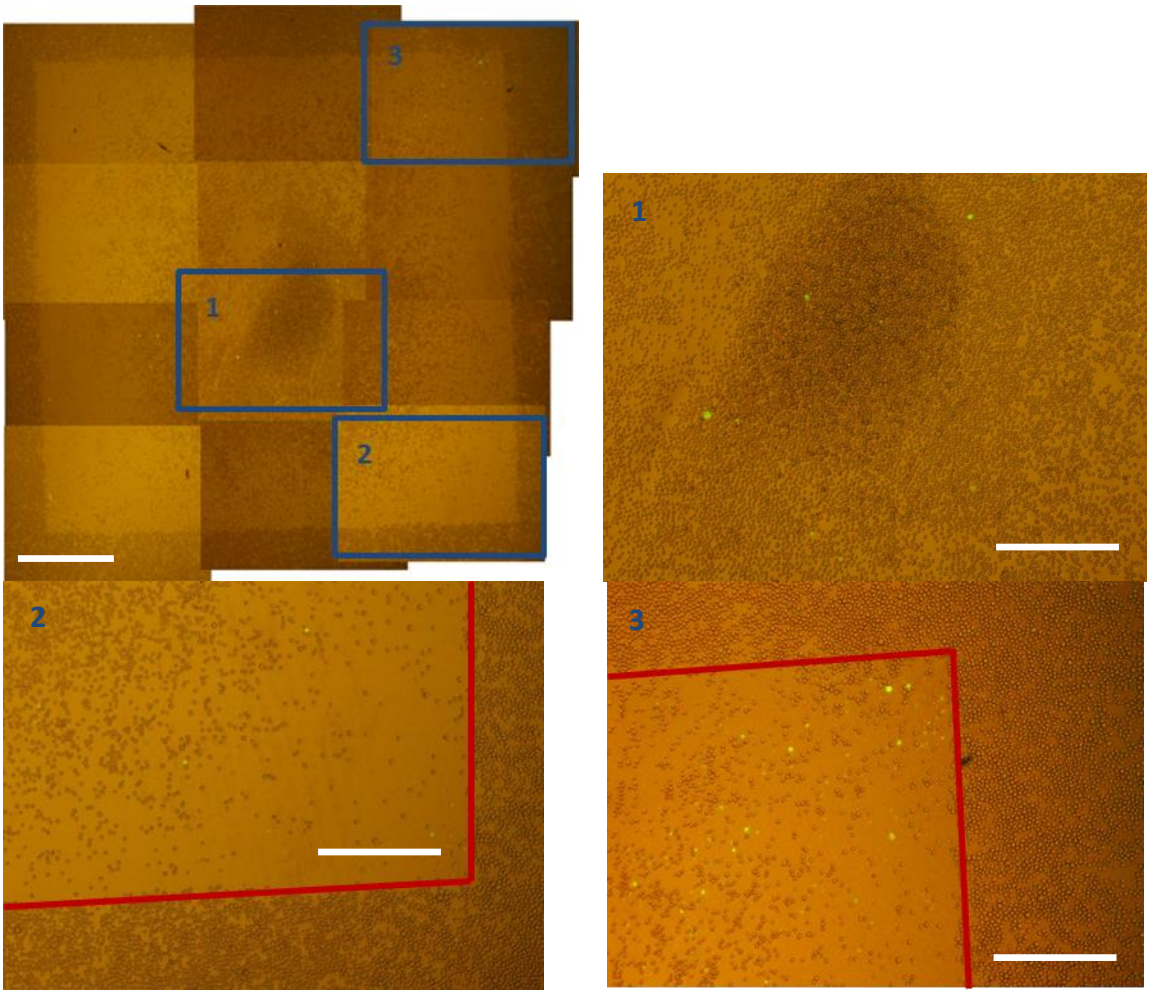

Figure 3.15. Brightfield images of K562 cells after puncture loading showing severe detachment along the edges and cell concentration at the center of the treated area. Top left image shows the entire area treated by the nanoneedles array. Dark blue lines indicate where the close-up views (1, 2, and 3) are. Red lines show where the edges of the nanoneedles array were. Scale bars are 1 mm (top left) and 500 µm (1, 2, and 3).

We further tested the immobilization of suspension cells on microfabricated surfaces, in collaboration with the laboratory of Wilbur Lam (Georgia Tech). The surface was patterned with square and circular wells, a few micrometers in depth, for the immobilization of individual cells in each well to minimize cell movement. After the

surface was treated with Cell-Tak, the cells were centrifuged at 300 g-force to promote attachment. Puncture loading was performed for intracellular delivery of 70 kDa FITC-dextran using 0.2 N for 30 s.

Cells were observed under the fluorescence microscope for detachment and intracellular uptake (Figure 3.16). The square and circular wells were seen in the brightfield view. While severe detachment was again observed, the majority of remaining cells were localized inside the well and showed uptake of fluorescent dextran molecules. Although we observed intracellular uptake of fluorescent molecules in suspension cells, we concluded that the immobilization techniques were not strong enough and not suitable to be used with puncture loading.

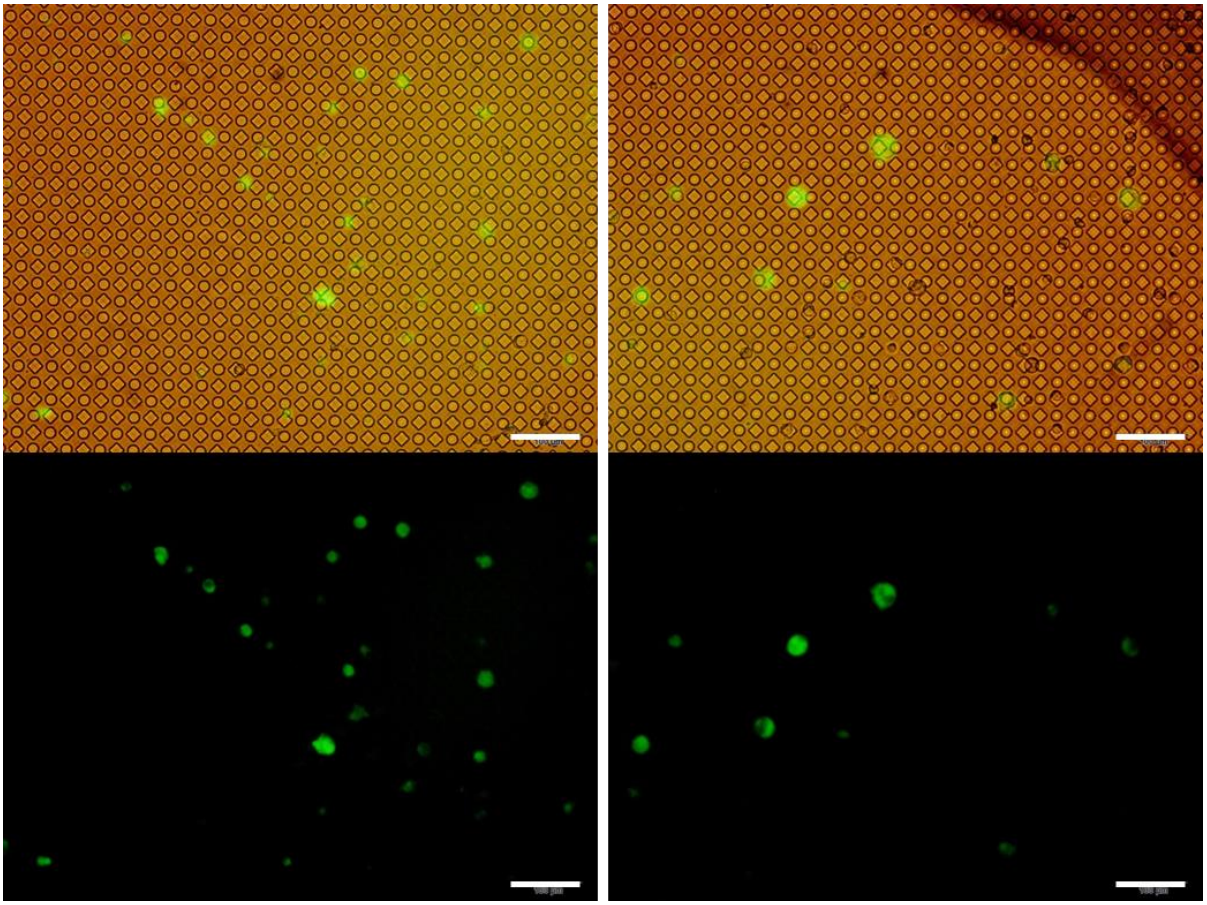

Figure 3.16. Brightfield and green fluorescence (intracellular uptake of 70 kDa FITC-dextran) images of K562 cells after the puncture loading on fabricated polystyrene surfaces (Lam lab). Scale bars are 100 µm.

3.3.4 Centrifuge loading

As an alternative approach to the method of puncture loading by bringing nanoneedles to a monolayer of cells, we developed a second method of centrifuge loading achieved by spinning cells down onto a nanoneedle array, which was fixed at the base of a centrifuge tube,. We hypothesized that the centrifugal force could bring the cells to the needles and result in impalement to promote uptake of molecules.

3.3.4.1 Effect of centrifugal force and time on intracellular uptake and viability

To test the feasibility of the centrifuge loading method, several centrifugation conditions were tested. We first quantified the uptake of calcein and the viability of DU145 cells over a broad range of centrifugal forces using all three types of nanoneedles: nanoneedles, nanoneedle tips and nanoblades (Figure 3.17). Centrifugal force was varied from 65 to 10000 g-force, while the centrifugation time was fixed at 2 min. At low centrifugal forces, 65 and 500 g-force, the viability of the cells treated with nanoneedles and nanoneedle tips were statistically same compared to the control (ANOVA, $p = 0.487$ and 0.200 for nanoneedles and nanoneedle tips, respectively). As the centrifugal force increased to 5000 and 10000 g-force, the decrease in viability was observed (ANOVA, $p = 0.000$). The increase in centrifugal force could have resulted in more cells sticking to the array and/or cell fragmentation. For all centrifugation conditions, the viability of the cells treated with nanoblades decreased significantly from the control and compared to the cells treated by other needle types (ANOVA, $p = 0.000$), which could be due to the bigger tip size of the nanoblades.

The delivery efficiency of calcein ranged between 10% and 50% of the cells collected after the centrifuge loading (Figure 3.17). We initially expected that as the centrifugal force increased, the delivery efficiency of calcein would increase as well due to stronger force to bring cells to the needles and puncture the cell membrane. Instead, we observed relatively high delivery efficiency at low centrifugal forces of 65 and 500 g-force and decreased uptake efficiency with higher centrifugal force (ANOVA, $p < 0.001$). Among the three needle types tested, we predicted the nanoblades to make bigger holes in the cell membrane, which would result in better uptake of molecules. However, the percentage of cells with calcein uptake after treatment with nanoblades was

approximately 10 – 15%, which was always lower than in the nanoneedle and nanoneedle tip samples (ANOVA, $p < 0.04$). Nanoneedles performed slightly better than nanoneedle tips at 65 and 500 g-force (Student's t-test, $p < 0.05$) and equivalently at 5000 g-force (Student's t-test, $p = 0.33$). For both nanoneedles and nanoneedle tips, the delivery efficiency did not vary significantly between 65 and 500 g-force (Student's t-test, $p > 0.2$). Based on these results, the optimal centrifuge condition was with nanoneedles or nanoneedle tips at 65 or 500 g-force.

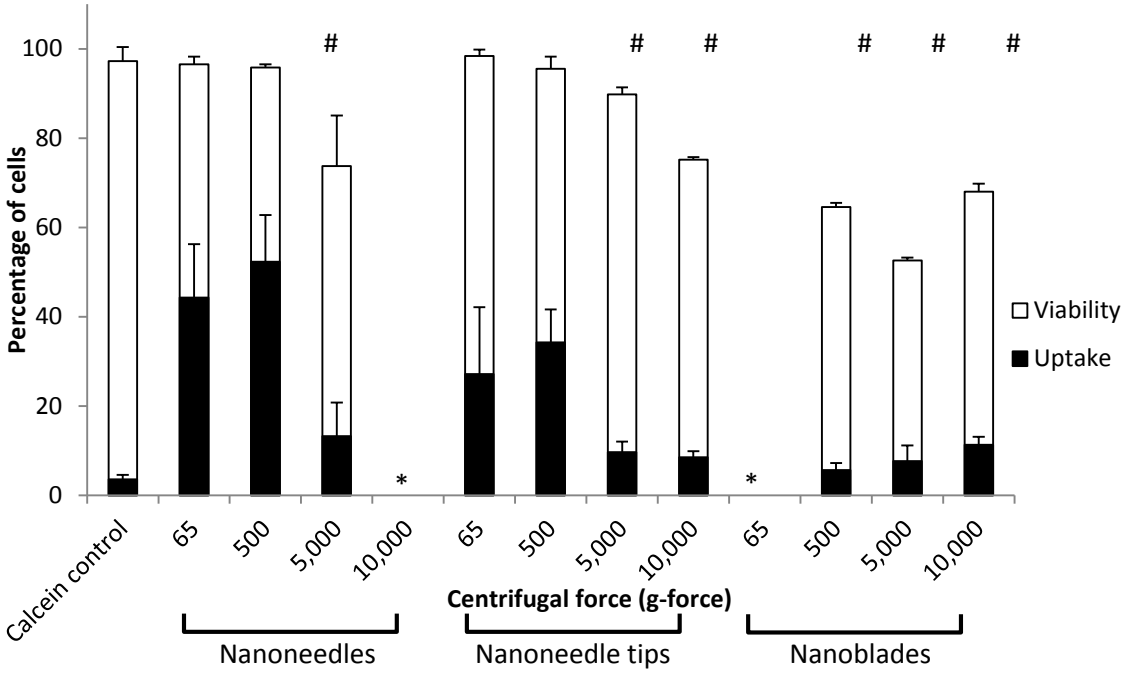

Figure 3.17. Effect of centrifugal force on the intracellular uptake of calcein and viability of DU145 cells. Centrifugation time was fixed at 2 min. Cells were treated with nanoneedles, nanoneedle tips, or nanoblades. Data were generated by flow cytometric analysis. Asterisk (*) indicate the conditions with no data available. Hash symbol (#) shows data where viability was lower than the untreated calcein control (Student's t-test, $p < 0.05$). Data show average ± SD, $n \geq 3$.

We next assessed the effect of centrifugation time on delivery efficiency and viability. Using a low centrifugal force of 0.65 g-force (100 rpm), the delivery efficiency of calcein and cell viability were quantified after centrifugation times of 5 min and 20 min for treatment with nanoneedles and nanoneedle tips (Figure 3.18). The viability of

cells collected after treatment was above 90% and did not differ significantly from the control (ANOVA, $p = 0.24$).

We expected the longer centrifugation time to give a greater chance for cells to come in contact with nanoneedles and thereby increase calcein uptake. However, for both nanoneedles and nanoneedle tips, the delivery efficiency of calcein was statistically the same at 5 min and 20 min (Student's t-test, $p > 0.1$). At both centrifuge conditions, the nanoneedles resulted in higher calcein uptake of approximately 40% compared to about 20% calcein uptake with the nanoneedle tips (Student's t-test, $p = 0.02$), which is consistent with the previous data at varied centrifugal force that also showed the superiority of nanoneedles.

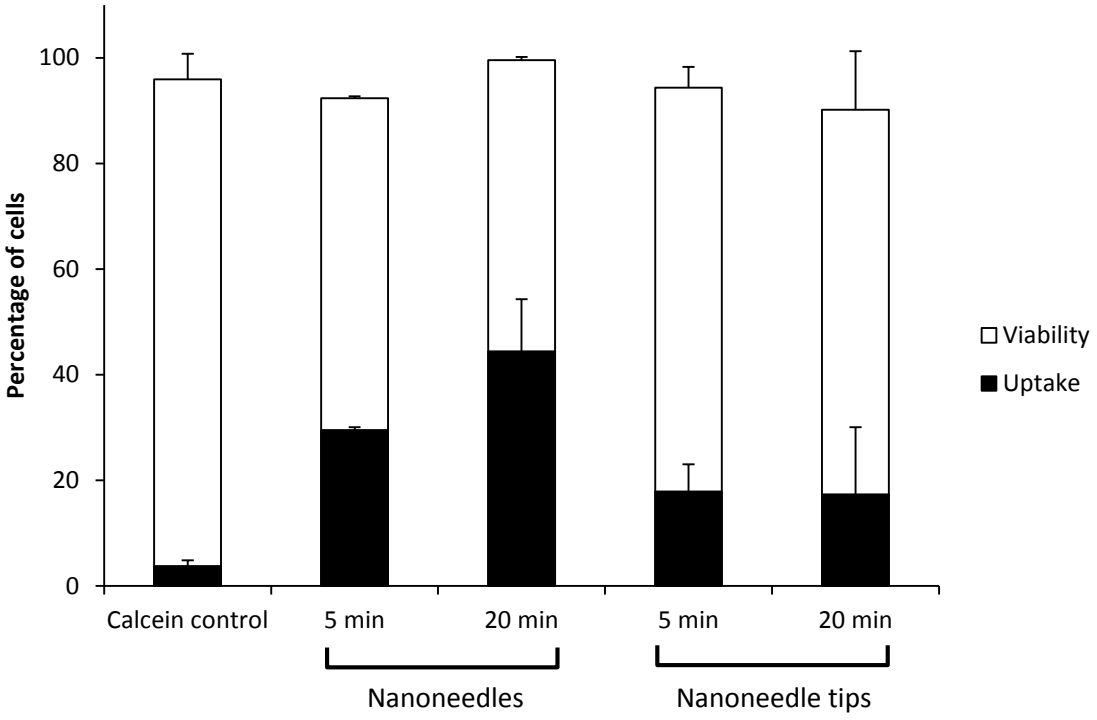

Figure 3.18. Effect of centrifugation time on intracellular uptake of calcein and cell viability. Centrifugation force was fixed at 0.65 g-force (100 rpm) for centrifugation times of 5 min and 20 min. Cells were treated with the nanoneedles or nanoneedle tips. Data were generated by flow cytometric analysis. Data show average ± SD, n ≥ 3.

3.3.4.2 Effect of sample size and number of treatments on uptake and viability

Because calcein uptake did not exceed 40 – 50% of cells at the optimal conditions, we hypothesized that calcein uptake could be increased further by reducing the number of cells per sample and by increasing the number of centrifugation treatments in order to increase the chances of a cell encountering, and thereby being punctured, by a nanoneedle. First, we reduced the number of cells per sample by reducing the cell concentration, guided by the estimate that spinning down approximately 125,000 cells of 15 – 20 μm diameter would form a monolayer on a 5 mm x 5 mm nanoneedle array. We therefore added 62,500, 125,000, and 250,000 cells per sample in order to form approximately half, one, and two monolayers, respectively.

We found that the number of cells per sample did not have a significant effect on viability compared to the untreated control (ANOVA, $p = 0.12$, Figure 3.19). Although we expected the percentage of cells with calcein uptake to increase with smaller sample size due to the increased probability of a cell encountering and thereby becoming impaled by a nanoneedle, the delivery efficiency of calcein was also not significantly affected by number of cells per sample (ANOVA, $p = 0.14$). Delivery efficiency was approximately 40% in all samples. Because the percentage of cells with uptake was unaffected by the number of cells per sample, the absolute number of cells with intracellular delivery was greater in the samples with more cells. Mechanistically, however, varying the number of cells per sample did not provide an explanation for why uptake did not exceed 40% - 50% of cells at optimal conditions.

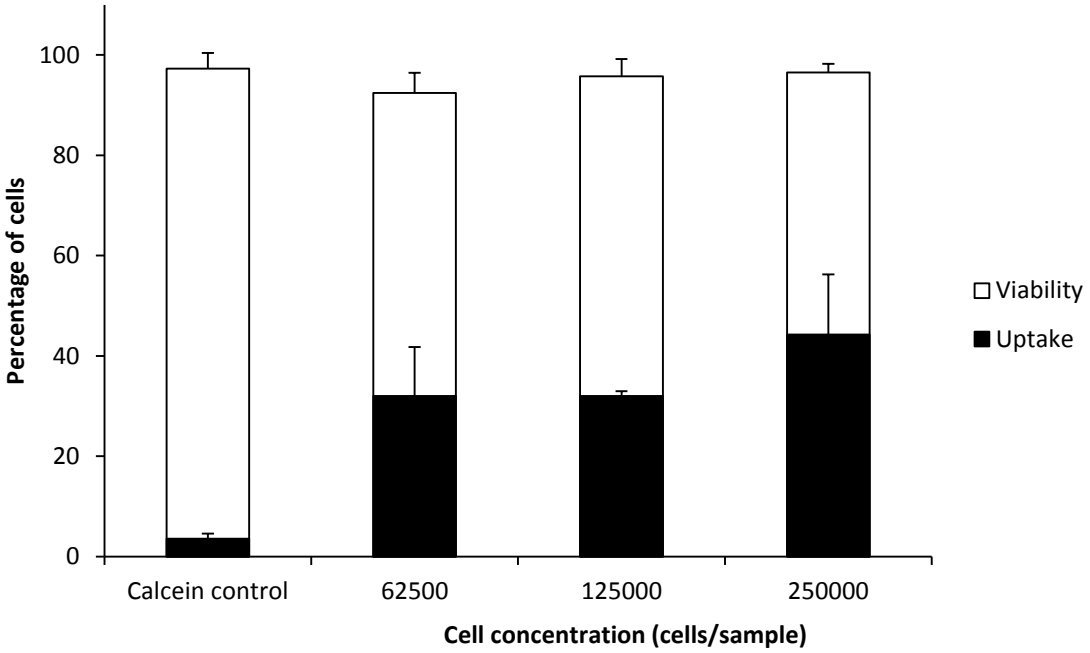

Figure 3.19. Effect of varying number of cells per sample on intracellular uptake of calcein and cell viability. Cell concentration was varied to achieve different numbers of cells per sample guided by their ability to form a monolayer on the nanoneedle array after being spun down. Cells were treated with nanoneedles at 65 g-force for 2 min. Data show average ± SD, n ≥ 3.

We next performed an experiment to test whether increasing the number of centrifugation treatments would result in higher delivery efficiency of calcein. Our hypothesis was that by increasing the number of treatments (with mixing of the cell suspension between each treatment), there would be more opportunities for a cell to come in contact with a nanoneedle for impalement. The cells were treated at 65 g-force for 2 minutes with both nanoneedles and nanoneedle tips using either a single centrifugation treatment or four centrifugation treatments.

Contrary to our hypothesis, multiple centrifugation treatments with nanoneedles and nanoneedle tips did not yield significant different delivery efficiency of calcein compared to the single treatment (Student's t-test, $p > 0.7$, Figure 3.20Figure 3.20). Nanoneedle tips achieved a delivery efficiency of 20 – 30% and nanoneedles performed slightly better, with a delivery efficiency of approximately 40%, but the data were statistically similar (Student's t-test, $p = 0.05$). Although we were concerned that multiple treatments with nanoneedles might result in lower cell viability, viability levels of the treated samples were all statistically the same (ANOVA, $p = 0.074$).

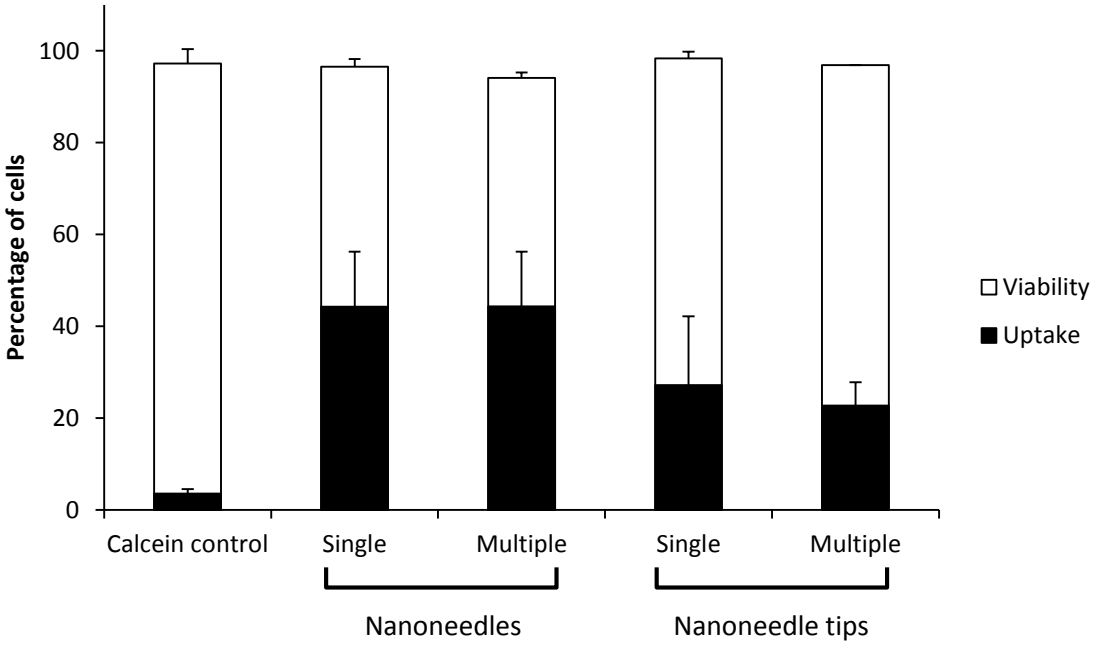

Figure 3.20. Effect of number of centrifugation treatments on intracellular uptake of calcein and cell viability. Cells were spun down either one time (single) or four times (multiple) at 65 g-force for 2 min with nanoneedles or nanoneedle tips. Data show average ± SD, n ≥ 3.

3.3.4.3 Effect of reusing nanoneedles on uptake and viability

We also assessed the feasibility of reusing the nanoneedles by comparing the delivery efficiency of calcein and cell viability after treatment with new nanoneedles versus used nanoneedles. The nanoneedles were soaked in bleach after the first experiment and rinsed with PBS before the second experiment.

Intracellular uptake of calcein decreased significantly in both nanoneedles and nanoneedle tips when these chips were used a second time compared to the first time (Student's t-test, $p < 0.01$, Figure 3.21Figure 3.21). As observed in previous experiments, the nanoneedles showed significantly higher delivery efficiency compared to the nanoneedle tips when use the first time (Student's t-test, $p = 0.009$). However, at the second use, there was negligible difference in delivery efficiency between nanoneedles and nanoneedle tips (Student's t-test, $p = 0.11$).

Cell viability also decreased for the used nanoneedles and nanoneedle tips, falling to approximately 80% while the viability associated with the new nanoneedles and nanoneedle tips remained similar to the control sample (ANOVA, $p \leq 0.001$). There was no difference between the viability after treatment with used nanoneedles and that after treatment with used nanoneedle tips (Student's t-test, $p = 0.40$).

The feasibility of using nanoneedles multiple times was investigated due to the time and effort put into nanoneedle fabrication. However, the performance decreased significantly after the first use in terms of lower viability and lower delivery efficiency of calcein. Nanoneedles were observed under SEM before and after the centrifuge loading to observe any significant difference on tips and structure of the nanoneedles (Figure 3.22**Error! Reference source not found.**). SEM images of nanoneedles after the centrifuge loading showed that the parts of the nanoneedles were covered by cells and cell debris. Cleaning the nanoneedles with bleach showed the minimal difference from before and suggested that the dimensions of the tips could have been altered. Although the nanoneedles can still be used after the first time by cleaning with bleach, there may be a decrease in the viability and delivery efficiency, possibly due to dull of damaged nanoneedle tip sharpness from remaining cell debris.

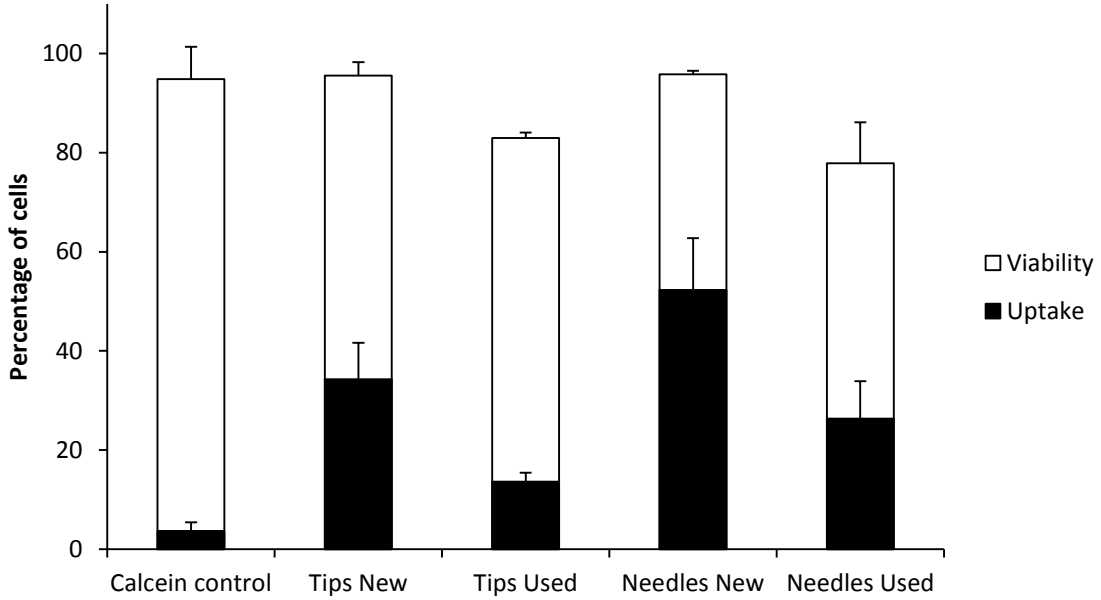

Figure 3.21. Effect of reuse of nanoneedles on intracellular uptake of calcein and cell viability. New nanoneedles or nanoneedle tips were used to treat cells, then cleaned with bleach, and then reused to treat a second cell sample by centrifugation at 500 g-force for 2 min. Data show average ± SD, n ≥ 3.

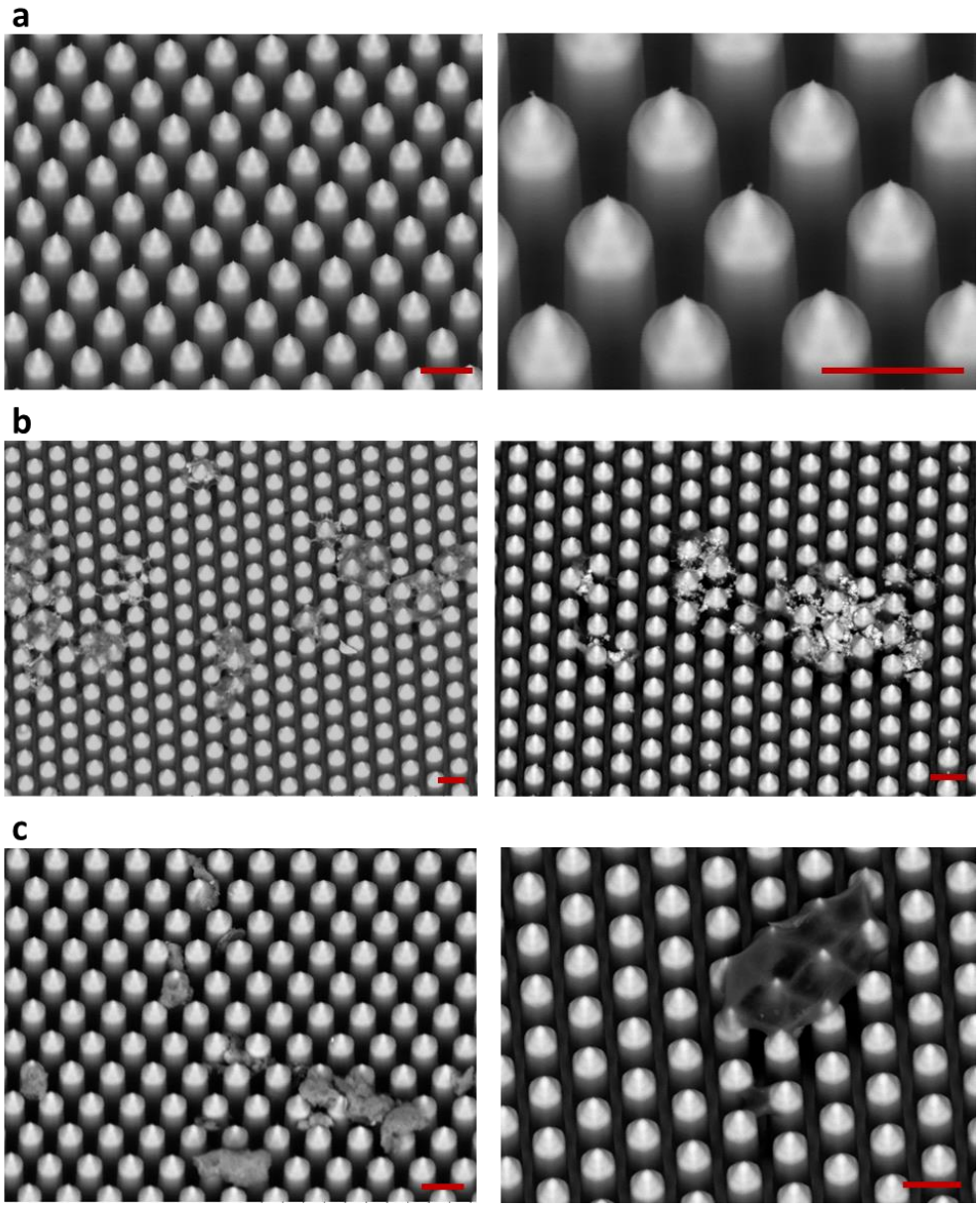

Figure 3.22. Scanning electron microscopy (SEM) images of the nanoneedles before the centrifuge loading (a), after the centrifuge loading (b), and after cleaning with bleach (c). Scale bars (red) are 10 μm.

3.3.4.4 Effects of molecular weight of uptake marker on uptake and viability

Lastly, we tested the feasibility of using centrifuge loading to deliver macromolecules, which have a molecular size similar to that of many proteins and plasmids of interest for biological applications. We first used nanoneedles and nanoneedle tips to promote intracellular delivery of FITC-BSA, which has a molecular

weight about two orders of magnitude bigger than calcein (Figure 3.23). The delivery efficiency of FITC-BSA was approximately 10% using both nanoneedles and nanoneedle tips, and was not significantly different between the two types of nanoneedle structures (Student's t-test, $p = 0.13$), in contrast to what we have seen with intracellular delivery of calcein. As we saw with puncture loading, the delivery efficiency of macromolecules was less than for small molecules, but this difference was more pronounced during centrifuge loading, which could mean the holes created by the nanoneedles were smaller and/or shorter-lived during centrifuge loading than puncture loading. As observed previously, the viability levels of the cells treated with FITC-BSA were not significantly different from the control sample (ANOVA, $p = 0.22$).

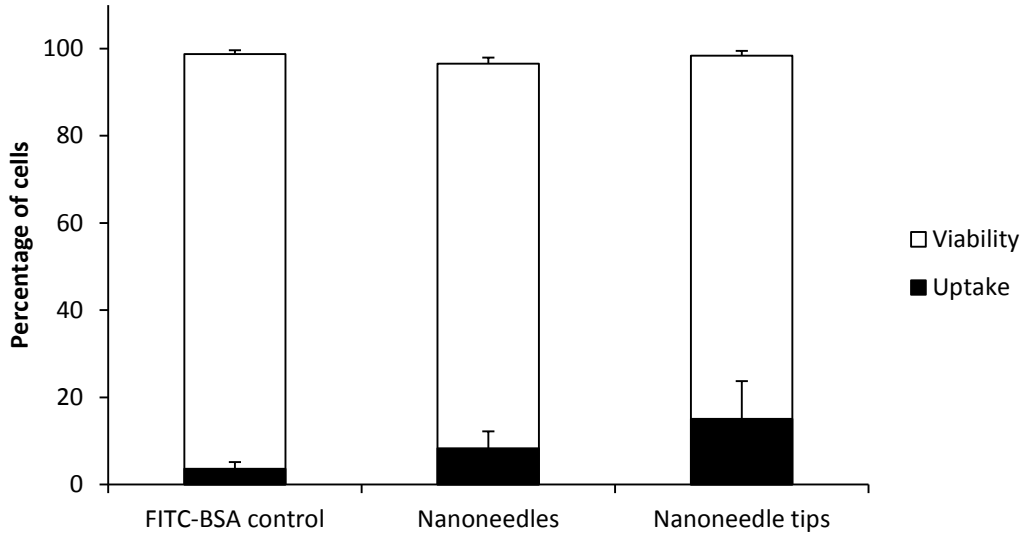

Figure 3.23. Intracellular uptake of FITC-BSA and cell viability. Cells were treated with centrifugation at 65 g-force for 2 min using nanoneedles and nanoneedle tips. Data show average ± SD, n = 5.

We also attempted the intracellular delivery of pGFP by collecting cells after treatment with centrifugation at 65 g-force for 2 min and quantifying the transfection efficiency 24 h post-treatment. Unfortunately, pGFP transfection efficiency was only about 1% at the tested condition (data not shown). This result further suggests that the delivery of macromolecules (i.e. proteins and plasmids) is difficult with the centrifuge loading method at the conditions used.

3.4 Discussion

This study developed nanoneedle-mediated intracellular delivery methods to deliver molecules directly into cells using a high-throughput issue approach. Toward this goal, we fabricated arrays of nanoneedles and studied their effect on intracellular delivery and cell viability at a variety of different experimental conditions using two different methods: puncture loading and centrifuge loading. These studies showed delivery of molecules into up to half of the treated cells with no significant loss of cell viability.

Intracellular delivery of molecules while maintaining high cell viability is of widespread interest. While single-cell microinjection is the gold standard for reliable delivery, it has extremely slow throughput [73, 74]. Viral delivery methods can have high efficiency, but are limited to DNA and RNA delivery and are associated with safety concerns [24, 40]. Chemical delivery methods, such as cationic lipids and polymers, can also be efficient, but utilize the endocytic uptake pathway that can degrade delivered molecules and reduce efficiency, and can also be limited by cell toxicity [45]. Physical methods, including electroporation, ultrasound and microfluidics, allow direct access to the cell cytosol avoiding endocytosis, but often have trade-offs between achieving high uptake levels and maintaining high cell viability [50, 164].

We sought to mimic the reliability of delivery associated with microinjection by using a similar approach of physically by-passing the cell membrane by directly puncturing with a microscopic needle. We also sought to overcome the main limitation of microinjection (i.e., very low throughput on the order of 10^2 cells per hour) by fabricating chips containing on the order of 10^5 nanoneedles for treatment of 10^4 to 10^5 cells at a time. Our approach differed, however, from conventional microinjection in that our needles were solid and served to create holes through with molecules could diffuse, whereas microinjection typically involves hollow microneedles through which molecules are delivered by convective flow into the cell.

There have been studies to accelerate the rate of microinjection using automation of the microinjection system for rapid sequential cell treatment [165, 166]. However, there are difficulties in using the automated microinjection system for large numbers of cells, especially for adherent cells. Reliability, repeatability, and accuracy of the method need further improvement and the system requires some amount of manual work [167].

This serial approach of rapidly puncturing one cell at a time by microinjection is still much slower than then the parallel approach using nanoneedles that treats thousands of cells simultaneously.

Other physical methods of intracellular delivery require significant optimization based the cell type used. For example, electroporation parameters, such as buffers, pulse voltage and pulse duration, need to be optimized for each cell type in order to achieve successful delivery with high cell viability [1, 5]. Ultrasound and microfluidic methods likewise require optimization for different cell types [8, 59] . These methods are also best suited for delivery to cells in suspension, although methods have been developed in some cases for adherent cells [168]. The nanoneedle-based approach was only studied here for one cell type (DU145 prostate cancer cells), but the microinjection literature suggests that cell puncture with nanoneedles may be broadly applicable to many cells types. In addition, the method can be used for both adherent cells, by puncture loading, and suspension cells, by centrifuge loading.

Although the centrifuge-loading method was well suited to treat cells in suspension, the delivery efficiency, especially for macromolecules, was significantly lower compared to puncture loading. This difference could be associated with different biophysical properties of adherent cells, which are spread out on an immobile substrate during puncture loading, versus suspension cells, which are roughly spherical and have no supporting substrate during centrifuge loading. The associated differences in cell morphology, membrane elasticity and other properties [169] could lead to different biomechanics during cell-nanoneedle contact, such that suspension cells might be more easily deformed by nanoneedles, making puncture across the cell membrane more difficult. Suspension cells might also deform into the spaces between the rows of nanoneedles during centrifuge loading, thereby avoiding puncture.

Intracellular delivery using nanoneedles is believed to depend on diffusion of molecules into cells through pores in the cell membrane. For this reason, delivery efficiency should depend on the pore size, the lifetime of the cell membrane pores and the diffusivity of the molecules being delivered. The observation that delivery of macromolecules was less efficient than small molecules could be explained by pore size on the order of 10 nm, which would allow easy access of small molecules, but hinder

transport of macromolecules. The small molecule used in this study, calcein (molecular weight of 0.6 kDa), has a radius of 0.6 nm [170]. The macromolecules are much bigger, where bovine serum albumin, 70 kDa dextran and 500 kDa dextran molecules have radii of 3.6 nm [171], 6 – 7 nm [172, 173] and 15 nm [174], respectively.

In addition to steric hindrance of transport through pores, the effect of molecular weight on diffusivity could also explain the reduce uptake of macromolecules. Because diffusivity is inversely proportional to molecular radius [175], the diffusion of 500 kDa dextran is almost 25 times slower than calcein. Thus, macromolecules will be taken up less efficiently due to slow diffusion through transient pores in the cell membrane.

Most previous work on intracellular delivery using nanowires or nanofiber arrays was achieved in a manner similar to the centrifuge loading method. Plasmid delivery using vertically aligned carbon nanofibers was conducted by spinning cells onto the array for 1 min at 600 g-force; however, an additional force was applied by manually pressing the arrays on the backside against PDMS after centrifugation [112]. Intracellular delivery was also demonstrated using CuO nanowire arrays by centrifugation with unspecified experimental conditions [114]. Another study achieved DNA delivery using carbon nanofiber arrays by manually pressing the array against a pellet of cells [176]. In other intracellular delivery studies, cells were simply incubated with arrays of carbon nanosyringes or silicon nanowires placed on the bottom of culture dishes for 12 – 72 h, where the gravity was used to slowly bring cells down to the nanostructures [113, 145, 177].

Although intracellular delivery was demonstrated in these studies, the experimental conditions required for cell impalement were not well characterized as in individual nanoneedle studies and were generally not varied to determine their effect on delivery efficiency and cell viability. When arrays were used in other studies, they were often non-uniform in the geometry and spacing between nanostructures. In this study, we used arrays of nanoneedles with well-defined geometry in a well-defined array and studied the effects of experimental parameters under controlled conditions on intracellular delivery and cell viability by both puncture and centrifuge loading. Using these data, we attempted to optimize the method for increased intracellular uptake and

cell viability and found conditions that had no significant loss of cell viability with up to ~50% of cells exhibiting intracellular delivery.

3.5 Conclusion

This study microfabricated arrays of nanoneedles with 20 – 30 nm tips and assessed their effects on intracellular delivery and cell viability using puncture loading and centrifuge loading. Puncture loading studies demonstrated effective intracellular delivery of fluorescent molecules by lowering nanoneedles onto confluent monolayers of adherent cells. Increasing puncture force increased intracellular uptake and decreased cell viability over the range of conditions studied. Increasing puncture time had no significant effect on uptake and reduced viability. Increasing molecular weight decreased uptake and had no effect on viability.

Centrifuge loading exploited the use of centrifugal force to bring cells onto the array of nanoneedles for impalement. Increasing centrifugal force decreased intracellular uptake and had no effect on cell viability over the range of conditions studied. Increasing centrifugation time, number of cells and number of treatments all had no significant effect on uptake or viability. The type of nanostructures mattered, where uptake was greatest when using nanoneedles, followed by nanoneedle tips and finally nanoblades, but viability was unchanged. The method was effective in the delivery of small molecules, such as calcein, but the delivery efficiency dropped significantly for macromolecules.

Overall, this study developed novel methods of intracellular delivery using nanoneedles, identified key operating parameters and determined their effects on optimizing intracellular delivery and cell viability and thereby advances the field of intracellular delivery using microfabricated nanoneedle arrays for future applications.

CHAPTER IV

EVALUATION OF THE MICROFLUIDIC DEVICE FOR THE EFFICIENT DELIVERY OF PROTEINS AND PLASMIDS IN THE TRAGET CELL LINES

4.1 Introduction

Fluid mechanical force has been studied for the permeabilization of the plasma membrane and delivery of macromolecules. Previous studies showed that the increase in shear stress caused the membrane fluidity to increase in endothelial cells [178, 179]. As a result, cell membrane poration was observed with the increase in membrane tension [60, 61]. The intracellular delivery was demonstrated by microchannel devices to induce shear stress on cells and the diffusion on fluorescent molecules of different sizes [63]. The intracellular uptake and cell viability was dependent on device design, shear force and time applied.

Similarly, the intracellular delivery of various molecules into different cell types was demonstrated using the new microfluidic device in literature [8]. The device with multiple constriction channels allowed the high-throughput treatment of cells by mechanical deformation and shear stress. In this study, we evaluated the feasibility of using these microfluidic devices for the efficient intracellular delivery of proteins and plasmids. In addition, we assessed the intracellular uptake and viability of different cells lines, which could be more relevant models for the future applications.

4.2 Methods

4.2.1 Cell culture

Human prostate cancer cells (DU145, American Type Culture Collection, Manassas, VA), human myelogenous leukemia cells (K562, American Type Culture Collection), and lymphoid leukemia cells (EU1, courtesy of Dr. Muxiang Zhou, Emory University, Atlanta, GA) were cultured in a humidified atmosphere of 95% air and 5%

CO_2 at 37°C. DU145 and K562 cells were cultured with RPMI-16490 medium (Cellgro, Herndon, VA), which was supplemented with 10% (v/v) heat-inactivated fetal bovine serum (FBS, Corning, Palo Alto, CA) and 1% penicillin/streptomycin (Cellgro) [137, 180]. EU1 cells were cultured with DMEM medium (Cellgro, Herndon, VA), which was also supplemented with 10% (v/v) heat-inactivated fetal bovine serum (FBS, Corning, Palo Alto, CA) and 1% penicillin/streptomycin (Cellgro) [181]. In addition to DU145 cells, K562 and EU1 cells were used as alternative cells for the experiment based on their cell size and characteristics.

4.2.2 Microfluidic loading

4.2.2.1 Sample preparation

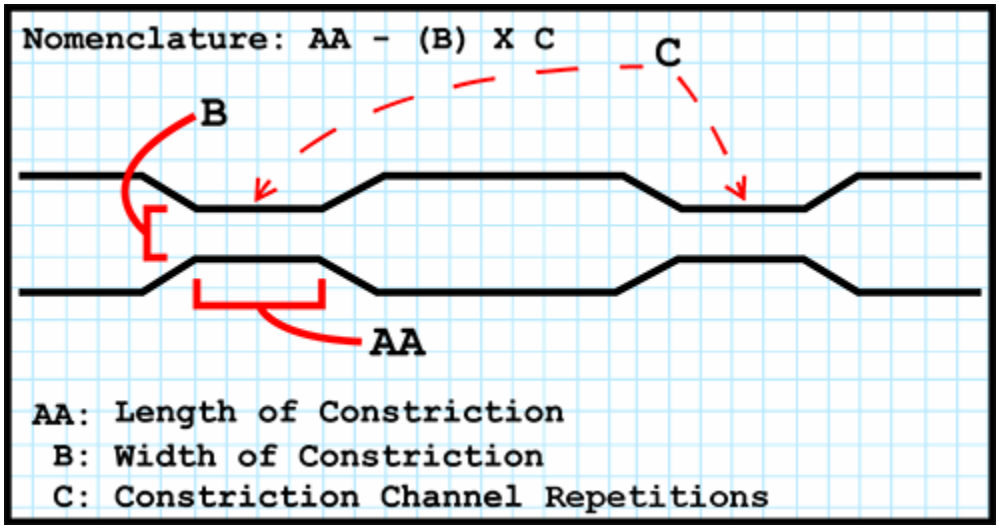

Figure 4.1. The microfluidic device schematic [182]

The silicon-based devices were fabricated to have tens of identical, parallel microfluidic channels. The channels have three main parameters as shown in Figure 4.1. The channel width and length of constriction varies from 4 – 8 µm, and 10 – 40 µm, respectively [8]. The devices were obtained (Courtesy of Drs. Armon Sharei, Klavs Jensen, and Robert Langer, MIT, Cambridge, MA and SQZ Biotechnologies, Boston, MA) and soaked in a 70% ethanol until used. Devices with varying constriction length,

width, and number were obtained and tested based on the cell size. Devices were assembled and completely dried prior to the experiment.

DU145 cells were harvested by trypsin/EDTA (Cellgro) and re-suspended in RPMI. K562 and EU1 cells were harvested and re-suspended in RPMI and DMEM, respectively. Cell concentration was measured by a Multisizer 3 Coulter Counter (Beckham Coulter, Fullerton, CA) and prepared for the experiment at 3x106 or 10x106 cells/ml based on the different versions of the holders used. Calcein (Molecular Probes, Eugene, OR) and 70 kDa FITC-labeled dextran (Sigma-Aldrich, St. Louis, MO) were added to cells at a final concentration of 0.2 mg/ml to serve as markers of intracellular uptake [8]. Allophycocyanin (APC, Sigma-Aldrich), another marker of intracellular uptake, was added to the cells at a final concentration of 0.05 μM due to the cytotoxicity associated with the marker at the concentration above 1 μM [183]. Halo TMR-tagged TALENs (Courtesy of Dr. William Dynan, Emory University) were added at a final concentration of 1.25 μM.

4.2.2.2 Delivery method

The volume of 100 – 150 μl of cells mixed with the desired delivery materials were placed in the assembled device's inlet reservoir. The reservoir was connected to a compressed air line (Airgas, Atlanta, GA) controlled by a regulator (McMaster-Carr, Atlanta, GA) and the pressure was adjusted from 50 – 150 psi to drive the fluid through the device at constant pressure. The constant flow rate to drive the fluid was also tested by connecting the reservoir to "Genie" programmable syringe pump (Kent Scientific Corporation, Litchfield, CT) and using the flow rate of 100 μl/min or 1 ml/min. The treated cells were then collected from the other reservoir by pipet.

Cells were incubated at room temperature for 15 minutes after the treatment for the cell membrane to reseal. Cells were washed three times with PBS (Cellgro) at 300 x g for 5 min to remove extracellular fluorescent molecules in the medium and on the surface of the cell membrane. After the third wash, the cells were resuspended in PBS for analysis. Propidium iodide (PI, Invitrogen, Grand Island, NY) or SYTOX Green nucleic acid stain (Invitrogen) was added at a final concentration of 5 μg/ml or 100 nM, respectively, 10 - 15 min before flow cytometry analysis to stain non-viable cells and

thereby measure cell viability. For nucleus stain, Hoechst 33342 (trihydrochloride, Invitrogen) was added at a final concentration of 2 µg/ml for 20 min.

4.2.3 Analysis and Quantification

Cell concentration was measured after the treatment to determine the cell loss due to clogging in the microfluidic channel and the fragmentation of cells. A volume of 50 ul of re-suspended cells was diluted in 10 ml of PBS, an electrolyte solution. The cell concentration was measured by a Coulter Counter and compared with the initial cell concentration to calculate the loss.

The uptake of fluorescent dyes and cell viability were measured using a bench-top flow cytometer (BD LSRII, BD Biosciences, San Jose, CA). The data were collected and analyzed in FACSDiva software (BD). Approximately 10,000 events were collected per sample. For cell viability, PI and SYTOX green were analyzed using a PerCP-Cy5, 670 nm longpass filter, and a FITC, 530/30 nm bandpass filter, respectively, for emission. The uptake of calcein and 70 kDa FITC-dextran was measured by a FITC, 530/30 nm bandpass filter for emission. The uptake of APC and Halo TMR-tagged TALENs were measured by an APC, 660/20 nm bandpass filter, and a PE, 575/26 nm bandpass filter, respectively, for emission.

The cell gate was constructed based on forward- and side-scatter light of the untreated control cells. Any events within this gate were considered to be intact cells while any events outside the gate were considered to be cell debris or other noise. To determine which cells had taken up fluorescent marker compounds (i.e., calcein, dextran, and APC for uptake; PI and SYTOX green for viability), histogram gates were set by the sham control which had fluorescent dyes in the solution but was not treated to account for extracellular staining and other noise. To set gates and account for possible spectral overlap between the dyes, compensation controls were prepared and tested.

Cells were imaged using an inverted fluorescence microscope (Olympus IX70, Olympus, Center Valley, PA). Using cellSense Standard software (Olympus), images were taken at 10x or 20x magnification and captured using appropriate filters.

4.2.4 Statistical analysis

A minimum of three replicates was performed for all conditions. Means and standard deviations were calculated from the replicates. An unpaired Student's t-test or analysis of variance (ANOVA) was performed using Minitab 17 (Minitab, State College, PA). A value of $p < 0.05$ was interpreted as significant.

4.3 Results

4.3.1 Intracellular delivery to DU145 cells

We first tested the feasibility of intracellular delivery to DU145 cells using the microfluidic devices with calcein and 70 kDa FITC-dextran. Cells were treated using a 10-6 microfluidic device, where 10 is the length of the constriction in μm and 6 is the width of the constriction in μm. The intracellular uptake of calcein and FITC-dextran as a function of pressure was quantified (Figure 4.2).

We observed the similar trend in calcein and FITC-dextran uptake as exhibited in previous work [8]. While the intracellular uptake of calcein was statistically similar (ANOVA, $p = 0.209$) in three pressures tested with 80 to 85% of cells exhibiting intracellular uptake of calcein, the delivery efficiency of FITC-dextran increased with the pressure from 20 to 40% of cells with uptake (ANOVA, $p = 0.001$). The delivery efficiency also depended on the size of the molecules; i.e. as the size of the molecule increased by about two orders of magnitude from calcein to FITC-dextran, the delivery efficiency was lower at each pressure tested (Student's t-test, $p < 0.05$). The viability of the cells collected after the treatment was 96 – 98% in all conditions tested (data not shown) and were not statically different (ANOVA, $p = 0.209$).

Based on these initial data on intracellular delivery of fluorescent molecules to DU145 cells, we treated the cells with plasmid DNA encoding for GFP using a 10-6 microfluidic device at 70 and 90 psi pressure to quantify the transfection efficiency 24 h post-treatment. Unfortunately, pGFP transfection efficiency was only 1 – 3% in all conditions tested (data not shown). This result further supports the idea that uptake decreases with increasing molecular size, such that delivery of large plasmid DNA molecules is difficult.

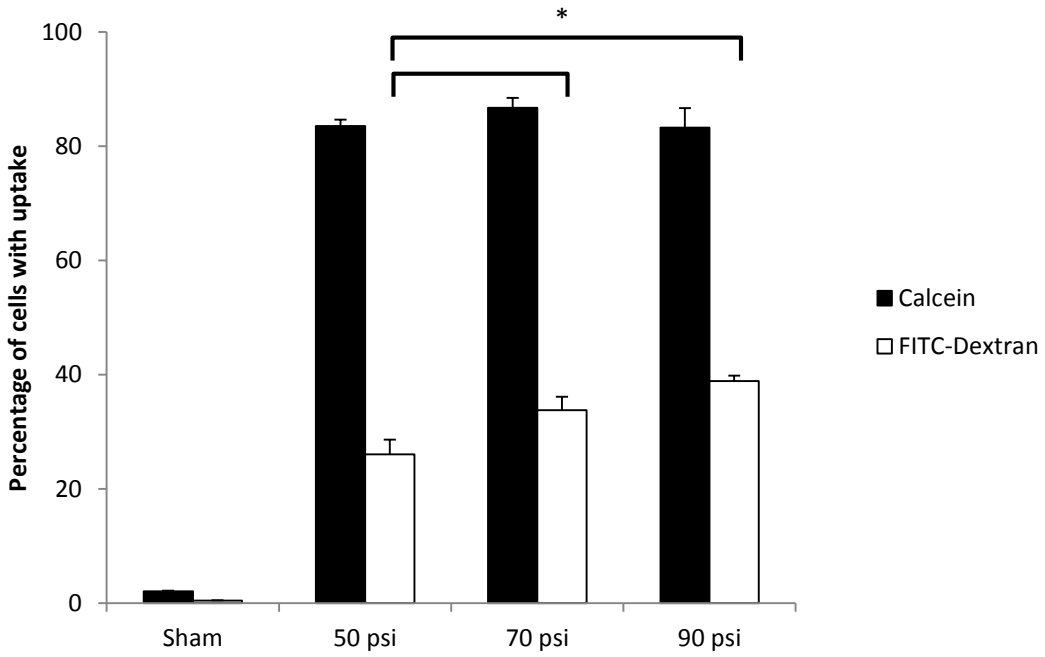

Figure 4.2. The delivery efficiency of fluorescent molecules, calcein and 70 kDa FITC-dextran, into DU145 cells collected after treating with a 10-6 microfluidic device at varying pressures of 50, 70, and 90 psi. Asterisk (*) shows statistically significant difference in uptake ($p < 0.05$). Data show average ± standard deviation (SD), n = 3.

The previous experiments were done using a constant-pressure system. We next tested a constant-flow rate system with the syringe pump to avoid the possibility of decrease in pressure of the system due to cells clogging in the constriction channels of the device. In our initial experiment with the two fluorescent molecules at two flow rates, 1.0 and 0.1 ml/min, we observed a low cell count and poor delivery efficiency of fluorescent molecules in flow cytometry analysis (data not shown). We counted the cells in each sample after treatment with 10-9 device to see the change in cell concentration (Figure 4.3). The noticeable decrease in cell concentration after treatment in the constant-flow rate system was observed due to the clogging in the constriction channels and the loss of intact cells. Percentage of cells remaining decreased to approximately 70% and 20% for the flow rates of 1.0 and 0.1 ml/min, respectively (ANOVA, $p < 0.001$). At both flow rates, there was no statistically significant difference in cell concentration before and after washing (Student's t-test, $p > 0.05$). We concluded from these studies that the

constant-flow rate system was less effective, because it led to extensive loss of cells in the microfluidic device.

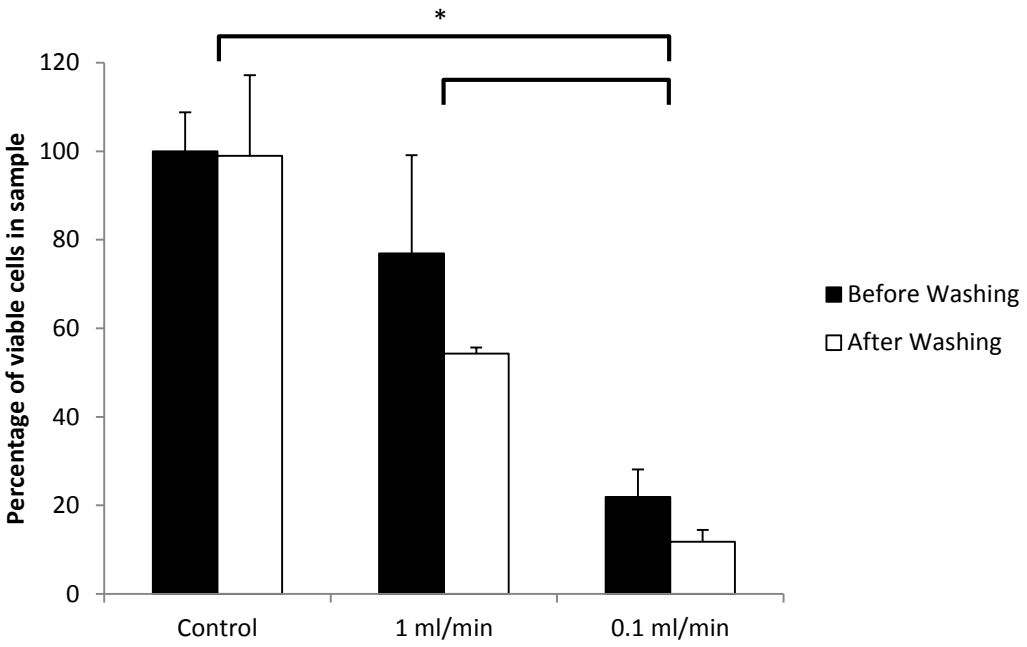

Figure 4.3. The concentration of DU145 cells before and after washing with centrifuge after treatment with a 10-9 device in the constant-flow rate system. Asterisk (*) shows statistically significant difference in percentage of cells remaining ($p < 0.05$). Data show average ± SD, n = 3.

4.3.2 Intracellular delivery to K562 cells

We hypothesized that due to the similar sizes of DU145 and K562 cells in the range of 15 – 20 μm in diameter, K562 cells can be treated with the microfluidic device for intracellular delivery as well and result in similar delivery efficiency. However, in our preliminary experiments with K562 cells and fluorescent molecules, the cell counts were low and the delivery efficiency was low as well in flow cytometry analysis (data not shown). After treating cells with a 10-6 device at 70 psi, the cell concentration was quantified before and after washing to observe the change (Figure 4.4). There was a significant decrease in the percentage of cells remaining before and after washing to 70% and 40%, respectively, after cells were treated with the microfluidic device (ANOVA, p = 0). Although the difference between before and after washing samples were negligible in

DU145 cells (Figure 4.3), there was a significant difference in before and after washing samples in K562 cells (Student's t-test, p = 0.036). We concluded that the difference between before and after washing was mainly due to the treatment with the microfluidic device since we validated the washing step that the cells are not lost by cell counts and the control samples also undergo the same washing steps.

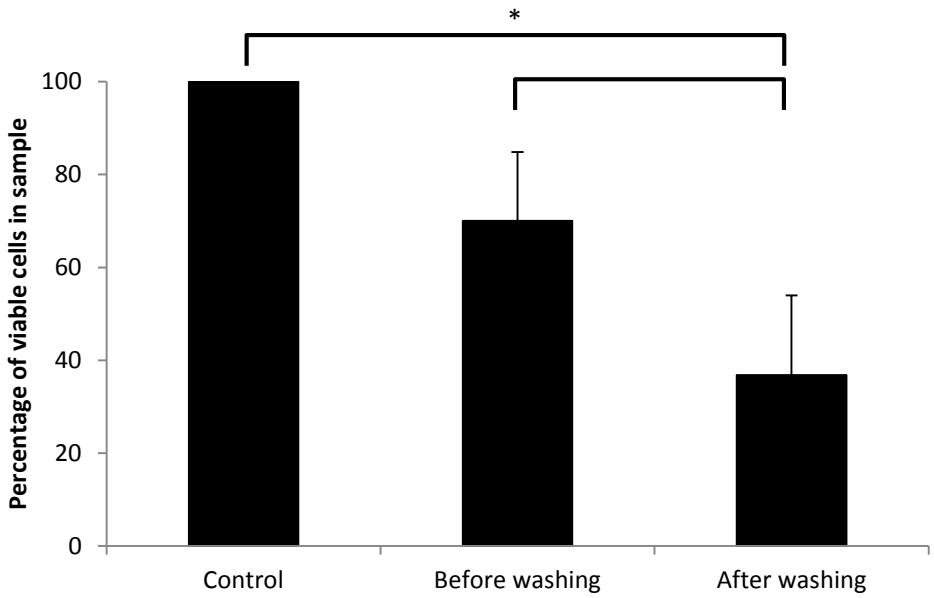

Figure 4.4. Percentage of K562 cells remaining after treating with a 10-6 device at 70 psi. Asterisk (*) shows statistically significant difference in percentage of cells remaining ($p < 0.05$). Data show average ± SD, n = 3.

4.3.3 Intracellular delivery of proteins to EU1 cells

As we did not see the promising result with K562 cells, we moved onto EU1 cells, which would be similar to K562 cells since they are both leukemia cells but smaller in size with 7 – 15 μm in diameter. To study the intracellular delivery of protein, APC was chosen as a model fluorescent protein since the size of APC (104 kDa) is comparable to that of TALENs (110 kDa). The initial study using a 10-8 device with the APC concentration of 1.5 μM showed the intracellular uptake of fluorescent proteins (data not shown). However, in order to reduce the high extracellular fluorescence observed in the sham control and reduce the possibility of toxicity associated with high APC

concentration, the following experiments were conducted using the APC concentration of 0.5 μM [183].

We quantified the delivery efficiency of APC in EU1 cells as a function of pressure and constriction width of the microfluidic device (Figure 4.5). We observed the similar trend in intracellular uptake with the change in constriction width as exhibited in previous work [8]. At each pressure tested, delivery efficiency increased with the decrease in constriction width of the device as cells undergo more deformation and are subject to greater shear force. The effect is more evident in the higher pressure of 120 psi (ANOVA, $p = 0.002$) compared to at 50 psi (ANOVA, $p = 0.056$). The data showed the similar trend for the effect of pressure on delivery efficiency as in DU145 cells with FITC-dextran. For the devices tested, the delivery efficiency was significantly different with pressure (ANOVA, $p < 0.05$) and increased by approximately four fold as pressure increased from 50 to 120 psi.

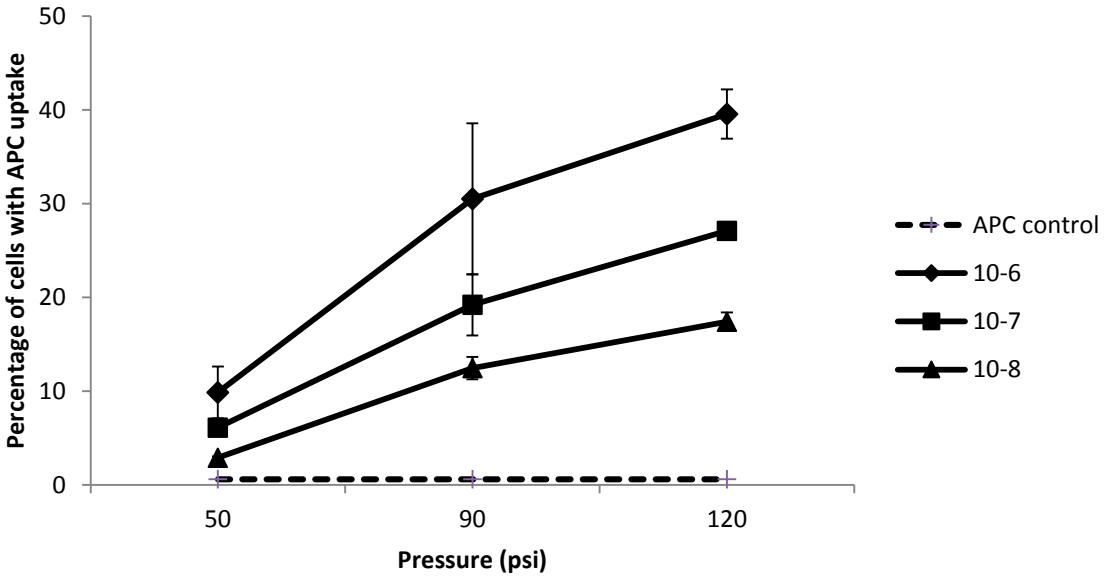

Figure 4.5. The effect of pressure and constriction width of the microfluidic device (10-6, 10-7, and 10-8) on the delivery efficiency of APC in the EU1 cells. Data show average ± SD, n = 3.

There are two ways to carry out viability analysis in our flow cytometry experiments. In one method, the fractions of cells detected by the flow cytometer are classified as viable or non-viable based on propidium iodide staining. In this method, cells that were lost at some point during the experiment (e.g., cells fragments into debris, cells remaining in the microfluidic device) are not accounted for. In the second method, the cells lost during the experiment are quantitatively accounted for by comparing cell concentration in experimental samples to cell concentration in negative control samples. In this second method, viability is determined on the basis of all cells treated by accounting for viable cells, nonviable cells and lost cells.

In both DU145 and EU1 experiments, we observed no significant difference in viability of the cells treated at varying experimental conditions (ANOVA, $p < 0.05$) using the first method of analysis, where we assumed that the cell loss due to clogging in the constriction channels or loss to fragmented cells in washing step have not been taken into account. Based on this assumption, the previous measurement on the viability and intracellular uptake is based on only the collected cells after the treatment. We therefore quantified the percentage of intact EU1 cells and viable cells out of total cells we started with using the second method of analysis at four different conditions (Figure 4.6). Percentages of intact cells (i.e., cells that were not lost) were in the range of 50 – 80% compared to almost 100% in negative control samples. Percentages of cells remaining after treating at lower pressure of 90 psi were not significantly different from the control sample (Student's t-test, $p = 0.084$ for 10-6 device, and $p = 0.054$ for 10-7 device), but were significantly smaller at higher pressure of 120 psi (Student's t-test, $p < 0.05$ for both devices). Percentages of viable cells were all statistically smaller than the control sample (Student's t-test, $p < 0.05$ for all experimental conditions) and were in the range of 30 – 60%. For both devices, the significant decrease in percentage of viable cells at higher pressure (Student's t-test, $p < 0.05$) was observed. At lower pressure of 90 psi, percentages of intact and viable cells were similar in both devices (Student's t-test, $p = 0.814$ and 0.826, respectively). However, with higher pressure of 120 psi, the device with smaller constriction width of 6 μm had significant decrease in percentage of viable cells (Student's t-test, $p = 0.032$). Although the cell viability of the collected cells remained high in the previous studies, we concluded from this study that the smaller constriction

width of microfluidic device and the higher pressure actually resulted in decrease of the cell viability (i.e. intact and viable cells).

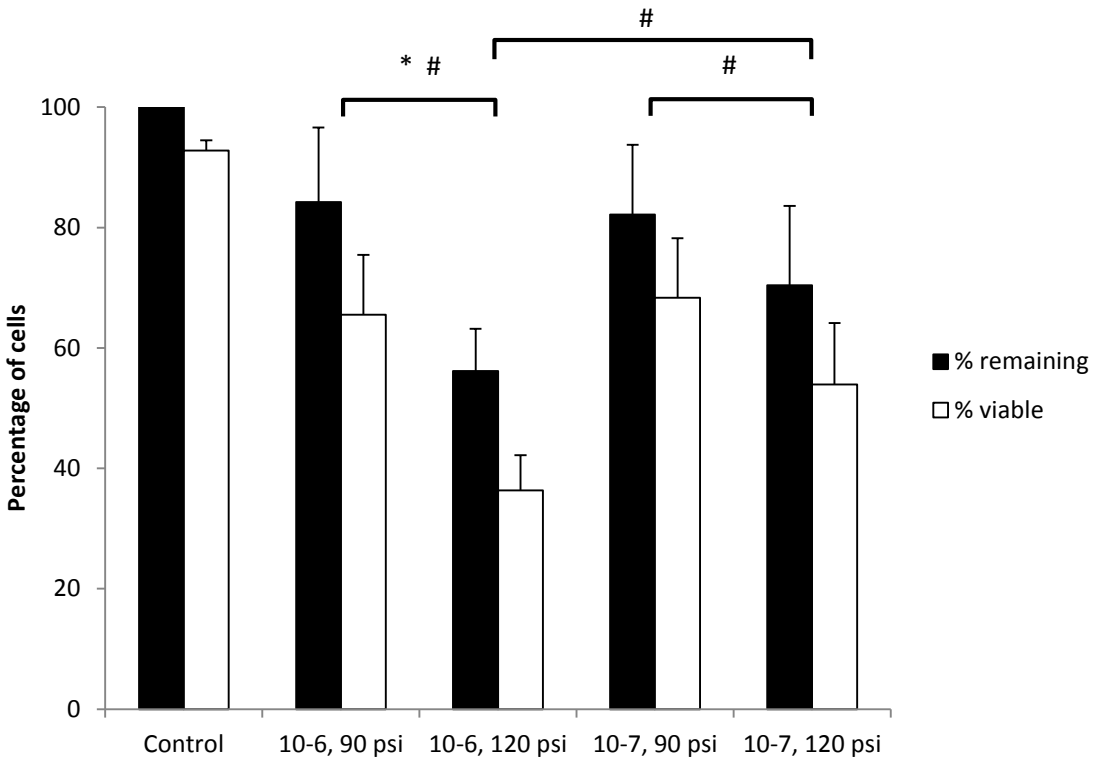

Figure 4.6. The percentage of remaining/intact and viable EU1 cells after the treatment using 10-6 and 10-7 devices at 90 and 120 psi. Asterisk (*) and hash symbol (#) show statistically significant differences in percentage of remaining and viable cells ($p < 0.05$), respectively. Data show average ± SD, n = 4.

We recalculated the intracellular delivery efficiency and viability based on the total number of cells we started with (i.e., the second method) instead of only the cells that were collected after the treatment (i.e., the first method) using the obtained values of percentages of intact and viable cells (Figure 4.7). While we saw the statistical difference in intracellular delivery efficiency across the conditions we tested, the recalculated delivery efficiency was about 20% out of total cells in all cases and did not show significant difference with the change of constriction width of the device and the pressure (ANOVA, $p > 0.05$). As for the viability, all of the samples were statistically different from the control except for the cells treated with 10-6 device at 90 psi (Student's t-test, $p > 0.05$). The viability decreased with increase in pressure for the 10-6 device (Student's t-

test, p = 0.01). These studies demonstrated that the recalculation was necessary in order to determine the correct delivery efficiency and cell viability out of all cells, not just the collected cells. While previous studies showed that the delivery efficiency was significantly influenced by the width of the microfluidic device or the pressure but the viability was not, the vice versa was observed in the recalculated data (i.e. the recalculated viability decreased significantly with the smaller width of the microfluidic device or the pressure but the recalculated delivery efficiency was similar regardless of the change in the system).

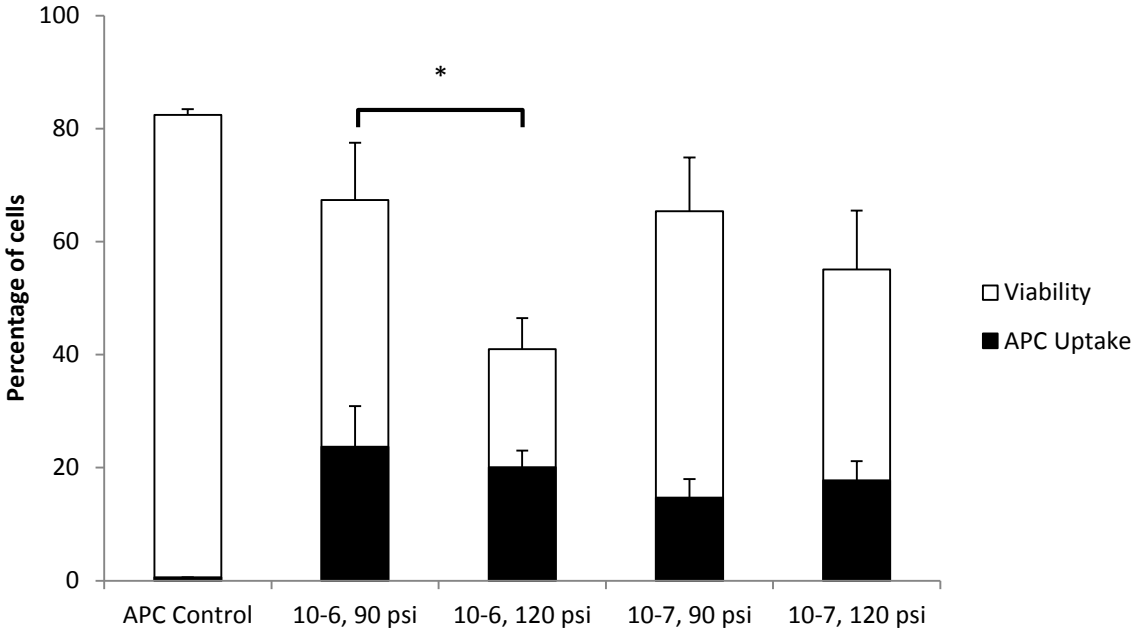

Figure 4.7. The delivery efficiency of APC and viability of EU1 cells from Figure 4.5 recalculated based on the viability values in Figure 4.6. Asterisk (*) shows statistically significant differences in viability ($p < 0.05$), respectively. Data show average ± SD, n = 3.

Based on our intracellular delivery result of APC to EU1 cells, we treated with two conditions for the intracellular delivery of halo TMR-tagged R4 TALEN. The treated cells were displayed on the histogram of the appropriate filter for the halo-tagged TALEN (Figure 4.8). Compared to the cells-only control sample, the samples with halo-tagged TALEN added to them showed the shift in the histogram even after several washing steps. In the samples treated with 10-6 and 10-7 microfluidic devices, the two

overlapping populations were noticeable to indicate the intracellular uptake of halo-tagged TALEN. The close overlap between two populations was likely due to the low concentration and the weak fluorescence of the halo-tagged TALEN used. This overlap made quantification of update difficult.

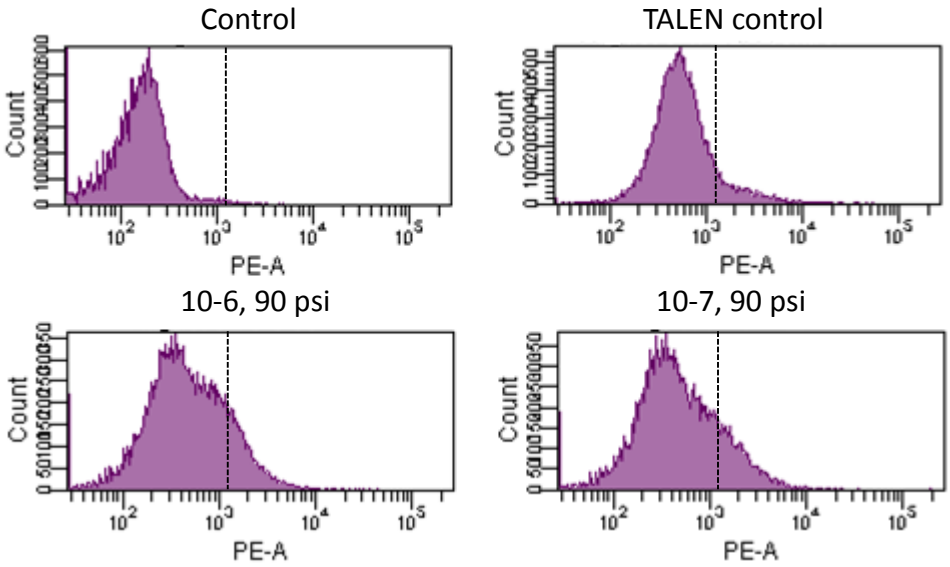

Figure 4.8. PE channel histogram for Halo-tagged TALEN (R4) uptake in to EU1 cells using two different microfluidic devices compared to control samples. Dotted lines indicate the upper limit on the background fluorescence signal in control cells.

4.4 Discussion

Consistent with previous studies showing that the microfluidic device can deliver various fluorescent and functional molecules to different cell lines [8], we also have demonstrated the intracellular delivery of fluorescent molecules and proteins into cells. Although the method works well for the delivery of fluorescent molecules and proteins, we saw the limitation of the method for the delivery of plasmid. We observed the low percentage of plasmid GFP transfection in DU145 cells. This could be possibly due to two factors; the size of the plasmid preventing intracellular uptake and/or the lack of plasmid delivery to nucleus. The size of the plasmid is a few MDa (r = 70 – 80 nm [184]) in general, which is about one or two order of magnitude larger than the proteins or fluorescent molecules we delivered ($r_{Calcein}$ = 0.6 nm [170], $r_{70\ kDa\ dextran}$ = 6 – 7 nm [172, 173], and r_{APC} = 11 nm [185]). According to the Stokes-Einstein equation, the bigger size

of the plasmid may result in the slower diffusion to and into the cells through the transient pores opened on the plasma membrane. Another possibility for the low transfection efficiency observed could be due to the cytosolic delivery of the method. Plasmids need to find the correct pathway to enter the nucleus, where the site of action is, and may be subject to rapid degradation in cytoplasm by other organelles or cytosolic nucleases [186]. Based on these points, the micronfluidic method may not be suitable for applications requiring intracellular plasmid delivery, such as gene therapy with the delivery of correct donor template along with nucleases, or the delivery to nucleus.

We experienced difficulty in using the microfluidic device for K562 cells unlike in DU145 or EU1 cells. Both DU145 and K562 cells show similar size measurement profile, with the peak of the cell diameter around 15 µm (Figure 4.9). Since the delivery method is based on the deformation and shear force at the constriction, we expected the comparable result for both cell lines due to similarity in physical characteristics, but the low delivery efficiency and the significant loss the K562 cell were observed after the treatment.

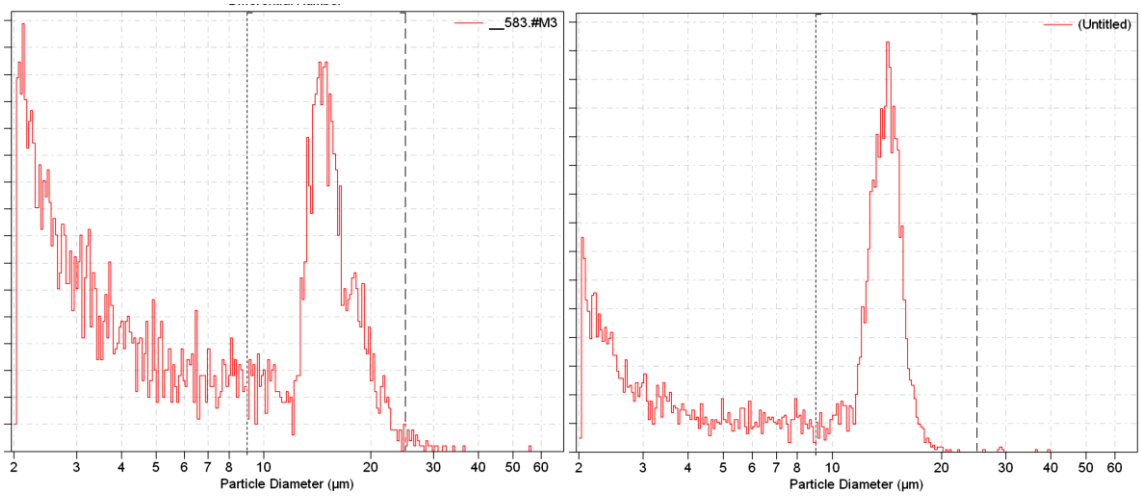

Figure 4.9. The Coulter counter measurement for the cell diameter (µm) of DU145 (left) and K562 (right) cells.

We considered a few factors that may have contributed to the unpredicted result with K562 cells. First, the difference in membrane structure or composition of DU145 and K562 cells can cause the difference in membrane rigidity. The decrease in plasma membrane fluidity is known to increase the membrane's resistance to shear in vitro [187].

The shape and membrane fluidity of different cells are determined by the composition of cytoskeleton, a network of complex biopolymeric molecules [188, 189]. Increase in resistance to shear is expected to decrease the intracellular uptake and can increase the chance of cells to become fragmented when force by pressure through constrictions instead of deforming to the constriction shape. Another possible factor for the cell loss of K562 cells could be the size or stiffness of the nucleus. In most types of leukemia cell lines, nuclei are known to be larger compared to normal leukocytes [190]. Nuclei size can dominate the leukemia cell deformability behavior, especially since nuclei of some cells are significantly stiffer than the whole cells [191-193]. We estimated the ratio of nucleus area to cell area (Figure 4.10) by taking fluorescence images of the cells stained for nucleus and plasma membrane. The nucleus:cell ratio (%) increased from 45% in DU145 cells to 55% in K562 cells and was significantly different (Student's t-test, $p = 0.038$). Although the change may not be substantial, there may be a threshold of the nucleus:cell ratio for the optimal result, high cell viability and high intracellular uptake, with the microfluidic device. These may suggest that the reason for low uptake and significant amount of K562 cell loss could be one or combination of these factors discussed.

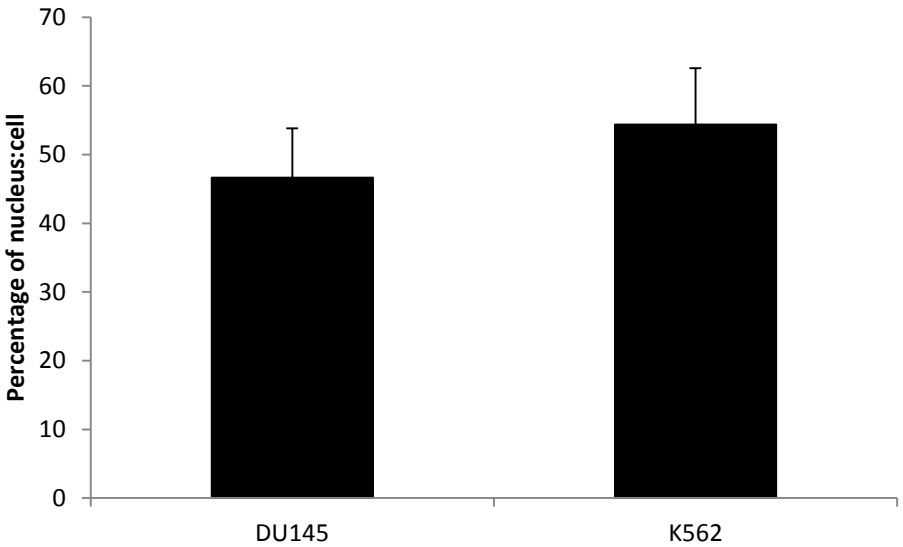

Figure 4.10. The nucleus:cell ratio (%) estimated by taking the cross-section images after staining both cell lines with Hoechst and CellMask orange plasma membrane stain for the nucleus and the plasma membrane, respectively. Data show average ± SD, n = 10.

As we observed the significant cell loss in K562 experiment and clogging in the microfluidic devices, we decided to look at the cell loss of EU1 after treatment and recalculate the uptake and viability based on the total number of cells we started with. Clogging in the constriction channel was observed with microscope after use and also visible with increase in time required to flow cells through the device, in some cases. We also noticed the significant number of cell loss after washing in K562 cells (Student's t-test, $p = 0.036$), which could be due to cells that were fragmented by the experiment and washed away after several washing steps. We concluded that the percentage of uptake and viability of EU1 cells were probably based on only the cells that were collected and intact after the treatment. While we observed the significant difference in intracellular uptake of fluorescent protein and high cell viability, comparable to the control, in all treated samples, the adjustment based on the total number of cells we started with changed the trend exhibited. Most of the treated sample had low viability compared to the control and the intracellular uptake did not vary significantly from sample to sample. This may be of a concern if the cells used are precious or the number of cells treated is critical for certain application.

4.5 Conclusion

This study examined the possibility of the intracellular delivery using a microfluidic device with constriction channels for cell deformation and shear. We have demonstrated the successful intracellular delivery of fluorescent molecules and proteins in DU145 and EU1 cells. Experimental factors, such as pressure, constriction width of the device, and size of the molecules, had effect on the delivery efficiency. However, we also identified a few drawbacks of the method that may limit the applications. Poor plasmid delivery and/or transfection efficiency and an incompatibility of the target cell lines may be considered when choosing the system. Also taking into account the cell loss in the device by clogging or fragmentation after treatment, the percentage of intracellular uptake and viability from the collected cells may not be accurate but probably have been overestimated as the denominator decreased with the cell loss.

CHAPTER V

NANOPARTICLE-MEDIATED INTRACELLULAR DELIVERY OF PROTEIN AND PLASMID

5.1 Introduction

Nanoparticles have gained interest over the years for many applications, especially in clinical applications of imaging, diagnosis and therapy. Nanoparticles can be synthesized in a number of different varieties based on the size, materials, synthesis methods, and shapes [117-121]. Especially in intracellular delivery, nanoparticles are advantageous since the small size of the particles allows the intracellular uptake by the endocytic pathway [194, 195]. The endocytosis kinetics depend on a number of factors, including materials and size [196]. In addition, different strategies allow the functionalization of the nanoparticle surface with a variety of ligands, based on the material properties, and the utilization for varying applications [197]. Therapeutic agents can be encapsulated into or coated on the surface of the nanoparticles for drug delivery across the cell membrane.

In this study, we exploited the use of nanoparticles for intracellular delivery to target leukemia cells, known as hard to transfect cells. First, we screened several materials of the nanoparticles for cell viability and a sign of intracellular uptake based on an initial study with HeLa cells. Next, we assessed the intracellular delivery using the chosen nanoparticles to demonstrate the delivery of therapeutic agents, such as proteins and plasmids.

5.2 Methods

5.2.1 Cell culture

Human myelogenous leukemia cells (K562, American Type Culture Collection, Manassas, VA), were cultured in a humidified atmosphere of 95% air and 5% CO_2 at 37°C. K562 cells were cultured with RPMI-16490 medium (Cellgro, Herndon, VA),

which was supplemented with 10% (v/v) heat-inactivated fetal bovine serum (FBS, Corning, Palo Alto, CA) and 1% penicillin/streptomycin (Cellgro) [180].

5.2.2 Nanoparticle preparation

Nanoparticles were prepared by first dissolving 0.5 g of hexadecyltrimethylammonium bromide (CTAB, Sigma-Aldrich, St. Louis, MO) in an aqueous solution of 70 ml of DI water, 0.8 ml of ammonium hydroxide (Sigma-Adlrich), and 20 ml of ethyl ether (Sigma-Adlrich), and stirring at room temperature. After 1.5 h, 2.5 ml of tetraethyl orthosilicate (TEOS, Sigma-Aldrich) was added quickly to the emulsion solution for the formation of silica particles and stirred at room temperature for an additional 4 h. The particle suspension formed was purified by washing three times with DI water and two times with 100% ethanol (KOPTEC, King of Prussia, PA) by centrifugation at 2500 g force for 5 min (Eppendorf, Hauppauge, NY). The precipitate was resuspended in 20 ml of 100% ethanol and added to etching solution, composed of 100 ml of 100% ethanol and 15 ml of hydrochloric acid (HCl, Sigma-Adlrich), to form mesoporous silica nanoparticles. The suspension was covered and continuously stirred at 70 ˚C for 16 h. Then the particle suspension was purified and washed three times with 100% ethanol and three times with DI water. The precipitate was resuspended in 20 ml of DI water and ultrasonicated using an ultrasonic processor VC 505 (Sonics & Materials, Newtown, CT) for 5 min at 25% amplification in an ice bath to prepare well-dispersed mesoporous silica nanoparticles.

The concentration of the nanoparticles was measured by drying 2 µl of the suspension on a glass slide and measuring the changes in weight before and after drying on the ultra-micro-balance (SE2, Sartorius, Bohemia, NY). The size and zeta potential of the nanoparticles were measured by a Zetasizer Nano ZS90 (Malvern Instruments, Westborough, MA).

5.2.2.1 Protein loading

To load protein inside the pores of the mesoporous nanoparticles, varying concentrations of FITC-BSA (Sigma-Aldrich) or tetramethylrhodamine (TMR)-BSA (Invitrogen, Grand Island, NY) were prepared in 200 µl of RPMI. An equal volume of

nanoparticle suspension was added to the solution of fluorescent proteins. The mixture was well dispersed by vortexing for 30 s and was continuously shaken at 270 rpm for 1 h at 25 °C. The protein-loaded nanoparticles were separated from the supernatant, containing excess proteins, by centrifugation at 5900 g force for 10 min in the microcentrifuge 5415R (Eppendorf). The amount of fluorescent protein loaded was calculated by subtracting the fluorescence measured by spectrofluorometer before and after the loading process.

5.2.2.2 Plasmid loading

The nanoparticles loaded with proteins were prepared for layer-by-layer assembly to modify the surface charge of the nanoparticles for the plasmid coating. Nanoparticles were re-dispersed in 500 µl of DI water and added to 500 µl of polyelectrolyte solution, a solution of 0.2 M NaCl (Sigma-Aldrich) with a final concentration of poly-L-lysine hydrochloride (PLL, Sigma-Aldrich) of 5 mg/ml. After 15 min of coating time, the nanoparticle suspension was purified from the polyelectrolyte solution by centrifugation and washed with DI water.

Poly-L-glutamic acid sodium salt (PGA, Sigma-Aldrich) was mixed with plasmid DNA at a ratio of 1:3.76 by weight for 20 min in 10 mM 4-(2-Hydroxyethyl)-1-piperazineethanesulfonic acid (HEPES, Sigma-Aldrich) buffer containing 150 mM NaCl. The plasmids used were Label IT Plasmid Delivery Controls, Fluorescein (Mirus Bio, Madison, WI) and the plasmid DNA (pDNA) encoding green fluorescent protein (GFP), gWIZ^{TM}-GFP (Aldevron, Fargo, ND). In a separate vial, protein-loaded nanoparticles were resuspended in a same HEPES buffer solution. The two solutions were mixed together by vortexing for 30 s, and incubated at room temperature for 30 min. The resulting plasmid-coated nanoparticles were purified from the polyelectrolyte/DNA solution by centrifugation and washed three times with DI water. The plasmid concentration in the supernatant was measured by a Nanodrop ND-1000 (NanoDrop Technologies, Wilmington, DE) to calculate the amount of plasmid adsorbed onto the surface of the nanoparticles.

5.2.3 Sample preparation

K562 cells were harvested and re-suspended in RPMI. Cell concentration was measured by a Multisizer 3 Coulter Counter (Beckham Coulter, Fullerton, CA) and prepared for the experiment by plating on 24-well cell culture plates (Corning, Corning, NY) with a final volume of 500 µl containing 1 – $2x10^5$ cells per sample. The nanoparticles loaded with protein and/or coated with plasmid were added to the cells. The positive controls for plasmids were prepared using Lipofectamine 200 transfection reagent (Invitrogen), following the manufacturers protocol.

The cells were incubated with nanoparticles at 37°C for 24 h to 72 h. The cells were washed three times with PBS (Cellgro) at 300 x g for 5 min to remove excess nanoparticles in the medium. After the third wash, the cells were resuspended in PBS for analysis. Propidium iodide (PI, Invitrogen) or SYTOX Green/Blue nucleic acid stain (Invitrogen) was added at a final concentration of 5 µg/ml or 100 nM, respectively, 10 - 15 min before flow cytometry analysis to stain non-viable cells and thereby determine cell viability. As a general nucleus stain, Hoechst 33342 (trihydrochloride, Invitrogen) was added at a final concentration of 2 µg/ml for 20 min.

5.2.4 Analysis and Quantification

The uptake of fluorescent dyes or plasmid transfection and cell viability were measured using a bench-top flow cytometer (BD LSRII, BD Biosciences, San Jose, CA). The data were collected and analyzed in FACSDiva software (BD). Approximately 10,000 events were collected per sample. For cell viability, PI, SYTOX green, and SYTOX blue were analyzed using a PerCP-Cy5, 670 nm longpass filter, a FITC, 530/30 nm bandpass filter, and a BV473/10, 473/10 nm bandpass filter, respectively, for emission. The uptake of FITC-BSA, fluorescein delivery control and pGFP transfection were measured by a FITC, 530/30 nm bandpass filter for emission. The uptake of TMR-BSA was measured by a PE, 575/26 nm bandpass filter for emission.

The cell gate was constructed based on forward- and side-scatter light of the untreated control cells. Any events within this gate were considered to be intact cells while any events outside the gate were considered to be cell debris or other noise. To determine which cells had taken up fluorescent marker compounds (i.e., FITC-BSA,

TMR-BSA, and fluorescein delivery control for uptake; PI, SYTOX green, and SYTOX blue for viability), histogram gates were set by the sham control which had fluorescent dyes in the solution but was not treated in order to account for extracellular staining and other noise. To set gates and account for possible spectral overlap between the dyes, compensation controls were prepared and tested.

Cells were imaged using an inverted fluorescence microscope (Olympus IX70, Olympus, Center Valley, PA). Using cellSense Standard software (Olympus), images were taken at 20x or 40x magnification and captured using appropriate filters.

5.2.5 Statistical analysis

A minimum of three replicates was performed for all conditions. Means and standard deviations were calculated from the replicates. An unpaired Student's t-test or analysis of variance (ANOVA) was performed using Minitab 17 (Minitab, State College, PA). A value of $p < 0.05$ was interpreted as significant.

5.3 Results

Note: In this collaborative study, the design and fabrication of the nanoparticles was carried out by Dr. Hong-Wei Yang and the intracellular delivery and transfection experiments were carried out by Seonhee Park.

5.3.1 Nanoparticle screening

As nanoparticles have gained popularity over the years for application in intracellular delivery, we screened for suitable nanoparticles to be used for the co-delivery of proteins and plasmids into K562 cells. Several materials of the nanoparticles were chosen based on the previous success with intracellular uptake in HeLa cells (Table 5.1). The nanoparticles were prepared by adsorbing the negatively charged plasmid DNA encoding for GFP onto the positively charged surface of the particles. The candidates were screened based on the cell viability and the transfection efficiency in K562 cells 24 h after incubation with nanoparticles. Despite the promising results with HeLa cells, most of results with K562 either resulted in low cell viability (< 50%) or low pGFP transfection efficiency (< 5%) (data not shown). There was only one exception among the

number of the candidates tested, which was the mesoporous silica poly-l-lysine (PLL) nanoparticles, which were chosen for further intracellular delivery experiments because of the good cell viability observed and for the feasibility of co-delivering protein and plasmid.

Table 5.1. List of nanoparticle tested

List of nanoparticles tested (Core + Shell)	
Core	**Shell**
PLGA (poly(lactic-co-glycolic) acid)	PEI (Polyethylenimine)
PLGA	Chitosan
PEO (Polyethylene oxide)	Chitosan
PAAMA (acrylic acid – maleic anhydride copolymer)	Chitosan
Silica	PEI
Poly-l-lysine	PEG (Polyethylene glycol)
Silica	Poly-l-lysine

The scanning electron microscope (SEM) image of the mesoporous silica poly-l-lysine (PLL) nanoparticles was obtained for visualization (Figure 5.1). The diameter of the nanoparticles appeared to vary but was approximately 100 nm. The size of the nanoparticles was suitable for intracellular uptake by endocytosis as demonstrated in the previous studies with gold and silica nanoparticles [198, 199]. The resolution of the SEM was not good enough to capture the mesoporous feature of the nanoparticles.

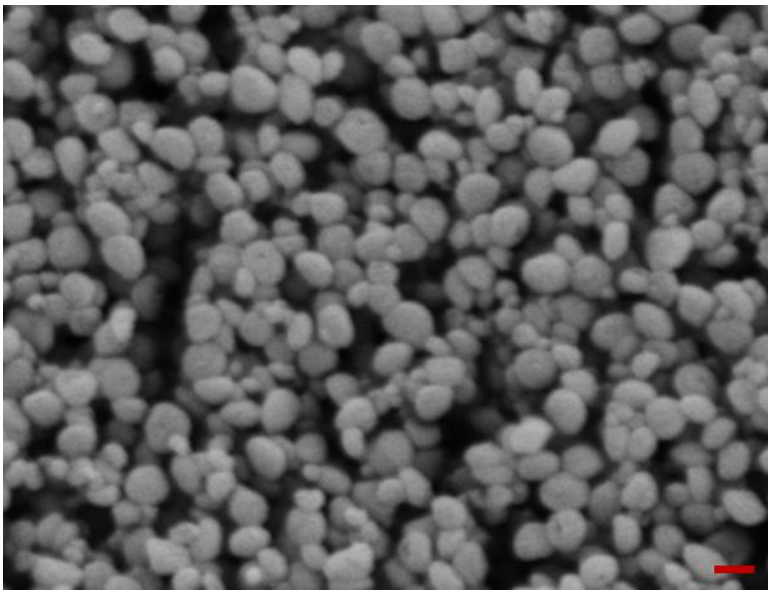

Figure 5.1. Scanning electron microscope (SEM) image of the mesoporous silica/PLL nanoparticles. Scale bar (red) is 100 nm.

The mesoporous silica/PLL nanoparticles were prepared for intracellular delivery by loading fluorescent protein and plasmid as shown in the schematic (Figure 5.2, top). The fluorescent protein was encapsulated within the pores of nanoparticles and was saturated at about 0.53 µg per 1 µg of nanoparticles (Figure 5.2, bottom left). The plasmid was adsorbed onto the surface of nanoparticles by coating the surface with positively charged poly-L-lysine. For 1 µg of nanoparticles, about 0.27 µg of plasmid GFP could be loaded (Figure 5.2, bottom right). Once the nanoparticles were loaded with protein and plasmid, they were incubated with cells for intracellular delivery to observe the delivery of proteins and the transfection of plasmid GFP.

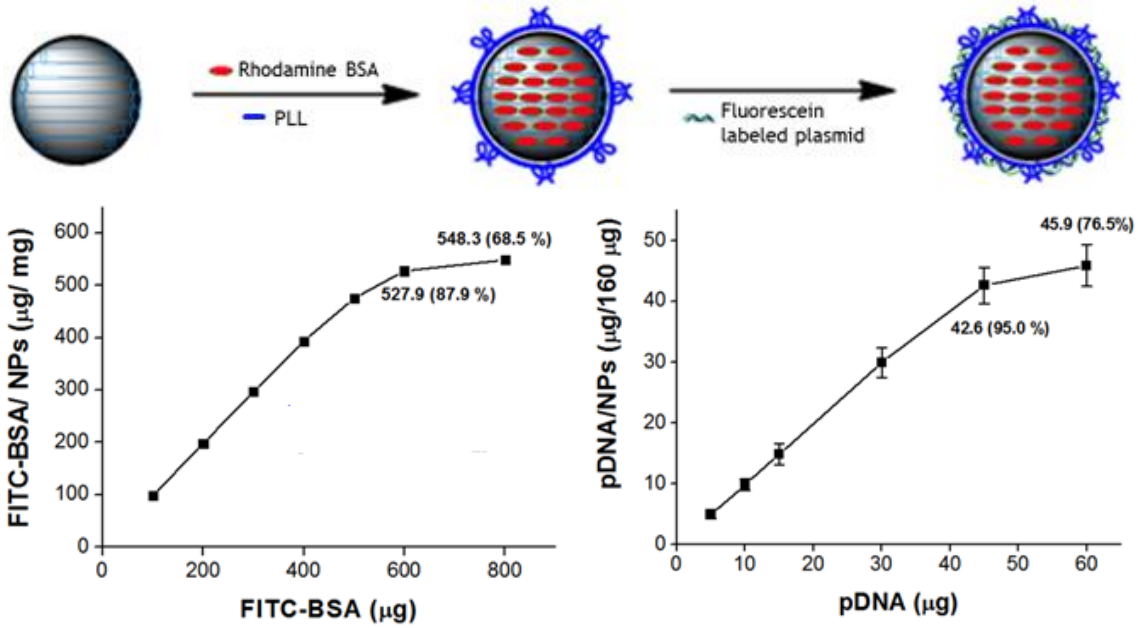

Figure 5.2. Protein and plasmid loading in the mesoporous silica/poly-l-lysine (PLL) nanoparticles. Schematic of the loading process (top) where red, blue and green corresponds to rhodamine BSA, PLL and fluorescein labeled plasmid, respectively. The loading efficiency of protein (bottom left) and plasmid DNA (bottom right) per 1 mg and 0.16 mg of nanoparticles, respectively. Data show average ± standard deviation (SD), n = 3.

5.3.2 Nanoparticle mediated intracellular delivery

The intracellular delivery was first studied in HeLa cells and examined under the fluorescence microscope 24 h post-incubation with nanoparticles (Figure 5.3). The red or green fluorescence was not observed in control samples (Figure 5.3, a and b), indicating that there was no intracellular uptake of naked plasmid or protein by endocytosis. However, the samples treated with nanoparticles (Figure 5.3, c) showed successful intracellular delivery of protein and plasmid as the corresponding red and green fluorescence was observed in the cytoplasm. Further study with nanoparticles loaded with rhodamine BSA and pGFP showed both the delivery of BSA and the transfection of GFP (data not shown). The percentage of BSA uptake was 82.55 ± 0.78% while the transfection efficiency was only 31.65 ± 3.89%, which was comparable to the transfection efficiency of about 32% by lipofectamine. The intracellular delivery of both protein and plasmid by nanoparticles was therefore demonstrated in HeLa cells and provided the basis for the further study in K562 cells.

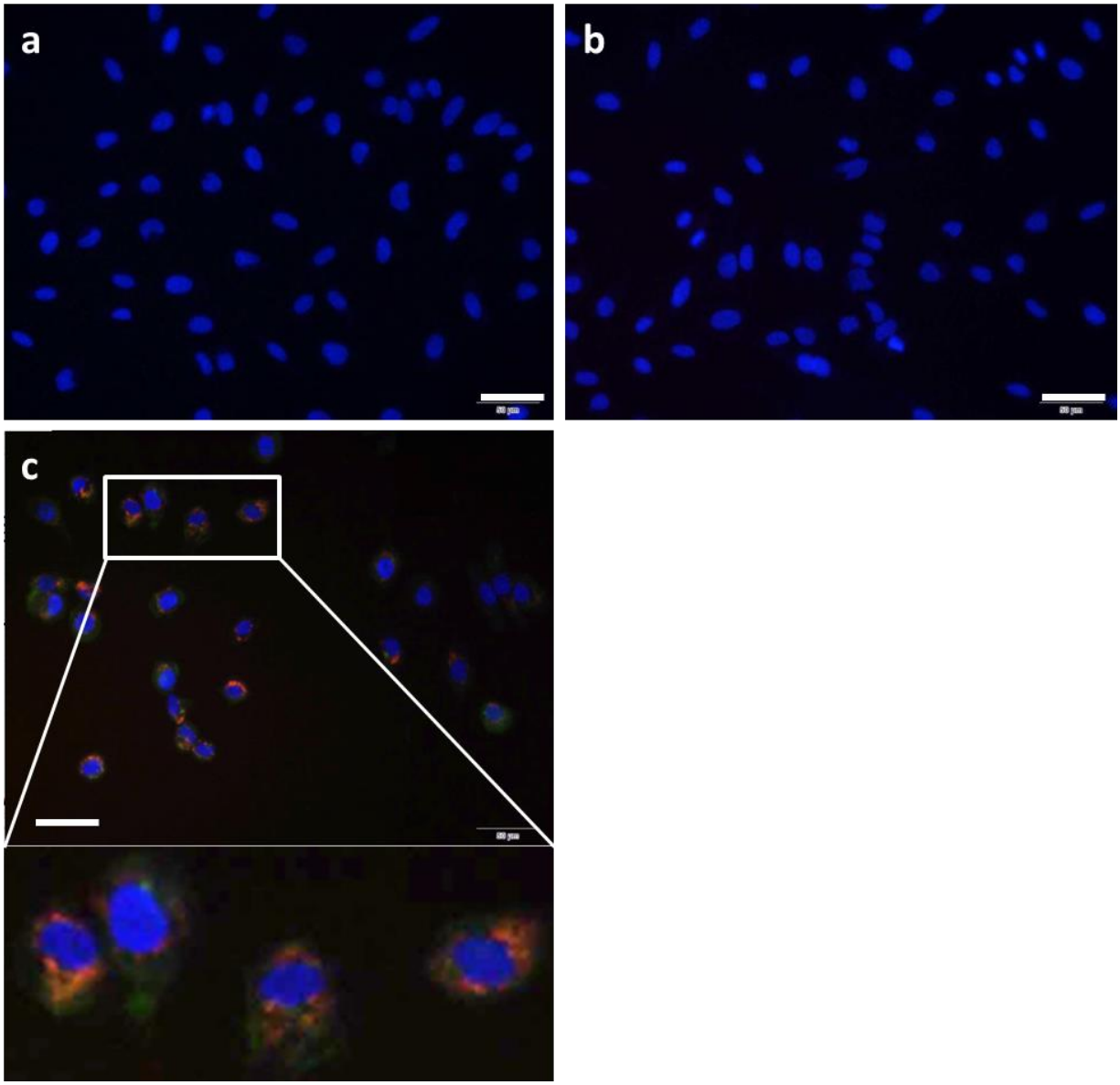

Figure 5.3. Fluorescence images showing the intracellular uptake of rhodamine BSA (red) and fluorescein-labeled plasmid (green) in HeLa cells. Cell nucleus was stained with Hoechst dye (blue). Each sample was treated with a) fluorescein-labeled plasmid control, b) rhodamine BSA control, and c) rhodamine BSA and fluorescein-labeled plasmid loaded nanoparticles. The higher magnification image of the image in c) shows the intracellular uptake both rhodamine BSA and fluorescein-labeled plasmid. Scale bars (white) are 50 µm.

Based on the results obtained with HeLa cells, we moved on to test the intracellular delivery in K562 cells. First, the delivery of both rhodamine BSA and fluorescein-labeled plasmid was observed with the fluorescence microscope after 24 h (Figure 5.4). The control samples incubated with naked fluorescein-labeled plasmid (and no rhodamine BSA) did not show any green fluorescence inside the cells (Figure 5.4, a). The positive control treated by lipofectamine with fluorescein-labeled plasmid (and no rhodamine BSA) showed weak green fluorescence, indicating the intracellular uptake of the naked plasmid (Figure 5.4, b). Both red and green fluorescence was observed in the cytoplasm of cells incubated with nanoparticles containing fluorescein-labeled plasmid and rhodamine BSA, as seen previously with HeLa cells (Figure 5.4, c).

Once the delivery of both protein and plasmid was demonstrated, we replaced the fluorescein-labeled plasmid with plasmid encoding GFP to determine the transfection efficiency. The delivery efficiency of fluorescein protein and transfection efficiency of pGFP after 24 h were quantified with flow cytometry (Figure 5.5). The delivery efficiency of rhodamine BSA with nanoparticles was approximately 65% which was slightly lower than the delivery efficiency in HeLa cells. The transfection efficiency of pGFP was only about 2% and decreased significantly from the transfection efficiency of 15% in lipofectamine (Student's t-test, $p = 0.000$). Although nanoparticles were loaded with both rhodamine BSA and pGFP, the transfection efficiency dropped significantly from the delivery efficiency (Student's t-test, $p = 0.000$). In K562 cells, the delivery efficiency or transfection efficiency was lower than HeLa cells, but co-delivery of protein and plasmid was demonstrated in both cell lines using the mesoporous silica/PLL nanoparticles.

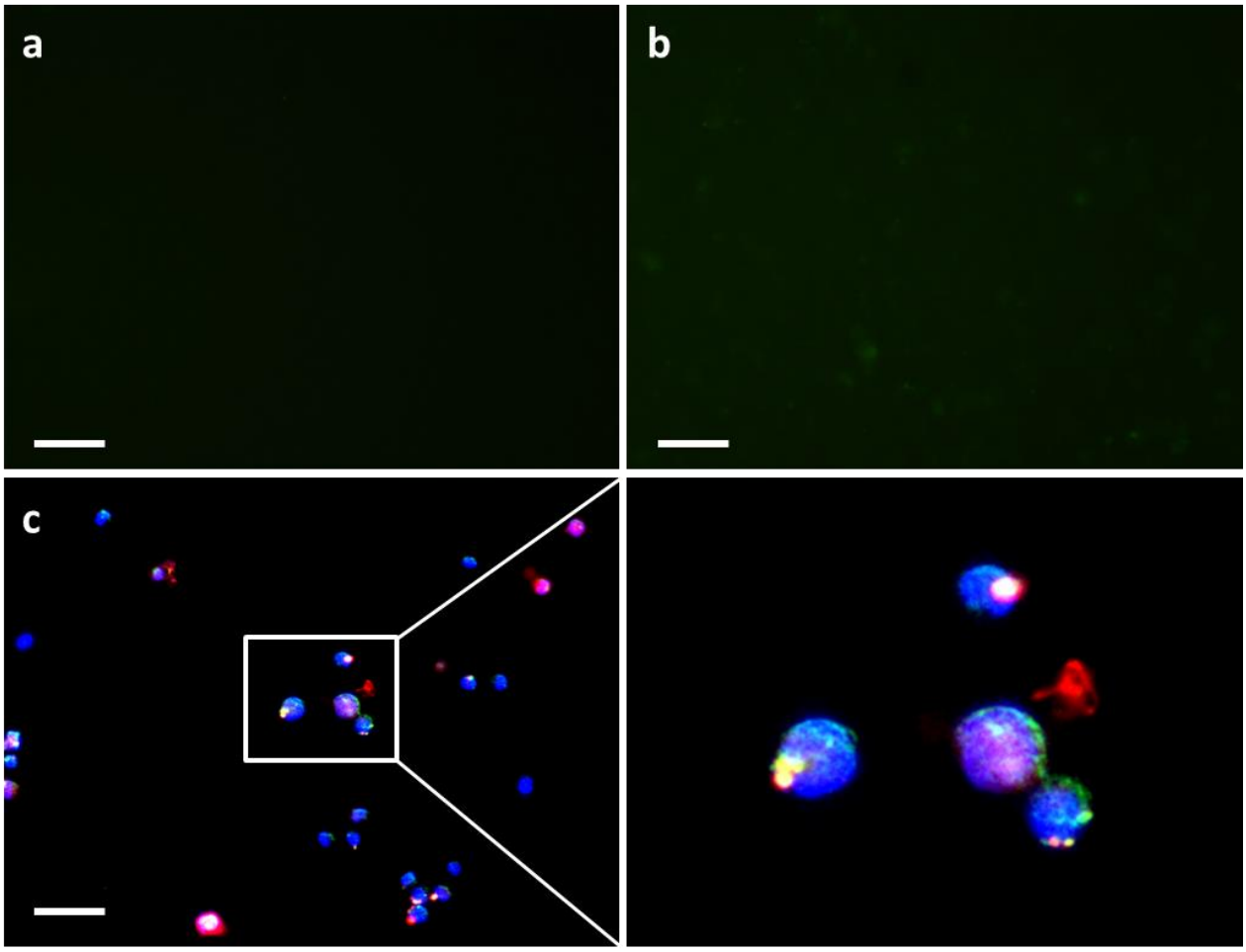

Figure 5.4. Fluorescence images showing the intracellular uptake of rhodamine BSA (red) and fluorescein-labeled plasmid (green) in K562 cells. Cell nucleus was stained with Hoechst dye (blue). Each sample was treated with a) fluorescein-labeled plasmid control, b) lipofectamine, and c) rhodamine BSA and fluorescein-labeled plasmid loaded nanoparticles. The higher magnification image of the c) shows the intracellular uptake both rhodamine BSA and fluorescein labeled plasmid. Scale bars (white) are 50 µm.

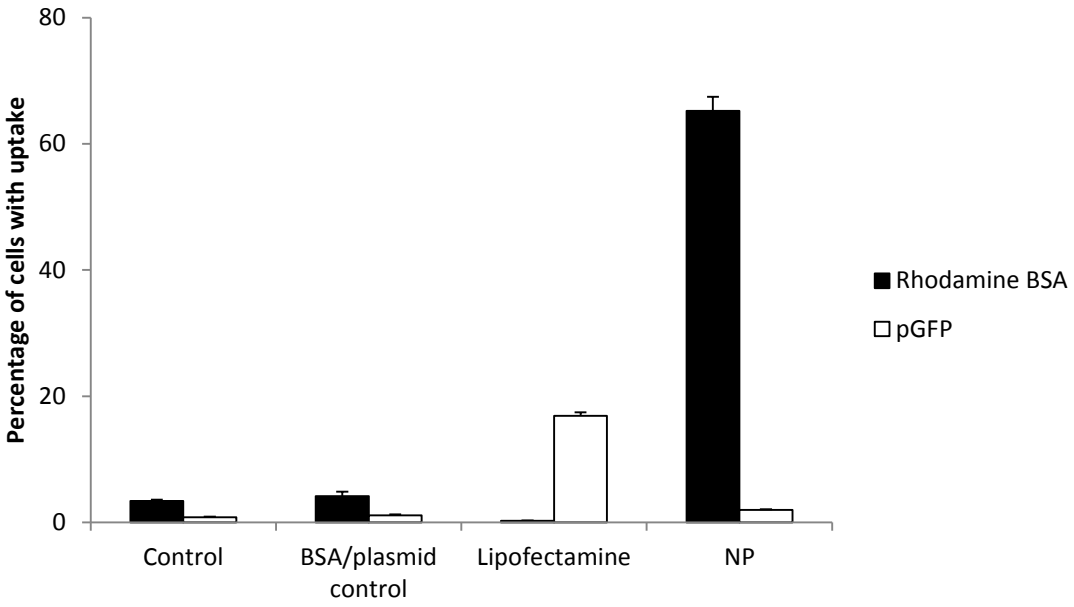

Figure 5.5. The delivery efficiency of rhodamine BSA (black) and the transfection of plasmid GFP (white) in K562 cells 24 h after treatment with lipofectamine or nanoparticles. Data show average ± standard deviation (SD), n = 3.

5.4 Discussion

From a number of nanoparticles tested, the mesoporous silica/PLL nanoparticles showed the most promising result on the intracellular delivery of protein and plasmid in both HeLa and K562 cells. Although nanoparticles were successfully used for the intracellular delivery in HeLa cells, the viability or the transfection efficiency was not as great in K562 cells. The suspension cells, especially primary and leukemia cells, were previously referred as "hard to transfect" cells and resulted in lower transfection efficiency compared to the adherent cells when commonly used transfection methods were used [200, 201]. This could be due to the dependence of many transfection methods on the cell cycle. Previous study showed that the rate of endocytosis increased with the increase in cell size and membrane expansion during mitosis [202]. As a result, the internalization of nanoparticles varied according to the different phases of cell cycle and was fastest at G2/M phase [203]. Similarly, the transfection efficiency of K562 cells using lipofectamine was found to depend heavily on the cell cycle due to change in cell size [204]. HeLa cells in suspension exhibited the similar behavior but the cell proliferation could be affected by the culture condition; i.e. suspended ovarian cancer

cells were found to have lower cell masses and to remain in a proliferation-quiescent sate compared to adherent monolayers [205]. Thus, the performance of nanoparticles could diminish significantly when used with suspension cells and may need to be optimized for cell viability and the intracellular uptake as the intracellular uptake depends on materials, size, and shape of the nanoparticles.

Although mesoporous silica/PLL nanoparticles were loaded with both protein and plasmid in this study, the transfection efficiency was significantly lower than the delivery efficiency of protein in both HeLa and K562 cells. This could be due to several factors in the process. First, the plasmid degradation over time could reduce the actual amount of active plasmid delivered inside the cells from the initial loading amount. In previous study with PLGA nanoparticles, the plasmid degradation due to the acidic microenvironment inside the particles resulted in the lower amount of active plasmid released [206]. The interaction between poly-L-lysine and the plasmid could result in degradation of active plasmid over time. Alternatively, the release of plasmid from the nanoparticle could be faster than the time required for the intracellular uptake of nanoparticles. Using gold nanoparticles, the intracellular uptake was fully achieved 6 h after incubation [207]. Due to the difference in size and materials, the estimate time would be different but the time required for the intracellular uptake of nanoparticles would be still a few hours after incubation. If the plasmid is dissociated from the PLL coating on the surface of nanoparticles at a faster rate than the uptake, the actual delivery amount of plasmid could reduce from the loading amount. Lastly, the difference in the intracellular uptake mechanism between lipofectamine and the nanoparticles could have attributed to the low transfection efficiency, especially in K562 cells. The intracellular uptake in lipofectamine is achieved as positively charged liposomes fuse with the negatively charged cell membrane [208]. The nanoparticles are taken inside the cells by endocytosis and the rate would depend on the cell-type, size, charge, and other surface properties [209]. It could be possible that in K562 cells, the intracellular uptake pathway of nanoparticles is not as tolerated as in HeLa cells. Overall, there are many possibilities that could explain the lower transfection efficiency compared to the delivery efficiency of protein; further study is required to more fully understand the problem.

5.5 Conclusion

The intracellular delivery using nanoparticles was evaluated and demonstrated in HeLa and K562 cells. From the several candidates of nanoparticles, mesoporous silica/PLL nanoparticles were chosen due to the good viability with K562 cells and the possibility of delivering both protein and plasmid. Intracellular delivery to HeLa and K562 cells was demonstrated by preparing the nanoparticles with protein encapsulated inside the pores and plasmid adsorbed onto the surface. Successful delivery of protein and plasmid were validated by the fluorescence inside the cytoplasm. Transfection of plasmid GFP was also compared to the positive control by lipofectamine; in HeLa cells, the nanoparticles performed comparably, while in K562 cells, the transfection efficiency dropped significantly. Overall, the nanoparticles performed better in HeLa cells than in K562 cells, but demonstrated the possibility of co-delivering protein and plasmid in both cells, which would be useful especially in gene therapy.

CHAPTER VI

DISCUSSION

The intracellular delivery methods have been studied for many years to efficiently deliver drugs across the cell membrane. Since the applications of intracellular delivery are widespread from research settings to clinical settings, the simple and effective methods need to be developed for successful results. In this study, we have developed and/or evaluated new intracellular delivery methods, including nanoneedle-mediated methods, microfluidic device, and nanoparticles, to address some of the limitations posed by the commercially available intracellular delivery methods. To evaluate the result and optimize the process, it was necessary to set few criteria based on the applications of the intracellular delivery. The criteria can be set for two major categories; in the laboratory and the clinical settings.

In the laboratory settings, the intracellular delivery would be conducted to perform biochemical assays and to develop stable cell lines for in vitro studies. For these types of studies, it would be ideal to treat as many cells as few thousands to millions and be dependent on the throughput of the intracellular delivery methods to achieve the required sample size. For experiments that are conducted on a daily basis, the methods also should be simple and quick to use and the cost of the materials should not be too expensive per each experiment. The cell types used in these applications may not be hard to obtain or culture and have homogeneous cell population. Accordingly, several experiments can be easily conducted until the methods are optimized and having a low viability would be acceptable as long as the number of treated cells reach the required level.

On the other hand, the examples of intracellular delivery application could be in the gene therapy using nanomedicines and the cellular engineering. In these applications, the cells types may come in a limited quantity and the efficient delivery would be necessary along with high cell viability to maximize the effort. The primary and progenitor cell types are heterogeneous and the patient to patient variability could result in varying viability and efficiency based on the methods. Thus, the delivery methods

should not require too much optimization based on the cell structure or type and the throughput of the method would depend on the number of cells required for each application, which could be still several hundreds to thousands. In addition, the therapeutic agents are macromolecules, such as proteins and plasmids, and may be available in small amounts, i.e. based on the production of engineered ZFNs, TALENs, and donor plasmids. The intracellular delivery methods should be designed to not waste the reagents and make best use of these.

Based on these guidelines, we assessed the feasibility of using commercially available methods and the new intracellular delivery methods for the applications in research and clinical settings. Among the number of biological, chemical, and physical intracellular delivery methods, we focused on lipofectamine, electroporation, and microinjection as a standard to compare to. Lipofectamine is a chemical method and has been used for years due to the simplicity of the method and well developed protocol. The method is great for laboratory settings, especially with the adherent cells. However, the efficiency decreases with suspension cells and the delivery materials are limited to plasmid and siRNA. Lipofectamine may not be suitable for the clinical applications due to varying efficiency in cell types and toxicity issues.

Electroporation is a physical method that has been used widely and studied extensively. Amaxa nucleofector and other commercially available equipment have optimized protocol for many cell types and would work well in research settings. However, for the cell types that are not optimized, especially for primary and progenitor cells, the electroporation conditions need to be optimized for cell viability and transfection efficiency. Once the optimized protocol is available for the desired cell type, the electroporation can be used for both laboratory and clinical applications since any macromolecules can be delivered.

Lastly, microinjection is another physical method and is very effective due to direct delivering molecules intracellularly by using glass pipettes. Despite this advantage, the method has limited potential due to the low throughput of the method since cells are poked one at a time manually. Not as much optimization is required for cell variability, but microinjection may be difficult to use in most of the laboratory or clinical settings where large number of cells need to be injected.

Our studies on the new methods may offer advantages of the existing intracellular delivery methods that would be beneficial to some of the applications. In both nanoneedle-mediated intracellular delivery methods, the delivery of fluorescent molecules was observed. In puncture loading, the delivery was possible by physical transient hole created on cell membrane by nanoneedles, similar to microinjection, and the possibility of the nuclear targeting was also observed with confocal microscopy, which would be favorable in case of protein and plasmid delivery. Since the intracellular uptake is possible with the physical puncture by nanoneedles, the methods may not need to be optimized meticulously for each cell type. While the results were not as promising in the suspension cells, the treatment of adherent cells showed the delivery of macromolecules and can be done without detaching the cells. The array of nanoneedles allowed the treatment of tens of thousands cells at once. Both puncture loading and centrifuge loading methods are relatively simple and easy to use, except the nanoneedles fabrication part. Overall, nanoneedle-mediated delivery methods can be integrated with number of laboratory applications, where large number of cells, especially adherent, needs to be treated.

The microfluidic device was effective in delivering molecules across the cell membrane by squeezing the cells through the constriction channels as demonstrated in the literature [8]. The treatment of several thousand cells at an experiment was possible by the tens of channels in parallel. Also the experiments can be done easy and quickly, within few seconds, once all the systems are set-up. The delivery of different protein molecules was achieved with the delivery efficiency of about 20% in EU1 cells using the optimized condition. Once the certain cell type can be optimized using the available chip designs, the microfluidic device would be useful for number of applications where the large number of cells need to be treated.

Lastly, nanoparticles were studied for the intracellular delivery of protein and plasmid. Among number of nanoparticles we tested, mesoporous silica/PLL nanoparticles was chosen for further investigation. Since the throughput of the nanoparticle delivery method would depend on the nanoparticle concentration, the sample size can be adjusted easily. The plasmid transfection efficiency of HeLa cells was comparable to that of the positive control by lipofectamine. The results suggests that nanoparticles can perform

similar to commercially available method and can be more favorable for other applications since the co-delivery of protein and plasmid by encapsulation and coating, respectively, is possible.

These intracellular delivery methods bring unique advantages in addition to already available methods, but there are still limitations, which can or cannot be further improved, as these methods are still early in the development stage. Nanoneedle-mediated methods exhibited the limited success with the suspension cells. The suspension cells could not be attached firmly to the surface for the puncture loading. Centrifuge loading could treat the cells in suspension but the delivery of macromolecules was challenging. The delivery of macromolecules, especially proteins and plasmid transfection, will need to be further studied in both delivery methods for the extended application in clinical or research settings. In order to minimize the diffusion limit of the macromolecules and reduce the amount of reagent required, the coated nanoneedle can be exploited. Finally, the use of nanoneedles may be limited to once or few times, as we have seen in the centrifuge loading. The limited use of nanoneedles would require mass production in order to be widely used for different applications.

The microfluidic device showed the intracellular uptake of protein, but the plasmid transfection was trivial. Due to the cytoplasmic delivery, the nuclear targeting is hard to achieve. Also as we have observed the low viability and lack of intracellular uptake with K562 cells, the device may not be feasible to use or optimize for certain cell lines, which could be based on the membrane or nucleus elasticity and the nucleus size. Similar to nanoneedles, the microfluidic device can be used for a limited number of times, as the clogging of the cells can cause the constriction channels to block. The microfluidic device could be challenging to use for the gene therapy, where delivery of plasmid may be necessary or target cells may be difficult to optimize with currently available device designs.

The nanoparticles showed the co-delivery of protein and plasmid in HeLa and K562 cells but the intracellular uptake was reduced in K562 compared to HeLa cells. The uptake efficiency and cell viability with nanoparticles can vary with different cell types and may need to be optimized. The optimization could be challenging as the only optimization option would be the size of the nanoparticles without changing the

materials. In addition, the clearance of the nanoparticles after treatment could be problematic since the nanoparticles can accumulate in body based on the size [210, 211]. The accumulation of nanoparticle can have additional effect in long-term and the better washing technique may need to be investigated.

Conventional and new intracellular delivery methods we studied and compared have been summarized in Table 6.1. Overall, we studied new intracellular delivery methods that can further improve the commercially available intracellular delivery methods in terms of delivery efficiency and possible applications. Although the novel intracellular delivery methods were not able to completely overcome the challenges of the conventional methods, these opened up new options for intracellular delivery applications in research and clinical settings.

Table 6.1 Summary of the intracellular delivery methods

Method	**Delivery method**	**Cell type[1]**	**Delivery of**			**Throughput**	**Advantage**	**Disadvantage**
			Fluorescent molecules[1]	**Proteins[1]**	**Plasmid[1]**	**(cells/sample)**		
Lipofectamine	Chemical	HeLa K562	-	-	pGFP	1000 – 1000000	Easy to use	No protein delivery Possible toxicity
Electroporation	Electrical	K562	Calcein	FITC-BSA	pGFP	250000 – 1000000	Easy to use	Requires cell-specific optimization Costly equipment
Microinjection	Needle	658D	Calcein	-	-	1	Nuclear targeting Little optimization required	Very low throughput
Puncture loading	Nanoneedles	DU145 K562	Calcein 70 kDa Dextran 500 kDa Dextran	Antibody	pGFP	30000 – 80000	High throughput Possible nuclear targeting	Cannot treat suspension cells
Centrifuge loading	Nanoneedles	DU145	Calcein	FITC-BSA	pGFP	62500 – 250000	High throughput	Low delivery efficiency of macromolecules
Microfluidic device	Shear stress	DU145 K562 EU1	Calcein	APC Halo-TALEN	-	300000	High throughput Effective protein delivery	No plasmid transfection
Nanoparticles	Endocytosis	HeLa K562	-	FITC-BSA Rhodamine-BSA	Fluorescein-labeled plasmid pGFP	1000 – 1000000	Co-delivery of protein and plasmid	Varying efficiency Clearance of nanoparticles

[1]used in this thesis.

CHAPTER VII

RECOMMENDATIONS

7.1 Nanoneedle-mediated intracellular delivery methods

7.1.1 Coated nanoneedles for the intracellular delivery

The intracellular delivery methods using nanoneedles were conducted mainly by mixing the fluorescent molecules in the solution before the experiment. Thus, the intracellular uptake process was dominated by the diffusion of the molecules through the transient holes on cell membrane. Instead, it would be beneficial to look into the possibility of coating or modifying a surface of the nanoneedles array to avoid the diffusion limitation and to directly deliver the molecules as in the microinjection. Nanoneedles array can be coated with molecules simply by dispensing small amount of solution and wait for the solution to evaporate as done similarly in the previous studies on nanofiber or nanowire arrays [112, 113]. Another possibility would be to use the surface chemistry to covalently bind and would be especially useful for the delivery of plasmid. Previously, the carodiimide-mediated condensation reaction was performed to bind plasmid to carbon nanofiber arrays [212]. Similarly, plasmid can bind to the silicon nanoneedles array by surface functionalization, i.e. making the surface hydrophobic or oxidation [213, 214].

The coating or the surface modification of the nanoneedles array would be a worthwhile study to observe the effect on the intracellular uptake. While these methods could be promising, several subsequent studies would be necessary to optimize the process as well. The amount of loading on nanoneedles should be optimized in order to not add too much thickness to the nanoneedles, which could affect the nanoneedle tip diameter. The loading of the molecules could not be evenly spread out through the array or mainly localized within the trenches, instead of the nanoneedles itself. In addition, the intracellular delivery methods should reflect the time required for the molecules to detach from the surface and enter the cell cytoplasm or the nucleus. Once the method is

established, the effect of the delivery efficiency, especially of macromolecules, can be studied by comparing with the existing experimental procedure.

7.1.2 Imaging

In order to understand and observe the intracellular delivery by nanoneedles in more details, the imaging with better spatial and temporal resolution would be essential. One of the possible techniques is scanning electron microscope (SEM), which utilizes the focused beam of electrons. Nanoneedles can be imaged after the experiments to observe the puncture by nanoneedles on the cell membrane. It would be also possible to determine the effect of various centrifuge loading parameters on the puncture depth and its correlation to the intracellular uptake. The SEM technique has been used for many decades for the imaging of samples in the nanoscale but the imaging of wet samples has been challenging. The samples can be imaged by either using an environmental SEM or a cryo-SEM technique. Environmental SEM is capable of imaging partially hydrated samples at low vacuum [215, 216], but obtaining the images with acceptable resolution and contrast may be difficult [217]. Another possibility is to prepare frozen samples by several dehydration steps prior to imaging [218]. The extensive sample preparation steps could be challenging to preserve the samples as it is without altering it. Both imaging techniques could make the imaging of cells after the treatment challenging, but it would be an interesting study to look at the interaction between cells and nanoneedles.

Further confocal microscopy imaging would be also important to validate the intracellular delivery process using nanoneedles. Real-time imaging of the intracellular uptake would be valuable to understand the time scale of the uptake and the cell membrane resealing process with nanoneedles. Capturing good quality real-time images would depend on the temporal resolution of the system as well as designing a simple system that would hold the nanoneedles in place instead of continuously pushing down on the cells and changing the focus. Although fluorescence and confocal microscopy images demonstrated the intracellular uptake of fluorescent molecules, the further studies of the intracellular uptake process were limited by the resolution of the microscope. Due to the limited spatial resolution, it is difficult to view the nanoneedles at the tip, where the diameter is about 20 nm, but nanoneedles are only visible when the tip diameter is about

few hundreds of nanometers diameter. Nanoneedles can be coated with fluorescent molecules to possibly enhance the view and observe the interaction with the cells, instead relying on the presence of black holes on the fluorescence filter. Another option would be to try the super resolution fluorescence microscopy, where the spatial resolution was enhanced by almost by an order of magnitude from the confocal microscopy [219, 220].

7.1.3 Extended application of the methods to alternative cell lines

For the nanoneedle-mediated intracellular delivery systems to be widely used, several cell lines will need to be tested to validate the intracellular uptake. We hypothesized that the intracellular delivery would be consistent across different cell lines using the nanoneedle-mediated methods, since the methods do not depend as much on the membrane characteristics as some other methods do. Most of the intracellular delivery methods rely on several physical characteristics of cells and the results can vary from cell to cell even if the experimental conditions are consistent. A number of different cell lines can be chosen based on the physical characteristics and further application to test the nanoneedle-mediated intracellular delivery methods. Primary and stem cells are known to be hard to transfect with commercially available methods and widely studied for the application in tissue engineering and gene therapy [221]. Many progenitors cells are heterogeneous and can vary from patient to patient, which makes existing transfection methods more difficult to use [222, 223]. In embryonic and hematopoietic stem cells, the terminal differentiation results in stiffer cell nucleus and the irreversible deformation of nucleus was observed [224]. Varying stiffness of cell nucleus could affect the cell viability and intracellular uptake as the confocal image of puncture loading showed some of the nanoneedles targeting the nucleus. Lastly, the physical characteristics of the cell can vary with the substrate stiffness [225, 226]. By adjusting substrate stiffness, cells can be prepared with varying stiffness, cytoskeletal structure, and adhesion for experiments. It is crucial in order to extend the application for the wider use across different cell lines and to study the dependence of the performance on cell characteristics, if there is any.

7.1.4 Cell viability and repair mechanism

The parameters for the nanoneedle-mediated intracellular delivery methods were varied based on the cell viability and the intracellular uptake. The bigger size and/or longer opening time of pores due to applied physical force can result in the potential risk of cell death due to apoptosis triggered by calcium efflux or necrosis [227]. A number of previous studies on physical delivery methods investigated the ways to increase the cell viability and can be applied with nanoneedle-mediated delivery methods to improve the cell viability, especially with puncture loading since the effect on viability was minimal with centrifuge loading.

One of the possible treatment options is adding poloxamer surfactants to protect the cells from shear-induced damage by increasing plasma membrane fluidity [228]. The increase in cell viability was observed with addition of poloxamer in several physical intracellular delivery methods, such as electroporation, ultrasound, and photoacoustic delivery [229-231]. Another treatment option is to increase the intracellular calcium concentration to achieve membrane recovery processes by calcium-mediated signaling [232]. In the micropuncture experiment on 3T3 cells, which would be similar to the nanoneedle-mediate methods, the membrane resealing time was delayed significantly with lower extracellular calcium concentration [149]. Calcium-mediated cell repair was also demonstrated in treatment with ultrasound and microfluidic device [233-235]. The effect on cell membrane resealing could be similar in nanoneedle-mediated methods since the size of holes would be in same order of magnitude, but since the effect could vary based on the cell type, cell state, and the methods, it would be interesting to observe how each treatment has effect on cell viability. The further study will not only be useful for improving the cell viability but also will provide valuable information for understanding the cell repair kinetics associated with the nanoneedle-mediated intracellular delivery methods.

7.2 Microfluidic devices

The newly developed microfluidic device was effective in delivering molecules to cytoplasm in a high-throughput manner. Based on our studies, the method was not suitable for the gene therapy, due to the lack of plasmid transfection observed. However, the preliminary result in the previous study showed the intracellular uptake of carbon nanotube wrapped with fluorescence labeled DNA [8]. The further work on the delivery of plasmid integrated with nanomaterials would be interesting in order to extend the application in gene therapy. By incorporating the plasmid on the nanomaterials, the degradation of plasmid can be delayed and the possible nuclear targeting could be achieved as well. The nuclear entry of gold nanoparticles could be achieved by making ultrasmall nanoparticles, smaller than 10 nm in size [236]. Another possible option would be to conjugate with nuclear localization signal (NLS) peptide, which assists the translocation to the nucleus, with nanoparticles [237, 238]. Although nanoparticles themselves can also enter the cytoplasm, the combination with the microfluidic device may increase the efficiency and can target cells that may have low efficiency by nanoparticles only.

7.3 Nanoparticles

The intracellular delivery of protein and plasmid by mesoporous silica/PLL nanoparticles was demonstrated in both HeLa and K562 cells. Both the delivery efficiency and transfection efficiency decreased when applied in the suspension cells. As this difference could be due to the cell cycle and the culture condition, the attachment of K562 cells on the surface prior to the experiment with nanoparticles could be a possible step to increase the delivery efficiency. Previously, the transfection efficiency of the suspension cells, using commercially available transfection reagents, improved by coating the surface by chicken egg white to promote the cell attachment to the culture plates [239]. As we have already studied several methods for the attachment of K562 cells on the surface for the puncture loading with nanoneedles, we can easily test for the nanoparticle-mediated intracellular delivery. The comparison of delivery and/or transfection efficiency of cells cultured in suspension and on the coated plates would be an interesting study, accompanied by the comparison of the cell cycle for validation of

the hypothesis. In addition to possible increase in the delivery and transfection efficiency, the attachment of K562 cells on the surface would be also advantageous in washing the excess nanoparticles. Since the suspension cells can be washed by centrifugation, the majority of the excess nanoparticles forms a pellet together with cells and is difficult to wash. By attaching the cells on the surface, the excess nanoparticles can be easily washed away as done in adherent cells. Clearance of nanoparticles would make the method also more favorable for the clinical applications; i.e. the transplantation of treated cells back into a patient.

CHAPTER VIII

CONCLUSION

In this study, we examined new intracellular delivery methods in order to address a number of limitations posed by conventional delivery methods and to further enable applications in research and clinical settings. We exploited novel intracellular delivery methods and evaluated various experimental parameters to study the effect on intracellular uptake and cell viability.

First, we demonstrated the possibility of using nanoneedles for high-throughput intracellular delivery. Arrays of nanoneedles with sharp tip were fabricated from silicon wafers to physically puncture the cell membrane for the diffusion of fluorescent molecules intracellularly. Two delivery methods, puncture loading and centrifuge loading, were developed and assessed. In puncture loading, the nanoneedles were inserted into the confluent monolayer of cells at varying puncture force and applied time. The intracellular uptake and cell viability were quantified at range of experimental parameters to determine the required conditions for intracellular delivery. Viability varied from 50% to 90% and the delivery efficiency of 70 kDa dextran ranged from 20% to 50% of cells. Macromolecules, up to 500 kDa, were delivered into the cells using the method. The method worked well for the treatment of adherent cells, but the further work may be necessary to attach the suspension cells with enough adhesion strength to remain in place during puncture loading.

In order to treat cells in suspension, the nanoneedles were fixed and the cells were centrifuged onto the needles at varying centrifugal force and time in the centrifuge loading method. Centrifuge conditions were optimized based on the cell viability and the delivery efficiency of small fluorescent molecules. Cell viability was relatively high (i.e., > 90%) in most of the conditions tested. The optimized conditions achieved up to 60% delivery efficiency of small molecules, but the delivery efficiency of macromolecules was only approximately 10%.

Novel microfluidic devices were studied as another physical intracellular delivery method to treat suspension cells in a high-throughput manner. The mechanical

deformation and shear stress in the constriction channels opened up transient holes in the cell membrane and allowed the diffusion of molecules intracellularly. Not all of the cells were compatible with the device, probably due to the variation in physical characteristics of cell membranes. Cell viability and intracellular uptake of various fluorescent molecules, including dextran and protein molecules, were quantified with the width of constriction channel or pressure tested.

Lastly, we studied intracellular delivery using nanoparticles. From several materials for nanoparticles, we screened for suitable materials to achieve intracellular delivery in a leukemia cell line. High cell viability and intracellular uptake were seen with mesoporous silica/poly-L-lysine nanoparticles. Therapeutics agents could be loaded onto the nanoparticles either by encapsulating within the pores and/or by coating on the surface of the nanoparticles. Successful uptake of fluorescent protein and plasmid transfection were observed in the leukemia cells.

APPENDIX A

ELECTROPORATION

Electroporation has been used widely for transfection experiments in laboratory and clinical settings. Protocol have been developed and optimized for many cell types to result in high cell viability and high delivery or transfection efficiency. The method is advantageous for many cell types with already developed protocols, but electroporation can be challenging if the cell types used for the experiments are rare and the protocol has not been developed yet [5].

We performed a series of electroporation experiments to demonstrate the intracellular delivery of proteins and to compare the delivery efficiency and viability with the other methods we studied. In addition to the optimized condition available from the manufacturer of the Amaxa Nucleofector II, we varied the pulse conditions with a CytoPulse electroporation unit to examine the effect on cell viability and intracellular uptake. The intracellular delivery of various fluorescent molecules, which were delivered in our other studies as well, was demonstrated with the optimized conditions of electroporation.

A.1 Methods

A.1.1 Cell culture

Human myelogenous leukemia cells (K562, American Type Culture Collection), and lymphoid leukemia cells (EU1, courtesy of Dr. Muxiang Zhou, Emory University, Atlanta, GA) were cultured in a humidified atmosphere of 95% air and 5% CO_2 at 37°C. K562 cells were cultured with RPMI-1640 medium (Cellgro, Herndon, VA), which was supplemented with 10% (v/v) heat-inactivated fetal bovine serum (FBS, Corning, Palo Alto, CA) and 1% penicillin/streptomycin (Cellgro) [137, 180]. EU1 cells were cultured with DMEM medium (Cellgro, Herndon, VA), which was also supplemented with 10% (v/v) heat-inactivated fetal bovine serum (FBS, Corning, Palo Alto, CA) and 1% penicillin/streptomycin (Cellgro) [181].

A.1.2 Electroporation

A.1.2.1 Sample Preparation

Cell concentration was measured by a Multisizer 3 Coulter Counter (Beckham Coulter, Fullerton, CA) and prepared for the experiment at 10^7 cells/ml in an electroporation solution. Electroporation solutions were either obtained from a commercially available kit (Lonza, Allendale, NJ) or made using the recipe from the laborator of Dr. Gang Bao's (Georgia Tech). FITC-labeled BSA (Sigma-Aldrich), allophycocyanin (APC) (Sigma-Aldrich) or pGFP (Aldevron) were added to the sample at a final concentration of 25 μM, 0.05 – 0.1 μM, and 100 μg/ml, respectively. Halo TMR-tagged TALENs (Courtesy of Dr. William Dynan, Emory University) were added at a final concentration of 1.25 μM.

A.1.2.2 Electroporation

Prepared samples (100 μl) were transferred to cuvettes with an electrode spacing of 2 mm for electroporation. Electroporation was performed using either Amaxa Nucleofector II (Lonza) or CytoPulse PA-4000 (Cyto Pulse Sciences. Columbia, MD). Immediately after treatment, 500 μl of pre-warmed media was added to the cuvette and transferred carefully to either 1.5 ml microcentrifuge tubes or 12-well plates.

The samples treated with FITC-BSA or APC were incubated for 15 min and washed with PBS four times at 300 x g for 5 min to remove the extracellular fluorescent molecules. After the last wash, the cells were resuspended in PBS and transferred to flow cytometry tubes for analysis. Propidium iodide (PI, Invitrogen, Grand Island, NY) was added at a final concentration of 5 μg/ml 10 min before flow cytometry analysis to stain non-viable cells.

The samples treated for plasmid transfection were incubated for 24 h post-electroporation. The cells were washed once at 300 x g for 5 min and resuspended in PBS. Afterwards, the cells were transferred to flow cytometry tubes and PI was added to stain non-viable cells.

A.1.3 Analysis and quantification

The uptake of fluorescent dyes and cell viability were measured using a bench-top flow cytometer (BD LSRII, BD Biosciences, San Jose, CA). The data were collected and analyzed in FACSDiva software (BD Biosciences). Approximately 10,000 events were collected per sample. For cell viability, PI was analyzed using a PerCP-Cy5, 670 nm longpass filter for emission. The uptake of FITC-BSA or transfection of pGFP was measured by a FITC, 530/30 nm bandpass filter for emission. The uptake of APC and Halo TMR-tagged TALENs were measured by an APC, 660/20 nm bandpass filter, and a PE, 575/26 nm bandpass filter, respectively, for emission.

The cell gate was constructed based on forward- and side-scatter light of the untreated control cells. Any events within this gate were considered to be intact cells while any events outside the gate were considered to be cell debris or other noise. To determine which cells had taken up fluorescent marker compounds (i.e., BSA, pGFP, and halo-tagged TALEN for uptake; PI for viability), histogram gates were set by the sham control which had fluorescent dyes in the solution but was not treated with electroporation to account for extracellular staining and other noise. To set gates and account for possible spectral overlap between the dyes, compensation controls were prepared and tested [50, 139].

A.2 Results

We first tested the feasibility of protein delivery into EU1 and K562 cells using the CytoPulse electroporator. A squarewave pulse of 1 or 2 kV/cm and fixed time of 1 ms was applied for the preliminary experiment on intracellular delivery of FITC-BSA. In EU1 cells, the delivery efficiency of FITC-BSA was similar at both pulse conditions (Student's t-test, $p = 0.391$) at about 60% (Figure A.1, top). The cell viability decreased by almost 30% as the voltage increased from 1 to 2 kV/cm (Student's t-test, $p = 0.016$). In K562 cells, the same pulse conditions resulted in different cell viability and delivery efficiency (Figure A.1, bottom). While cell viability did not vary significantly with pulse conditions (ANOVA, $p = 0.276$), delivery efficiency of FITC-BSA increased from 5% at 1 kV/cm to 50% at 2 kV/cm (Student's t-test, $p = 0.002$). In both cell lines, intracellular delivery was confirmed by fluorescence microscopy and very low fluorescence detected

in the control samples. These results showed that intracellular delivery of protein can be achieved with electroporation and the further optimization for each cell type can improve the method.

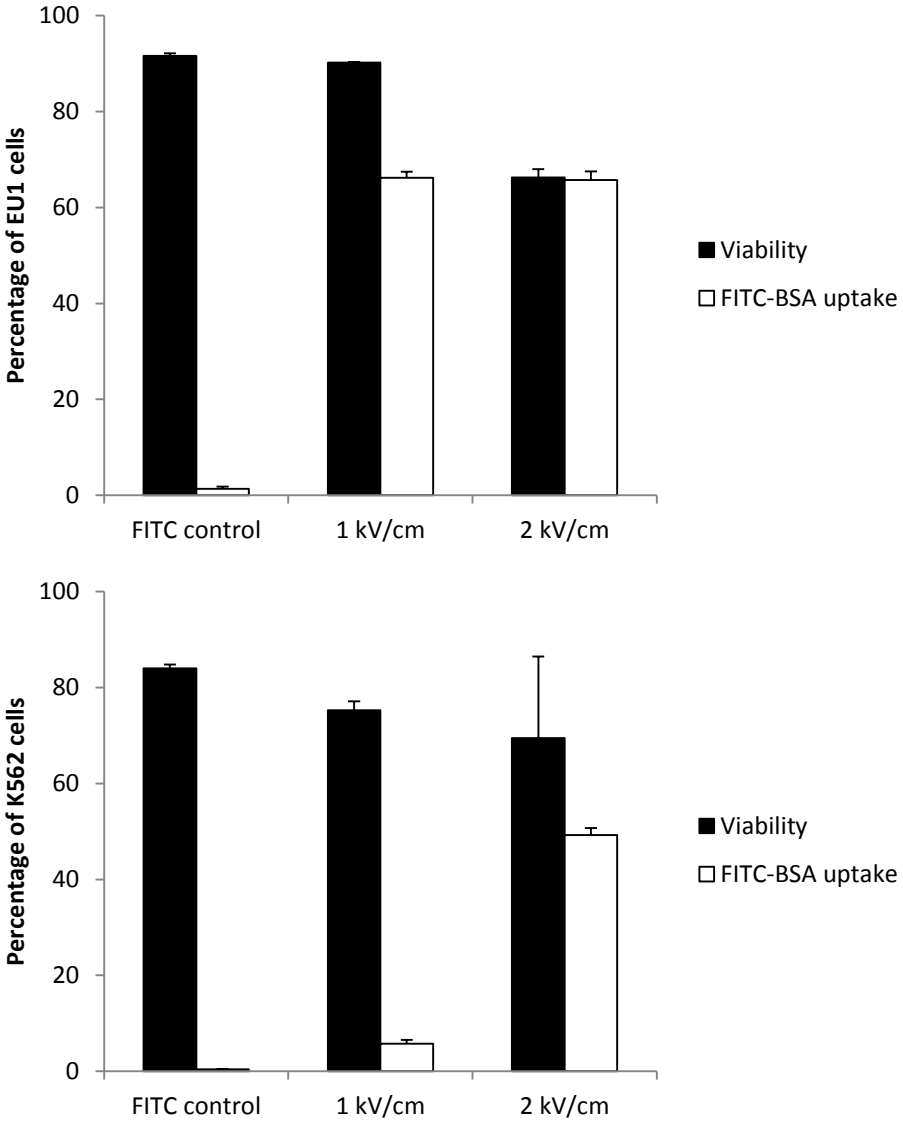

Figure A.1. Cell viability and delivery efficiency of FITC-BSA into EU1 cells (top) and K562 cells (bottom) after electroporation using the CytoPulse electroporator at 1 kV/cm and 2 kV/cm for 1 ms. Data show average ± standard deviation (SD), n = 3.

Once we demonstrated the uptake of FITC-BSA, we varied the pulse conditions with the CytoPulse instrument to examine the effect on cell viability and intracellular uptake. The pulse conditions were varied from 0.88 to 1.75 kV/cm with a fixed time of 5 ms. Cell viability and delivery efficiency of FITC-BSA is summarized in Figure A.2. Intracellular uptake of FITC-BSA was observed at all conditions tested. However, the delivery efficiency was approximately 70% in the range of voltage from 0.88 to 1.25 kV/cm, but started to decrease at higher voltage (ANOVA, $p = 0.000$). Cell viability also decreased with the increase in voltage applied (ANOVA, $p = 0.000$); cell viability was similar to the control sample at 0.88 kV/cm but decreased below 50% at 1.75 kV/cm. At 1 kV/cm, the delivery efficiency of FITC-BSA improved significantly as pulse length increased from 1 ms to 5 ms (Student's t-test, $p = 0.001$), while cell viability was not affected as much and remained similar to control samples in both cases (Student's t-test, $p = 0.05$ and 0.07 for 1 and 5 ms, respectively). The optimized pulse conditions for protein delivery into K562 cells was 0.88 – 1.25 kV/cm for 5 ms.

We also compared the result to the samples treated with the optimized condition (T-016) reported for the Amaxa Nucleofector II. The pulse condition of the Amaxa device was measured by oscilloscope and was a semi-square pulse of 0.4 kV/cm for 30 ms. While we used a higher electric field strength for a shorter time with the CytoPulse instrument, the pulse condition on the Amaxa device used a lower field strength for a longer time. Cell viability was comparable to the control sample (Student's t-test, $p = 0.106$), but the delivery efficiency of FITC-BSA was only about 50%. Compared to the optimized condition using the CytoPulse instrument, the viability was slightly better (ANOVA, $p = 0.014$) but the delivery efficiency of FITC-BSA was lower (ANOVA, $p = 0.000$).

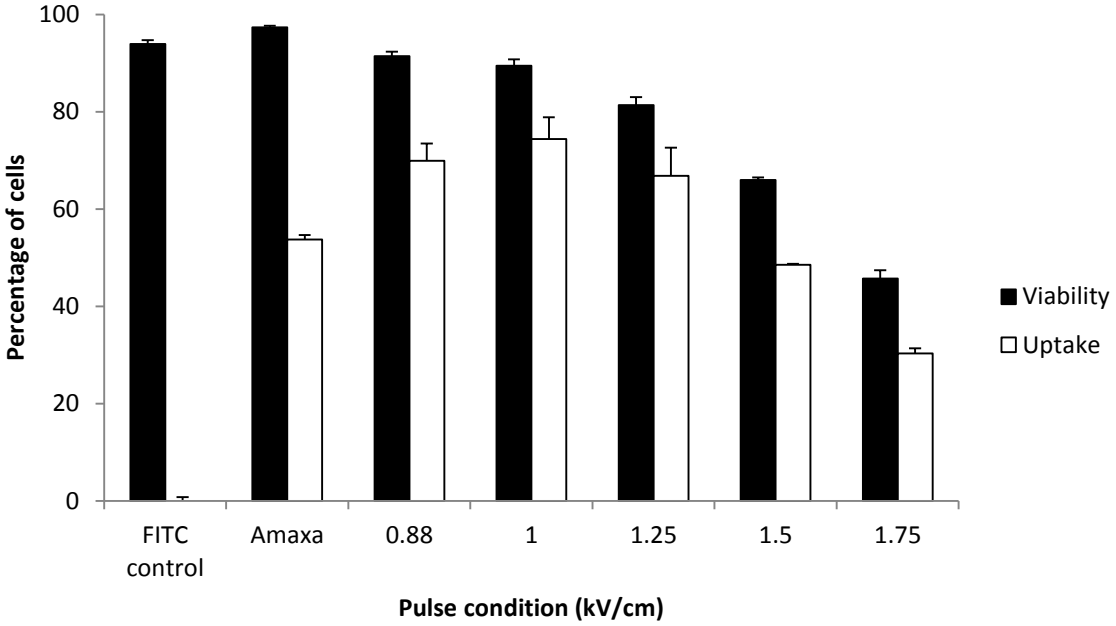

Figure A.2. Cell viability and delivery efficiency of FITC-BSA into K562 cells at varying pulse conditions using the CytoPulse and Amaxa Nucleofector instruments. The pulse conditions tested with the CytoPulse device were treated for 5 ms. Data show average ± standard deviation (SD), n = 3.

After optimizing the pulse conditions for FITC-BSA delivery with the CytoPulse device, we moved on to plasmid delivery and examined plasmid transfection efficiency using the optimized conditions (Figure A.3). Cell viability was similar in all samples 24 h after electroporation. The optimized CytoPulse conditions resulted in relatively lower transfection efficiency compared to the Amaxa Nucleofector (ANOVA, $p = 0.000$). The transfection efficiency using the Amaxa instrument was about 50% and similar to the delivery efficiency of FITC-BSA (Student's t-test, $p = 0.295$). However, both pulse conditions with the CytoPulse instrument resulted in transfection efficiency below 20%. As the Amaxa nucleofector protocol is optimized for plasmid transfection, it is possible that the condition may be more efficient in targeting the nuclear membrane compared to the CytoPulse conditions.

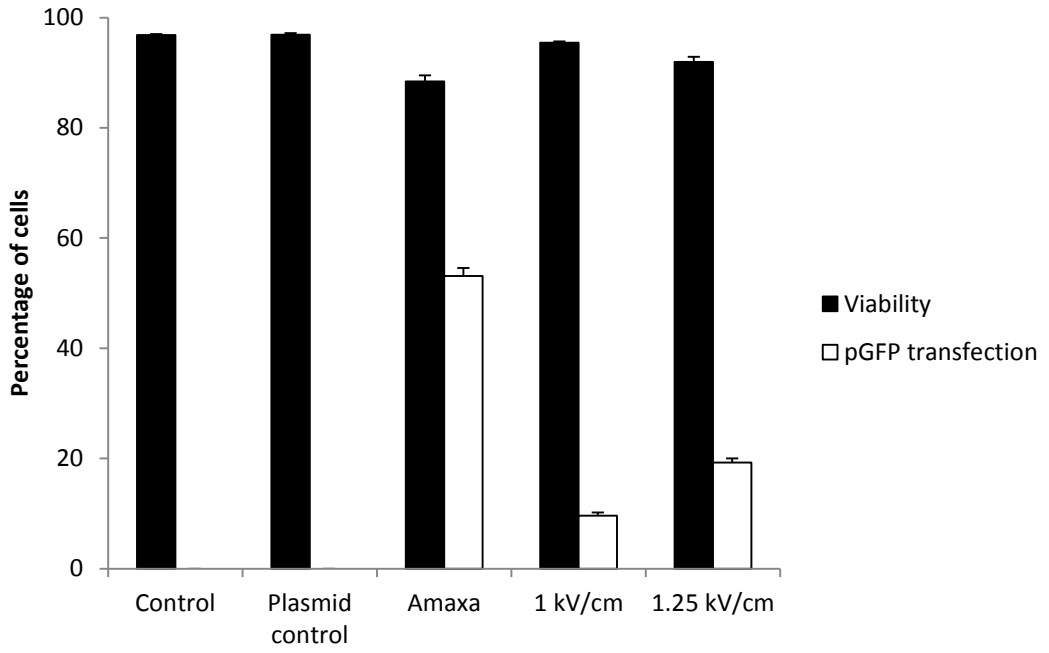

Figure A.3. Cell viability and plasmid transfection efficiency in K562 cells 24 h after electroporation with the Amaxa Nucleofector and CytoPulse instruments. Data show average ± standard deviation (SD), n = 3.

Next, we treated the cells for intracellular delivery of proteins used in Chapter 4 as a comparison. Although we used EU1 cells for microfluidic device and K562 cells in electroporation, the results of the optimized conditions may provide the sense of possible efficiency and viability achieved with each method. First, we quantified cell viability and delivery efficiency of APC in K562 cells using the optimized pulse conditions of the CytoPulse device (Figure A.4). We hypothesized that lower cell viability would be associated with higher APC concentration due to possible toxicity of intracellular APC; however, cell viability was similar at each condition (Student's t-test, $p = 0.164$ and 0.195 for 1 and 1.25 kV/cm, respectively). Delivery efficiency of APC increased with the higher concentration of APC (Student's t-test, $p = 0.001$ and 0.006 for 1 and 1.25 kV/cm, respectively) from 30% to 50% (probably due to increased detection sensitivity of the stronger APC fluorescence signal) but did not vary significantly with the voltage (Student's t-test, $p = 0.070$ and 0.113 for 0.05 and 0.1 μM APC). Successful intracellular uptake of APC was observed at the optimized CytoPulse conditions and the results (cell viability and delivery efficiency) were comparable to the microfluidic data at the same APC concentration.

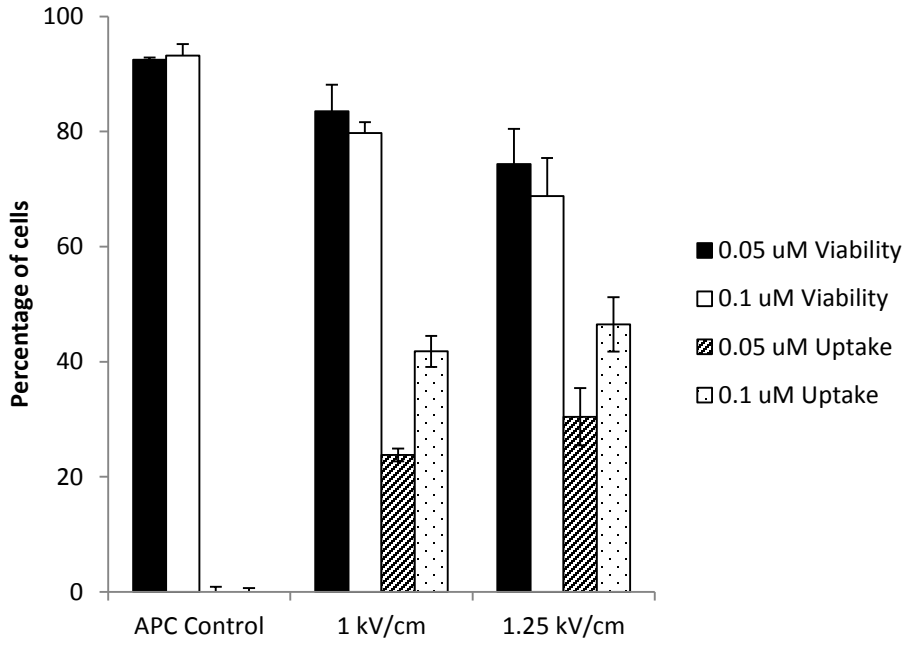

Figure A.4. Cell viability and delivery efficiency of APC into K562 cells at varying APC concentration (0.05 and 0.1 µM) and pulse conditions (1 and 1.25 kV/cm). Data show average ± standard deviation (SD), n = 3.

Based on previous results, we tested intracellular delivery of halo TMR-tagged R4 TALEN into K562 cells. The same cell concentration (1 million cells/sample) and TALEN concentration (1 uM) was used as in the experiment with the microfluidic device. The control and treated samples were displayed on the histogram of the appropriate filter for the halo-tagged TALEN (Figure A.5). Similar to the results in the microfluidic devices, the control sample with halo-tagged TALEN showed a shift in the histogram after washing steps and was used as a basis for setting the gate for background fluorescence signal. While we observed two overlapping populations in the samples treated with microfluidic devices, we observed a shift in the histogram of the cells treated with electroporation, using both the Amaxa Nucleofector II and CytoPulse device. This indicates the intracellular uptake of halo-tagged TALEN and the efficiency was about 60 – 70% based on the gate.

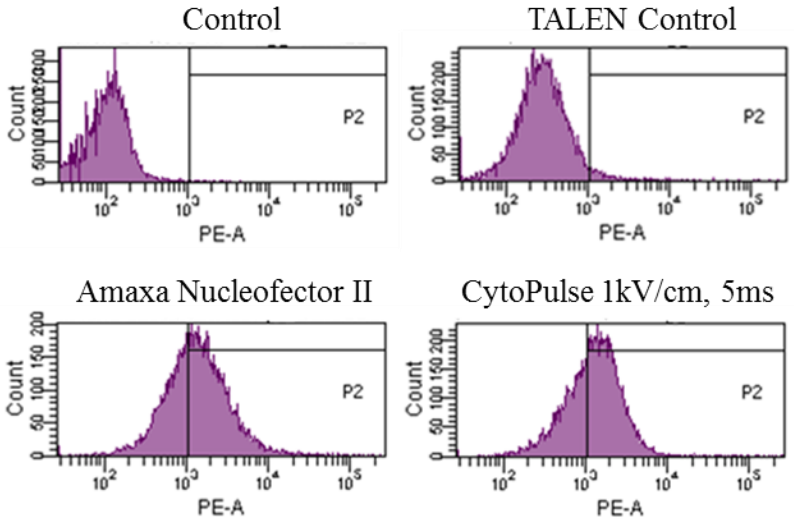

Figure A.5. PE channel histogram for Halo-tagged TALEN (R4) uptake into K562 cells using the Amaxa Nucleofector and CytoPulse electroporator compared to non-electroporated control samples. Dotted lines indicate the upper limit on the background fluorescence signal in control cells.

A.3 Conclusion

In this study, we demonstrated the intracellular delivery of various fluorescent proteins in K562 cells using electroporation. Along with the Amaxa Nucleofector, we tested varying pulse conditions with the CytoPulse electroporation device and identified optimized conditions for K562 cells with high cell viability and high delivery efficiency. As electroporation is used widely in many applications, the electroporation results can be referenced as a standard for new intracellular delivery methods.

APPENDIX B

LIPOFECTION

Lipofection is a chemical intracellular delivery method and can be prepared easily using a number of commercially available kits. The positively charged lipid and negatively charged plasmid form a complex that can easily fuse with the cell membrane for intracellular delivery [42]. The efficient delivery of nucleic acids has been demonstrated in various cells types.

In this study, we performed lipofection experiments on a hard-to-transfect leukemia cell line as a positive control for the plasmid transfection. In addition, the lipofection results are suitable to use as a standard for the optimization of nanoparticle experiments.

B.1 Methods

B.1.1 Cell culture

Human myelogenous leukemia cells (K562, American Type Culture Collection) were cultured in a humidified atmosphere of 95% air and 5% CO_2 at 37°C. K562 cells were cultured with RPMI-1640 medium (Cellgro, Herndon, VA), which was supplemented with 10% (v/v) heat-inactivated fetal bovine serum (FBS, Corning, Palo Alto, CA) and 1% penicillin/streptomycin (Cellgro) [137, 180].

B.1.2 Lipofection

Cell concentration was measured by a Multisizer 3 Coulter Counter (Beckham Coulter, Fullerton, CA) and prepared for the experiment at 1.5 x 10^5 cells per well in 24-well plates. Lipofectamine 2000 reagent (Invitrogen, Grand Island, NY) was prepared according to the manufacturer's protocol with pGFP (Aldevron). The reagents were prepared either in Opti-MEM medium (Invitrogen) or RPMI medium. The plasmid-lipid complex was added to the cells and incubated for 24 – 48 h for transfection. The cells were washed four times with PBS at 300 x g for 5 min after incubation. After the last

wash, the cells were resuspended in PBS and transferred to flow cytometry tubes for analysis. Propidium iodide (PI, Invitrogen) was added at a final concentration of 5 µg/ml 10 min before flow cytometry analysis to stain non-viable cells.

B.1.3 Analysis and quantification

The uptake of fluorescent dyes and cell viability were measured using a bench-top flow cytometer (BD LSRII, BD Biosciences, San Jose, CA). The data were collected and analyzed in FACSDiva software (BD Biosciences). Approximately 10,000 events were collected per sample. For cell viability, PI was analyzed using a PerCP-Cy5, 670 nm longpass filter for emission. The transfection of pGFP was measured by a FITC, 530/30 nm bandpass filter for emission.

B.2 Results

Among a number of commercially available kits for lipofection, we observed the highest efficiency of plasmid transfection in our cells using our conditions with Lipofectamine 2000 from Invitrogen. We tested two variables (amount of Lipofectamine 2000 reagent, and medium) in the study to examine the effect on cell viability and transfection efficiency. The amount of reagent was varied according to the range provided by the protocol. The media tested were Opti-MEM, which was recommended in the protocol, and RPMI, which was used for the culture of K562 cells. Two variables did not have a significant effect on the cell viability (ANOVA, $p = 0.005$) and cell viability was above 90% after 24 h incubation (Figure B.1, top). However, the transfection efficiency of pGFP (Figure B.1, bottom) was higher when Opti-MEM was used compared to when RPMI was used (Student's t-test, $p < 0.05$). The transfection efficiency also increased slightly with an increasing amount of Lipofectamine reagent added (ANOVA, $p = 0.033$ and 0.016 for Opti-MEM and RPMI, respectively). While successful transfection was observed, the efficiency only ranged from 20 to 30% in K562 cells. Further optimization of the method would be challenging since the number of variables in lipofection is limited.

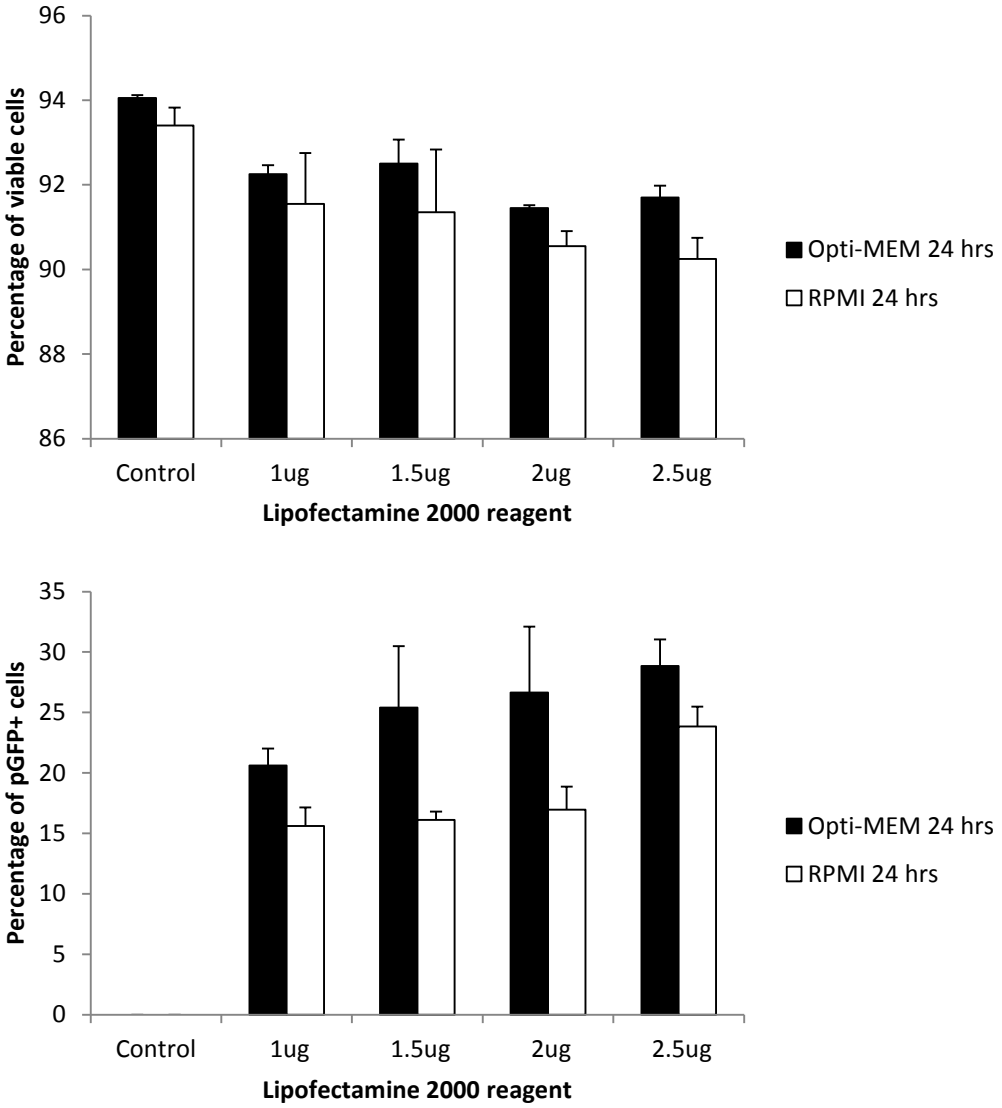

Figure B.1 Cell viability (top) and transfection efficiency of pGFP (bottom) in K562 cells with varying amount of lipofectamine 2000 reagent. Data show average ± standard deviation (SD), n = 3.

B.3 Conclusion

In this study, we performed a lipofection experiment on K562 cells to study the effect of medium and amount of Lipofectamine reagent on cell viability and transfection efficiency of pGFP. The maximum transfection efficiency achieved was approximately 30% and could be set as a target for the optimization of intracellular delivery by nanonparticles.

REFERENCES

1. Gehl, J., *Electroporation: theory and methods, perspectives for drug delivery, gene therapy and research.* Acta Physiol Scand, 2003. **177**(4): p. 437-47.

2. Gardlik, R., et al., *Vectors and delivery systems in gene therapy.* Med Sci Monit, 2005. **11**(4): p. RA110-21.

3. Torchilin, V.P., *Recent approaches to intracellular delivery of drugs and DNA and organelle targeting.* Annual Review of Biomedical Engineering, 2006. **8**: p. 343-375.

4. Varga, C.M., T.J. Wickham, and D.A. Lauffenburger, *Receptor-mediated targeting of gene delivery vectors: Insights from molecular mechanisms for improved vehicle design.* Biotechnology and Bioengineering, 2000. **70**(6): p. 593-605.

5. Santos, J.L., et al., *Non-Viral Gene Delivery to Mesenchymal Stem Cells: Methods, Strategies and Application in Bone Tissue Engineering and Regeneration.* Current Gene Therapy, 2011. **11**(1): p. 46-57.

6. King, R., *Gene delivery to mammalian cells by microinjection.* Methods Mol Biol, 2004. **245**: p. 167-74.

7. McAllister, D.V., et al., *Microfabricated needles for transdermal delivery of macromolecules and nanoparticles: fabrication methods and transport studies.* Proc Natl Acad Sci U S A, 2003. **100**(24): p. 13755-60.

8. Sharei, A., et al., *A vector-free microfluidic platform for intracellular delivery.* Proc Natl Acad Sci U S A, 2013. **110**(6): p. 2082-7.

9. Chou, L.Y., K. Ming, and W.C. Chan, *Strategies for the intracellular delivery of nanoparticles.* Chem Soc Rev, 2011. **40**(1): p. 233-45.

10. Varkouhi, A.K., et al., *Endosomal escape pathways for delivery of biologicals.* J Control Release, 2011. **151**(3): p. 220-8.

11. Michalet, X., et al., *Quantum dots for live cells, in vivo imaging, and diagnostics.* Science, 2005. **307**(5709): p. 538-544.

12. Smith, A.M., et al., *Engineering luminescent quantum dots for In vivo molecular and cellular imaging.* Annals of Biomedical Engineering, 2006. **34**(1): p. 3-14.

13. Sutton, E.J., et al., *Cell tracking with optical imaging.* European Radiology, 2008. **18**(10): p. 2021-2032.

14. Derfus, A.M., W.C.W. Chan, and S.N. Bhatia, *Intracellular delivery of quantum dots for live cell labeling and organelle tracking.* Advanced Materials, 2004. **16**(12): p. 961-+.

15. Nerem, R.M., *Cellular Engineering.* Annals of Biomedical Engineering, 1991. **19**(5): p. 529-545.

16. Takahashi, K., et al., *Induction of pluripotent stem cells from adult human fibroblasts by defined factors.* Cell, 2007. **131**(5): p. 861-872.

17. Doulatov, S. and G.Q. Daley, *A Stem Cell Perspective on Cellular Engineering.* Science, 2013. **342**(6159): p. 700-702.

18. Vierbuchen, T. and M. Wernig, *Molecular Roadblocks for Cellular Reprogramming.* Molecular Cell, 2012. **47**(6): p. 827-838.

19. Morris, S.A. and G.Q. Daley, *A blueprint for engineering cell fate: current technologies to reprogram cell identity.* Cell Research, 2013. **23**(1): p. 33-48.

20. Cathomen, T. and J.K. Joung, *Zinc-finger nucleases: The next generation emerges.* Molecular Therapy, 2008. **16**(7): p. 1200-1207.

21. Zhang, F., et al., *Efficient construction of sequence-specific TAL effectors for modulating mammalian transcription.* Nature Biotechnology, 2011. **29**(2): p. 149-U90.

22. Gasiunas, G., et al., *Cas9-crRNA ribonucleoprotein complex mediates specific DNA cleavage for adaptive immunity in bacteria.* Proceedings of the National

Academy of Sciences of the United States of America, 2012. **109**(39): p. E2579-E2586.

23. Miller, J.C., et al., *A TALE nuclease architecture for efficient genome editing.* Nat Biotechnol, 2011. **29**(2): p. 143-8.

24. Young, L.S., et al., *Viral gene therapy strategies: from basic science to clinical application.* J Pathol, 2006. **208**(2): p. 299-318.

25. Ljunggren, H.G. and K.J. Malmberg, *Prospects for the use of NK cells in immunotherapy of human cancer.* Nature Reviews Immunology, 2007. **7**(5): p. 329-339.

26. Matter, M., et al., *Decreased tumor surveillance after adoptive T cell therapy.* Cancer Research, 2007. **67**(15): p. 7467-7476.

27. Kwon, E.D., et al., *Manipulation of T cell costimulatory and inhibitory signals for immunotherapy of prostate cancer.* Proceedings of the National Academy of Sciences of the United States of America, 1997. **94**(15): p. 8099-8103.

28. Porter, D.L., et al., *Chimeric Antigen Receptor-Modified T Cells in Chronic Lymphoid Leukemia.* New England Journal of Medicine, 2011. **365**(8): p. 725-733.

29. Kloss, C.C., et al., *Combinatorial antigen recognition with balanced signaling promotes selective tumor eradication by engineered T cells.* Nature Biotechnology, 2013. **31**(1): p. 71-+.

30. Kochenderfer, J.N., et al., *Eradication of B-lineage cells and regression of lymphoma in a patient treated with autologous T cells genetically engineered to recognize CD19.* Blood, 2010. **116**(20): p. 4099-4102.

31. Dazzi, F. and N.J. Horwood, *Potential of mesenchymal stem cell therapy.* Current Opinion in Oncology, 2007. **19**(6): p. 650-655.

32. Au, P., et al., *Bone marrow-derived mesenchymal stem cells facilitate engineering of long-lasting functional vasculature.* Blood, 2008. **111**(9): p. 4551-4558.

33. Johnson, F.L., et al., *Bone-marrow transplantation in a patient with sickle-cell anemia.* N Engl J Med, 1984. **311**(12): p. 780-3.

34. Cao, Y.A., et al., *Shifting foci of hematopoiesis during reconstitution from single stem cells.* Proc Natl Acad Sci U S A, 2004. **101**(1): p. 221-6.

35. Osawa, M., et al., *Long-term lymphohematopoietic reconstitution by a single CD34-low/negative hematopoietic stem cell.* Science, 1996. **273**(5272): p. 242-5.

36. Asahara, T., C. Kalka, and J.M. Isner, *Stem cell therapy and gene transfer for regeneration.* Gene Therapy, 2000. **7**(6): p. 451-457.

37. Zhang, X.J. and W.T. Godbey, *Viral vectors for gene delivery in tissue engineering.* Advanced Drug Delivery Reviews, 2006. **58**(4): p. 515-534.

38. Kay, M.A., J.C. Glorioso, and L. Naldini, *Viral vectors for gene therapy: the art of turning infectious agents into vehicles of therapeutics.* Nature Medicine, 2001. **7**(1): p. 33-40.

39. Hacein-Bey-Abina, S., et al., *Insertional oncogenesis in 4 patients after retrovirus-mediated gene therapy of SCID-X1.* Journal of Clinical Investigation, 2008. **118**(9): p. 3132-3142.

40. Stein, S., et al., *Genomic instability and myelodysplasia with monosomy 7 consequent to EVI1 activation after gene therapy for chronic granulomatous disease.* Nature Medicine, 2010. **16**(2): p. 198-U105.

41. Lundstrom, K. and T. Boulikas, *Viral and non-viral vectors in gene therapy: technology development and clinical trials.* Technol Cancer Res Treat, 2003. **2**(5): p. 471-86.

42. Felgner, P.L., et al., *Lipofection: a highly efficient, lipid-mediated DNA-transfection procedure.* Proc Natl Acad Sci U S A, 1987. **84**(21): p. 7413-7.

43. Vinogradov, S.V., E. Kohli, and A.D. Zeman, *Comparison of nanogel drug carriers and their formulations with nucleoside 5'-triphosphates.* Pharm Res, 2006. **23**(5): p. 920-30.

44. Stone, D., et al., *Viral vectors for gene delivery and gene therapy within the endocrine system.* Journal of Endocrinology, 2000. **164**(2): p. 103-118.

45. Conwell, C.C. and L. Huang, *Recent Advances in Non-viral Gene Delivery.* Non-Viral Vectors for Gene Therapy, 2nd Edition: Part 1, 2005. **53**: p. 3-18.

46. Meacham, J.M., et al., *Physical methods for intracellular delivery: practical aspects from laboratory use to industrial-scale processing.* J Lab Autom, 2014. **19**(1): p. 1-18.

47. Rodriguez-Devora, J.I., et al., *Physically facilitating drug-delivery systems.* Ther Deliv, 2012. **3**(1): p. 125-39.

48. Mehier-Humbert, S. and R.H. Guy, *Physical methods for gene transfer: Improving the kinetics of gene delivery into cells.* Advanced Drug Delivery Reviews, 2005. **57**(5): p. 733-753.

49. Wells, D.J., *Electroporation and ultrasound enhanced non-viral gene delivery in vitro and in vivo.* Cell Biology and Toxicology, 2010. **26**(1): p. 21-28.

50. Canatella, P.J., et al., *Quantitative study of electroporation-mediated molecular uptake and cell viability.* Biophysical Journal, 2001. **80**(2): p. 755-764.

51. Liu, Y., J. Yan, and M.R. Prausnitz, *Can ultrasound enable efficient intracellular uptake of molecules? A retrospective literature review and analysis.* Ultrasound Med Biol, 2012. **38**(5): p. 876-88.

52. Guzman, H.R., et al., *Ultrasound-mediated disruption of cell membranes. I. Quantification of molecular uptake and cell viability.* Journal of the Acoustical Society of America, 2001. **110**(1): p. 588-596.

53. Mehier-Humbert, S., et al., *Plasma membrane poration induced by ultrasound exposure: Implication for drug delivery.* Journal of Controlled Release, 2005. **104**(1): p. 213-222.

54. Hallow, D.M., et al., *Measurement and correlation of acoustic cavitation with cellular bioeffects.* Ultrasound Med Biol, 2006. **32**(7): p. 1111-22.

55. Schlicher, R.K., et al., *Mechanism of intracellular delivery by acoustic cavitation.* Ultrasound Med Biol, 2006. **32**(6): p. 915-24.

56. Kinoshita, M. and K. Hynynen, *Intracellular delivery of Bak BH3 peptide by microbubble-enhanced ultrasound.* Pharm Res, 2005. **22**(5): p. 716-20.

57. Mohan, P. and N. Rapoport, *Doxorubicin as a molecular nanotheranostic agent: effect of doxorubicin encapsulation in micelles or nanoemulsions on the ultrasound-mediated intracellular delivery and nuclear trafficking.* Mol Pharm, 2010. **7**(6): p. 1959-73.

58. Miller, D.L., S.V. Pislaru, and J.E. Greenleaf, *Sonoporation: mechanical DNA delivery by ultrasonic cavitation.* Somat Cell Mol Genet, 2002. **27**(1-6): p. 115-34.

59. Brayman, A.A., et al., *Transient poration and cell surface receptor removal from human lymphocytes in vitro by 1 MHz ultrasound.* Ultrasound Med Biol, 1999. **25**(6): p. 999-1008.

60. Lokhandwalla, M., et al., *Mechanical haemolysis in shock wave lithotripsy (SWL): II. In vitro cell lysis due to shear.* Physics in Medicine and Biology, 2001. **46**(4): p. 1245-1264.

61. Netz, R.R. and M. Schick, *Pore formation and rupture in fluid bilayers.* Physical Review E, 1996. **53**(4): p. 3875-3885.

62. Clarke, M.S.F. and P.L. Mcneil, *Syringe Loading Introduces Macromolecules into Living Mammalian-Cell Cytosol.* Journal of Cell Science, 1992. **102**: p. 533-541.

63. Hallow, D.M., et al., *Shear-induced intracellular loading of cells with molecules by controlled microfluidics.* Biotechnology and Bioengineering, 2008. **99**(4): p. 846-854.

64. Scherer, F., et al., *Magnetofection: enhancing and targeting gene delivery by magnetic force in vitro and in vivo.* Gene Therapy, 2002. **9**(2): p. 102-109.

65. Mykhaylyk, O., et al., *Generation of magnetic nonviral gene transfer agents and magnetofection in vitro.* Nature Protocols, 2007. **2**(10): p. 2391-2411.

66. Plank, C., et al., *The magnetofection method: Using magnetic force to enhance gene delivery.* Biological Chemistry, 2003. **384**(5): p. 737-747.

67. Klein, T.M., et al., *High-Velocity Microprojectiles for Delivering Nucleic-Acids into Living Cells.* Nature, 1987. **327**(6117): p. 70-73.

68. Yang, N.S., et al., *Invivo and Invitro Gene-Transfer to Mammalian Somatic-Cells by Particle Bombardment.* Proceedings of the National Academy of Sciences of the United States of America, 1990. **87**(24): p. 9568-9572.

69. Liu, C.J., et al., *CAP-1A is a novel linker that binds clathrin and the voltage-gated sodium channel Na(v)1.8.* Molecular and Cellular Neuroscience, 2005. **28**(4): p. 636-649.

70. Praitis, V., *Creation of transgenic lines using microparticle bombardment methods.* Methods Mol Biol, 2006. **351**: p. 93-107.

71. Kitagawa, T., et al., *Advantages and limitations of particle-mediated transfection (gene gun) in cancer immuno-gene therapy using IL-10, IL-12 or B7-1 in murine tumor models.* J Gene Med, 2003. **5**(11): p. 958-65.

72. Dib-Hajj, S.D., et al., *Transfection of rat or mouse neurons by biolistics or electroporation.* Nature Protocols, 2009. **4**(8): p. 1118-1127.

73. Adamo, A. and K.F. Jensen, *Microfluidic based single cell microinjection.* Lab on a Chip, 2008. **8**(8): p. 1258-1261.

74. Noori, A., P.R. Selvaganapathy, and J. Wilson, *Microinjection in a microfluidic format using flexible and compliant channels and electroosmotic dosage control.* Lab on a Chip, 2009. **9**(22): p. 3202-3211.

75. Bohr, M.T., *Nanotechnology goals and challenges for electronic applications.* Ieee Transactions on Nanotechnology, 2002. **1**(1): p. 56-62.

76. van den Heuvel, M.G.L. and C. Dekker, *Motor proteins at work for nanotechnology.* Science, 2007. **317**(5836): p. 333-336.

77. Whitesides, G.M., *The 'right' size in nanobiotechnology.* Nature Biotechnology, 2003. **21**(10): p. 1161-1165.

78. Bustillo, J.M., R.T. Howe, and R.S. Muller, *Surface micromachining for microelectromechanical systems.* Proceedings of the Ieee, 1998. **86**(8): p. 1552-1574.

79. Lee, K.Y., et al., *Micromachining applications of a high resolution ultrathick photoresist.* Journal of Vacuum Science & Technology B, 1995. **13**(6): p. 3012-3016.

80. Voldman, J., M.L. Gray, and M.A. Schmidt, *Microfabrication in biology and medicine.* Annual Review of Biomedical Engineering, 1999. **1**: p. 401-425.

81. Xia, Y.N. and G.M. Whitesides, *Soft lithography.* Angewandte Chemie-International Edition, 1998. **37**(5): p. 551-575.

82. Robbins, H. and B. Schwartz, *Chemical Etching of Silicon .2. The System Hf, Hno3, H2o, and Hc2h3o2.* Journal of the Electrochemical Society, 1960. **107**(2): p. 108-111.

83. Seidel, H., et al., *Anisotropic Etching of Crystalline Silicon in Alkaline-Solutions .1. Orientation Dependence and Behavior of Passivation Layers.* Journal of the Electrochemical Society, 1990. **137**(11): p. 3612-3626.

84. Seidel, H., et al., *Anisotropic Etching of Crystalline Silicon in Alkaline-Solutions .2. Influence of Dopants.* Journal of the Electrochemical Society, 1990. **137**(11): p. 3626-3632.

85. Louizos, L.A., P.G. Athanasopoulos, and K. Varty, *Microelectromechanical Systems and Nanotechnology: A Platform for the Next Stent Technological Era.* Vascular and Endovascular Surgery, 2012. **46**(8): p. 605-609.

86. Yum, K., N. Wang, and M.F. Yu, *Nanoneedle: A multifunctional tool for biological studies in living cells.* Nanoscale, 2010. **2**(3): p. 363-372.

87. Yum, K., et al., *Mechanochemical Delivery and Dynamic Tracking of Fluorescent Quantum Dots in the Cytoplasm and Nucleus of Living Cells.* Nano Letters, 2009. **9**(5): p. 2193-2198.

88. Chen, X., et al., *A cell nanoinjector based on carbon nanotubes.* Proceedings of the National Academy of Sciences of the United States of America, 2007. **104**(20): p. 8218-8222.

89. Dai, H.J., et al., *Nanotubes as nanoprobes in scanning probe microscopy.* Nature, 1996. **384**(6605): p. 147-150.

90. Wilson, N.R. and J.V. Macpherson, *Carbon nanotube tips for atomic force microscopy.* Nature Nanotechnology, 2009. **4**(8): p. 483-491.

91. Han, S.W., et al., *High-efficiency DNA injection into a single human mesenchymal stem cell using a nanoneedle and atomic force microscopy.* Nanomedicine-Nanotechnology Biology and Medicine, 2008. **4**(3): p. 215-225.

92. Suryavanshi, A.P. and M.F. Yu, *Probe-based electrochemical fabrication of freestanding Cu nanowire array.* Applied Physics Letters, 2006. **88**(8).

93. Suryavanshi, A.P., J. Hu, and M.F. Yu, *Meniscus-controlled continuous fabrication of arrays and rolls of extremely long micro- and nano-fibers.* Advanced Materials, 2008. **20**(4): p. 793-+.

94. Liu, Z., et al., *Carbon Nanotubes in Biology and Medicine: In vitro and in vivo Detection, Imaging and Drug Delivery.* Nano Research, 2009. **2**(2): p. 85-120.

95. Lu, F.S., et al., *Advances in Bioapplications of Carbon Nanotubes.* Advanced Materials, 2009. **21**(2): p. 139-152.

96. Yum, K.S., et al., *Individual nanotube-based needle nanoprobes for electrochemical studies in picoliter microenvironments.* Acs Nano, 2007. **1**(5): p. 440-448.

97. Yum, K., et al., *Biofunctionalized nanoneedles for the direct and site-selective delivery of probes into living cells.* Biochimica Et Biophysica Acta-General Subjects, 2011. **1810**(3): p. 330-338.

98. Schrlau, M.G., et al., *Carbon nanopipettes characterize calcium release pathways in breast cancer cells.* Nanotechnology, 2008. **19**(32).

99. Freedman, J.R., et al., *Magnetically assembled carbon nanotube tipped pipettes.* Applied Physics Letters, 2007. **90**(10).

100. Hernandez-Ramirez, F., et al., *High response and stability in CO and humidity measures using a single SnO2 nanowire.* Sensors and Actuators B-Chemical, 2007. **121**(1): p. 3-17.

101. Li, Z., et al., *Silicon nanowires for sequence-specific DNA sensing: device fabrication and simulation.* Applied Physics a-Materials Science & Processing, 2005. **80**(6): p. 1257-1263.

102. Samitsu, S., et al., *Conductivity measurements of individual poly(3,4-ethylenedioxythiophene)/poly(styrenesulfonate) nanowires on nanoelectrodes using manipulation with an atomic force microscope.* Applied Physics Letters, 2005. **86**(23).

103. Elibol, O.H., et al., *Integrated nanoscale silicon sensors using top-down fabrication.* Applied Physics Letters, 2003. **83**(22): p. 4613-4615.

104. Hochbaum, A.I., et al., *Controlled growth of Si nanowire arrays for device integration.* Nano Letters, 2005. **5**(3): p. 457-460.

105. Goldberger, J., et al., *Silicon vertically integrated nanowire field effect transistors.* Nano Letters, 2006. **6**(5): p. 973-977.

106. Lu, B., et al., *Synthesis and characterization of hollow-cavity-stacked one-dimensional carbon nanostructures.* Chinese Journal of Inorganic Chemistry, 2004. **20**(4): p. 469-473.

107. Boettcher, S.W., et al., *Energy-Conversion Properties of Vapor-Liquid-Solid-Grown Silicon Wire-Array Photocathodes.* Science, 2010. **327**(5962): p. 185-187.

108. Kelzenberg, M.D., et al., *Enhanced absorption and carrier collection in Si wire arrays for photovoltaic applications.* Nature Materials, 2010. **9**(3): p. 239-244.

109. Park, I., et al., *Top-down fabricated silicon nanowire sensors for real-time chemical detection.* Nanotechnology, 2010. **21**(1).

110. Hahm, J. and C.M. Lieber, *Direct ultrasensitive electrical detection of DNA and DNA sequence variations using nanowire nanosensors.* Nano Letters, 2004. **4**(1): p. 51-54.

111. Zheng, G.F., et al., *Multiplexed electrical detection of cancer markers with nanowire sensor arrays.* Nature Biotechnology, 2005. **23**(10): p. 1294-1301.

112. McKnight, T.E., et al., *Tracking gene expression after DNA delivery using spatially indexed nanofiber Arrays.* Nano Letters, 2004. **4**(7): p. 1213-1219.

113. Shalek, A.K., et al., *Vertical silicon nanowires as a universal platform for delivering biomolecules into living cells.* Proceedings of the National Academy of Sciences of the United States of America, 2010. **107**(5): p. 1870-1875.

114. Mumm, F. and P. Sikorski, *Oxidative fabrication of patterned, large, non-flaking CuO nanowire arrays.* Nanotechnology, 2011. **22**(10).

115. Skold, N., et al., *Nanofluidics in hollow nanowires.* Nanotechnology, 2010. **21**(15).

116. Faraji, A.H. and P. Wipf, *Nanoparticles in cellular drug delivery.* Bioorganic & Medicinal Chemistry, 2009. **17**(8): p. 2950-2962.

117. Liong, M., et al., *Multifunctional inorganic nanoparticles for imaging, targeting, and drug delivery.* Acs Nano, 2008. **2**(5): p. 889-896.

118. Kumari, A., S.K. Yadav, and S.C. Yadav, *Biodegradable polymeric nanoparticles based drug delivery systems.* Colloids and Surfaces B-Biointerfaces, 2010. **75**(1): p. 1-18.

119. Junghanns, J.U.A.H. and R.H. Muller, *Nanocrystal technology, drug delivery and clinical applications.* International Journal of Nanomedicine, 2008. **3**(3): p. 295-309.

120. Wissing, S.A., O. Kayser, and R.H. Muller, *Solid lipid nanoparticles for parenteral drug delivery.* Advanced Drug Delivery Reviews, 2004. **56**(9): p. 1257-1272.

121. Sun, Y.G. and Y.N. Xia, *Shape-controlled synthesis of gold and silver nanoparticles.* Science, 2002. **298**(5601): p. 2176-2179.

122. Hewakuruppu, Y.L., et al., *Plasmonic "pump-probe" method to study semi-transparent nanofluids.* Applied Optics, 2013. **52**(24): p. 6041-6050.

123. Alivisatos, A.P., *Semiconductor clusters, nanocrystals, and quantum dots.* Science, 1996. **271**(5251): p. 933-937.

124. Medintz, I.L., et al., *Quantum dot bioconjugates for imaging, labelling and sensing.* Nature Materials, 2005. **4**(6): p. 435-446.

125. Hutten, A., et al., *New magnetic nanoparticles for biotechnology.* Journal of Biotechnology, 2004. **112**(1-2): p. 47-63.

126. Seo, W.S., et al., *FeCo/graphitic-shell nanocrystals as advanced magnetic-resonance-imaging and near-infrared agents.* Nature Materials, 2006. **5**(12): p. 971-976.

127. Panyam, J. and V. Labhasetwar, *Biodegradable nanoparticles for drug and gene delivery to cells and tissue.* Advanced Drug Delivery Reviews, 2003. **55**(3): p. 329-347.

128. Moghimi, S.M., A.C. Hunter, and J.C. Murray, *Long-circulating and target-specific nanoparticles: Theory to practice.* Pharmacological Reviews, 2001. **53**(2): p. 283-318.

129. Desai, M.P., et al., *The mechanism of uptake of biodegradable microparticles in Caco-2 cells is size dependent.* Pharmaceutical Research, 1997. **14**(11): p. 1568-1573.

130. Desai, M.P., et al., *Gastrointestinal uptake of biodegradable microparticles: Effect of particle size.* Pharmaceutical Research, 1996. **13**(12): p. 1838-1845.

131. Kim, H.J., et al., *Diamond Nanogel-Embedded Contact Lenses Mediate Lysozyme-Dependent Therapeutic Release.* Acs Nano, 2014. **8**(3): p. 2998-3005.

132. Taratula, O., et al., *Nanostructured lipid carriers as multifunctional nanomedicine platform for pulmonary co-delivery of anticancer drugs and siRNA.* Journal of Controlled Release, 2013. **171**(3): p. 349-357.

133. Tseng, W.C., F.R. Haselton, and T.D. Giorgio, *Transfection by cationic liposomes using simultaneous single cell measurements of plasmid delivery and transgene expression.* Journal of Biological Chemistry, 1997. **272**(41): p. 25641-25647.

134. Zhang, Y., *Microinjection technique and protocol to single cells.* 2007.

135. Patel, S.R., et al., *Suprachoroidal Drug Delivery to the Back of the Eye Using Hollow Microneedles.* Pharmaceutical Research, 2011. **28**(1): p. 166-176.

136. Sullivan, S.P., et al., *Dissolving polymer microneedle patches for influenza vaccination.* Nature Medicine, 2010. **16**(8): p. 915-U116.

137. Stone, K.R., et al., *Isolation of a Human Prostate Carcinoma Cell Line (Du 145).* International Journal of Cancer, 1978. **21**(3): p. 274-281.

138. Schlicher, R.K., et al., *Mechanism of intracellular delivery by acoustic cavitation.* Ultrasound in Medicine and Biology, 2006. **32**(6): p. 915-924.

139. Sengupta, A., et al., *Efficient Intracellular Delivery of Molecules with High Cell Viability Using Nanosecond-Pulsed Laser-Activated Carbon Nanoparticles.* Acs Nano, 2014. **8**(3): p. 2889-2899.

140. Taur, Y. and T.H. Ning, *Fundamentals of VLSI devices*. 2nd ed. 2009: Cambridge University Press. 680.

141. Campbell, S.A., *Fabrication Engineering at the Micro- and Nanoscale* 4th ed. The Oxford Series in Electrical and Computer Engineering. 2012: Oxford University Press. 688.

142. Hong, C.Y. and A.I. Akinwande, *Oxidation sharpening mechanism for silicon tip formation.* Electrochemical and Solid State Letters, 2005. **8**(5): p. F13-F15.

143. Paik, S.-J., et al. *A highly dense nanoneedle array for intracellular gene delivery*. in *14th Solid State Sensors, Actuators, and Microsystems Workshop*. 2012. Hilton Head, SC.

144. Ocqueteau, C., et al., *Three-dimensional morphometry of mammalian cells. I. Diameters.* Arch Biol Med Exp (Santiago), 1989. **22**(2): p. 89-95.

145. Kim, W., et al., *Interfacing silicon nanowires with mammalian cells.* Journal of the American Chemical Society, 2007. **129**(23): p. 7228-+.

146. Wang, W.H.H., X.Y.Y. Liu, and Y. Sun, *High-Throughput Automated Injection of Individual Biological Cells.* Ieee Transactions on Automation Science and Engineering, 2009. **6**(2): p. 209-219.

147. Liu, X.Y. and Y. Sun, *Microfabricated glass devices for rapid single cell immobilization in mouse zygote microinjection.* Biomedical Microdevices, 2009. **11**(6): p. 1169-1174.

148. Weaver, J.C. and Y.A. Chizmadzhev, *Theory of electroporation: A review.* Bioelectrochemistry and Bioenergetics, 1996. **41**(2): p. 135-160.

149. Steinhardt, R.A., G.Q. Bi, and J.M. Alderton, *Cell-Membrane Resealing by a Vesicular Mechanism Similar to Neurotransmitter Release.* Science, 1994. **263**(5145): p. 390-393.

150. Ciechanover, A. and A.L. Schwartz, *The Ubiquitin-Mediated Proteolytic Pathway - Mechanisms of Recognition of the Proteolytic Substrate and Involvement in the Degradation of Native Cellular Proteins.* Faseb Journal, 1994. **8**(2): p. 182-191.

151. Ziegler, U. and P. Groscurth, *Morphological features of cell death.* News in Physiological Sciences, 2004. **19**: p. 124-128.

152. Majno, G. and I. Joris, *Apoptosis, Oncosis, and Necrosis - an Overview of Cell-Death.* American Journal of Pathology, 1995. **146**(1): p. 3-15.

153. Khademhosseini, A., et al., *Layer-by-layer deposition of hyaluronic acid and poly-L-lysine for patterned cell co-cultures.* Biomaterials, 2004. **25**(17): p. 3583-3592.

154. Winblade, N.D., et al., *Blocking adhesion to cell and tissue surfaces by the chemisorption of a poly-L-lysine-graft-(poly(ethylene glycol); phenylboronic acid) copolymer.* Biomacromolecules, 2000. **1**(4): p. 523-533.

155. Cooper, G.M., *The Cell: A Molecular Approach*. 2nd ed. 2000, Sunderland, MA: Sinauer Associates.

156. Alberts, B., et al., *Molecular Biology of the Cell*. 4th ed. 2002, New York: Garland Science.

157. Notter, M.F.D., *Selective Attachment of Neural Cells to Specific Substrates Including Cell-Tak, a New Cellular Adhesive.* Experimental Cell Research, 1988. **177**(2): p. 237-246.

158. Waite, J.H. and M.L. Tanzer, *Polyphenolic Substance of Mytilus-Edulis - Novel Adhesive Containing L-Dopa and Hydroxyproline.* Science, 1981. **212**(4498): p. 1038-1040.

159. Pankov, R. and K.M. Yamada, *Fibronectin at a glance.* Journal of Cell Science, 2002. **115**(20): p. 3861-3863.

160. Kane, R.S., et al., *Patterning proteins and cells using soft lithography.* Biomaterials, 1999. **20**(23-24): p. 2363-2376.

161. Pierschbacher, M.D. and E. Ruoslahti, *Variants of the Cell Recognition Site of Fibronectin That Retain Attachment-Promoting Activity.* Proceedings of the National Academy of Sciences of the United States of America-Biological Sciences, 1984. **81**(19): p. 5985-5988.

162. Hanenberg, H., et al., *Colocalization of retrovirus and target cells on specific fibronectin fragments increases genetic transduction of mammalian cells.* Nature Medicine, 1996. **2**(8): p. 876-882.

163. Davis, B.R., et al., *Glass needle-mediated microinjection of macromolecules and transgenes into primary human blood stem/progenitor cells.* Blood, 2000. **95**(2): p. 437-444.

164. Liu, Y., J. Yan, and M.R. Prausnitz, *Can Ultrasound Enable Efficient Intracellular Uptake of Molecules? A Retrospective Literature Review and Analysis.* Ultrasound in Medicine and Biology, 2012. **38**(5): p. 876-888.

165. Fukuda, T. and F. Arai. *Prototyping Design and Automation of Micro/nano Manipulation System*. in *IEEE International Conference on Robotics & Automation*. 2000. San Francisco, CA.

166. Tan, K., D. Ng, and Y. Xie. *Optimal Intra-Cytoplasmic Sperm Injection with a Piezo Micromanipulator*. in *4th World Congress on Intelligent Control and Automation*. 2002. Shanghai, China.

167. Kallio, P. and J. Kuncova, *Capillary pressure microinjection of living adherent cells: challenges in automation.* Journal of Micromechatronics, 2006. **3**(3): p. 189 - 220.

168. Tlaxca, J.L., et al., *Analysis of in Vitro Transfection by Sonoporation Using Cationic and Neutral Microbubbles.* Ultrasound in Medicine and Biology, 2010. **36**(11): p. 1907-1918.

169. Bacabac, R.G., et al., *Round versus flat: Bone cell morphology, elasticity, and mechanosensing.* Journal of Biomechanics, 2008. **41**(7): p. 1590-1598.

170. Edwards, D.A., et al., *Analysis of Enhanced Transdermal Transport by Skin Electroporation.* Journal of Controlled Release, 1995. **34**(3): p. 211-221.

171. Guzman, H.R., et al., *Equilibrium loading of cells with macromolecules by ultrasound: Effects of molecular size and acoustic energy.* Journal of Pharmaceutical Sciences, 2002. **91**(7): p. 1693-1701.

172. Lebrun, L. and G.A. Junter, *Diffusion of Dextran through Microporous Membrane Filters.* Journal of Membrane Science, 1994. **88**(2-3): p. 253-261.

173. Thorne, R.G. and C. Nicholson, *In vivo diffusion analysis with quantum dots and dextrans predicts the width of brain extracellular space.* Proceedings of the National Academy of Sciences of the United States of America, 2006. **103**(14): p. 5567-5572.

174. Jaiswal, J.K., et al., *Synaptotagmin VII restricts fusion pore expansion during lysosomal exocytosis.* Plos Biology, 2004. **2**(8): p. 1224-1232.

175. Wilke, C.R. and P. Chang, *Correlation of Diffusion Coefficients in Dilute Solutions.* Aiche Journal, 1955. **1**(2): p. 264-270.

176. Peckys, D.B., et al., *Immobilization and release strategies for DNA delivery using carbon nanofiber arrays and self-assembled monolayers.* Nanotechnology, 2009. **20**(14).

177. Park, S., et al., *Carbon Nanosyringe Array as a Platform for Intracellular Delivery.* Nano Letters, 2009. **9**(4): p. 1325-1329.

178. Butler, P.J., et al., *Shear stress induces a time- and position-dependent increase in endothelial cell membrane fluidity.* American Journal of Physiology-Cell Physiology, 2001. **280**(4): p. C962-C969.

179. Haidekker, M.A., N. L'Heureux, and J.A. Frangos, *Fluid shear stress increases membrane fluidity in endothelial cells: a study with DCVJ fluorescence.* American Journal of Physiology-Heart and Circulatory Physiology, 2000. **278**(4): p. H1401-H1406.

180. Andersson, L.C., K. Nilsson, and C.G. Gahmberg, *K562 - Human Erythroleukemic Cell-Line.* International Journal of Cancer, 1979. **23**(2): p. 143-147.

181. Zhou, M.X., et al., *Characterization of a Myeloperoxidase Mrna(+) Acute Lymphoblastic-Leukemia Cell-Line (Eu-1/All) Established from a Child with an Apparent Case of All.* Leukemia, 1994. **8**(4): p. 659-663.

182. Biotech, S. [cited 2014 August]; Available from: http://sqzbiotech.com/.

183. Shih, S.R., et al., *Inhibition of enterovirus 71-induced apoptosis by allophycocyanin isolated from a blue-green alga Spirulina platensis.* Journal of Medical Virology, 2003. **70**(1): p. 119-125.

184. Tsoi, M., et al., *Characterization of condensed plasmid DNA models for studying the direct effect of ionizing radiation.* Biophysical Chemistry, 2010. **147**(3): p. 104-110.

185. Brejc, K., et al., *Isolation, Crystallization, Crystal-Structure Analysis and Refinement of Allophycocyanin from the Cyanobacterium Spirulina-Platensis at 2.3 Angstrom Resolution.* Journal of Molecular Biology, 1995. **249**(2): p. 424-440.

186. Lechardeur, D., et al., *Metabolic instability of plasmid DNA in the cytosol: a potential barrier to gene transfer.* Gene Therapy, 1999. **6**(4): p. 482-497.

187. Ramirez, O.T. and R. Mutharasan, *The Role of the Plasma-Membrane Fluidity on the Shear Sensitivity of Hybridomas Grown under Hydrodynamic Stress.* Biotechnology and Bioengineering, 1990. **36**(9): p. 911-920.

188. Bao, G. and S. Suresh, *Cell and molecular mechanics of biological materials.* Nature Materials, 2003. **2**(11): p. 715-725.

189. Zhu, C., G. Bao, and N. Wang, *Cell mechanics: Mechanical response, cell adhesion, and molecular deformation.* Annual Review of Biomedical Engineering, 2000. **2**: p. 189-226.

190. Tkachuk, D.C., J.V. Hirschmann, and J.R. McArthur, *White cell disorders. In Atlas of Clinical Hematology*. 2002, Philadelphia: W.B. Sanuders. 101-114.

191. Lichtman, M.A., *Rheology of leukocytes, leukocyte suspensions, and blood in leukemia. Possible relationship to clinical manifestations.* J Clin Invest, 1973. **52**(2): p. 350-8.

192. Dong, C., R. Skalak, and K.L.P. Sung, *Cytoplasmic Rheology of Passive Neutrophils.* Biorheology, 1991. **28**(6): p. 557-567.

193. Guilak, F., J.R. Tedrow, and R. Burgkart, *Viscoelastic properties of the cell nucleus.* Biochemical and Biophysical Research Communications, 2000. **269**(3): p. 781-786.

194. Shukla, R., et al., *Biocompatibility of gold nanoparticles and their endocytotic fate inside the cellular compartment: A microscopic overview.* Langmuir, 2005. **21**(23): p. 10644-10654.

195. Raynal, I., et al., *Macrophage endocytosis of superparamagnetic iron oxide nanoparticles - Mechanisms and comparison of Ferumoxides and Ferumoxtran-10.* Investigative Radiology, 2004. **39**(1): p. 56-63.

196. Li, W., et al., *The translocation of fullerenic nanoparticles into lysosome via the pathway of clathrin-mediated endocytosis.* Nanotechnology, 2008. **19**(14).

197. Mout, R., et al., *Surface functionalization of nanoparticles for nanomedicine.* Chemical Society Reviews, 2012. **41**(7): p. 2539-2544.

198. Jiang, W., et al., *Nanoparticle-mediated cellular response is size-dependent.* Nature Nanotechnology, 2008. **3**(3): p. 145-150.

199. Kong, L.G., et al., *Synthesis of silica nanoparticles using oil-in-water emulsion and the porosity analysis.* Journal of Sol-Gel Science and Technology, 2012. **64**(2): p. 309-314.

200. Larsen, H.O., et al., *Nonviral transfection of leukemic primary cells and cells lines by siRNA-a direct comparison between Nucleofection and Accell delivery.* Experimental Hematology, 2011. **39**(11): p. 1081-1089.

201. Gresch, O., et al., *New non-viral method for gene transfer into primary cells.* Methods, 2004. **33**(2): p. 151-163.

202. Raucher, D. and M.P. Sheetz, *Membrane expansion increases endocytosis rate during mitosis.* Journal of Cell Biology, 1999. **144**(3): p. 497-506.

203. Moon, D.O., Y.H. Choi, and G.Y. Kim, *Role of p21 in SP600125-induced cell cycle arrest, endoreduplication, and apoptosis.* Cellular and Molecular Life Sciences, 2011. **68**(19): p. 3249-3260.

204. Brunner, S., et al., *Cell cycle dependence of gene transfer by lipoplex polyplex and recombinant adenovirus.* Gene Therapy, 2000. **7**(5): p. 401-407.

205. Xu, S., et al., *Construction and characteristics of an E-cadherin-related three-dimensional suspension growth model of ovarian cancer.* Scientific Reports, 2014. **4**.

206. Walter, E., et al., *Microencapsulation of DNA using poly(DL-lactide-co-glycolide): stability issues and release characteristics.* Journal of Controlled Release, 1999. **61**(3): p. 361-374.

207. Chithrani, B.D., A.A. Ghazani, and W.C.W. Chan, *Determining the size and shape dependence of gold nanoparticle uptake into mammalian cells.* Nano Letters, 2006. **6**(4): p. 662-668.

208. Dalby, B., et al., *Advanced transfection with Lipofectamine 2000 reagent: primary neurons, siRNA, and high-throughput applications.* Methods, 2004. **33**(2): p. 95-103.

209. Iversen, T.G., T. Skotland, and K. Sandvig, *Endocytosis and intracellular transport of nanoparticles: Present knowledge and need for future studies.* Nano Today, 2011. **6**(2): p. 176-185.

210. Alexis, F., et al., *Factors affecting the clearance and biodistribution of polymeric nanoparticles.* Molecular Pharmaceutics, 2008. **5**(4): p. 505-515.

211. Longmire, M., P.L. Choyke, and H. Kobayashi, *Clearance properties of nano-sized particles and molecules as imaging agents: considerations and caveats.* Nanomedicine, 2008. **3**(5): p. 703-717.

212. McKnight, T.E., et al., *Intracellular integration of synthetic nanostructures with viable cells for controlled biochemical manipulation.* Nanotechnology, 2003. **14**(5): p. 551-556.

213. Braun, G., et al., *Gold nanoparticle decoration of DNA on silicon.* Langmuir, 2005. **21**(23): p. 10699-701.

214. Christel, L.A., et al., *Rapid, automated nucleic acid probe assays using silicon microstructures for nucleic acid concentration.* J Biomech Eng, 1999. **121**(1): p. 22-7.

215. Robinson, V.N.E., *Wet Stage Modification to a Scanning Electron-Microscope.* Journal of Microscopy-Oxford, 1975. **103**(Jan): p. 71-77.

216. Danilatos, G.D., *Review and Outline of Environmental Sem at Present.* Journal of Microscopy-Oxford, 1991. **162**: p. 391-402.

217. Thiberge, S., et al., *Scanning electron microscopy of cells and tissues under fully hydrated conditions.* Proceedings of the National Academy of Sciences of the United States of America, 2004. **101**(10): p. 3346-3351.

218. Walther, P., *High-resolution cryoscanning electron microscopy of biological samples*, in *Biological Low-Voltage Scanning Electron Microscopy*, H. Schatten and J.B. Pawley, Editors. 2008, Springer: New York. p. 245 - 267.

219. Bates, M., B. Huang, and X.W. Zhuang, *Super-resolution microscopy by nanoscale localization of photo-switchable fluorescent probes.* Current Opinion in Chemical Biology, 2008. **12**(5): p. 505-514.

220. Huang, B., et al., *Three-dimensional super-resolution imaging by stochastic optical reconstruction microscopy.* Science, 2008. **319**(5864): p. 810-813.

221. Hamm, A., et al., *Efficient transfection method for primary cells.* Tissue Engineering, 2002. **8**(2): p. 235-245.

222. Russell, K.C., et al., *In Vitro High-Capacity Assay to Quantify the Clonal Heterogeneity in Trilineage Potential of Mesenchymal Stem Cells Reveals a Complex Hierarchy of Lineage Commitment.* Stem Cells, 2010. **28**(4): p. 788-798.

223. Maloney, J.M., et al., *Mesenchymal Stem Cell Mechanics from the Attached to the Suspended State.* Biophysical Journal, 2010. **99**(8): p. 2479-2487.

224. Pajerowski, J.D., et al., *Physical plasticity of the nucleus in stem cell differentiation.* Proceedings of the National Academy of Sciences of the United States of America, 2007. **104**(40): p. 15619-15624.

225. Yeung, T., et al., *Effects of substrate stiffness on cell morphology, cytoskeletal structure, and adhesion.* Cell Motility and the Cytoskeleton, 2005. **60**(1): p. 24-34.

226. Discher, D.E., P. Janmey, and Y.L. Wang, *Tissue cells feel and respond to the stiffness of their substrate.* Science, 2005. **310**(5751): p. 1139-1143.

227. Hutcheson, J.D., et al., *Saving Cells from Ultrasound-Induced Apoptosis: Quantification of Cell Death and Uptake Following Sonication and Effects of*

Targeted Calcium Chelation. Ultrasound in Medicine and Biology, 2010. **36**(6): p. 1008-1021.

228. Wu, G.H., et al., *Interaction between lipid monolayers and poloxamer 188: An X-ray reflectivity and diffraction study.* Biophysical Journal, 2005. **89**(5): p. 3159-3173.

229. Tsoneva, I., et al., *Electrodelivery of Drugs into Cancer Cells in the Presence of Poloxamer 188.* Journal of Biomedicine and Biotechnology, 2010.

230. Chen, Y.C., et al., *Pluronic block copolymers: Novel functions in ultrasound-mediated gene transfer and against cell damage.* Ultrasound in Medicine and Biology, 2006. **32**(1): p. 131-137.

231. Sengupta, A., *Intracellular drug delivery using laser activated carbon nanoparticles*, in *Chemical and Biomolecular Engineering*. 2014, Georgia Institute of Technology: Atlanta, GA.

232. McNeil, P.L. and T. Kirchhausen, *An emergency response team for membrane repair.* Nature Reviews Molecular Cell Biology, 2005. **6**(6): p. 499-505.

233. Sharei, A., et al., *Plasma membrane recovery kinetics of a microfluidic intracellular delivery platform.* Integrative Biology, 2014. **6**(4): p. 470-475.

234. Honda, H., et al., *Role of intracellular calcium ions and reactive oxygen species in apoptosis induced by ultrasound.* Ultrasound in Medicine and Biology, 2004. **30**(5): p. 683-692.

235. Kumon, R.E., et al., *Ultrasound-induced calcium oscillations and waves in Chinese hamster ovary cells in the presence of microbubbles.* Biophysical Journal, 2007. **93**(6): p. L29-L31.

236. Huo, S.D., et al., *Ultrasmall Gold Nanoparticles as Carriers for Nucleus-Based Gene Therapy Due to Size-Dependent Nuclear Entry.* Acs Nano, 2014. **8**(6): p. 5852-5862.

237. Kang, B., M.A. Mackey, and M.A. El-Sayed, *Nuclear Targeting of Gold Nanoparticles in Cancer Cells Induces DNA Damage, Causing Cytokinesis Arrest*

and Apoptosis. Journal of the American Chemical Society, 2010. **132**(5): p. 1517-+.

238. Nakielny, S. and G. Dreyfuss, *Transport of proteins and RNAs in and out of the nucleus*. Cell, 1999. **99**(7): p. 677-690.

239. Basiouni, S., H. Fuhrmann, and J. Schumann, *High-efficiency transfection of suspension cell lines.* Biotechniques, 2012: p. 1 - 4.